NUCLEAR ISOMERISM IN THE N = 127 ISOTONES

NUCLEAR ISOMERISM IN THE N = 127 ISOTONES

by

DAVID FRANKLYN TORGERSON, B.Sc.(Hons),M.Sc.

A thesis

Submitted to the Faculty of Graduate Studies

in Partial Fulfilment of the Requirements

for the degree

Doctor of Philosophy

McMaster University

July 1969

DOCTOR OF PHILOSOPHY (1969)
(Chemistry)

McMASTER UNIVERSITY
Hamilton, Ontario

TITLE: Nuclear Isomerism in the N = 127 Isotones

AUTHOR: David Franklyn Torgerson, B.Sc.(Hons) (Manitoba)
M.Sc. (Manitoba)

SUPERVISOR: Dr. R. D. Macfarlane

NUMBER OF PAGES: viii, 103

SCOPE AND CONTENTS:

The alpha decay properties of nuclei decaying across the N = 126 closed neutron configuration are examined. A systematic occurrence of isomerism is established in the odd-odd N = 127 isotones from a detailed study of ^{214}Fr and ^{216}Ac. Energy level spacings of the odd-odd N = 125 isotones ^{208}Bi, ^{210}At, and ^{212}Fr are found to exhibit a distinct correspondence. The Mang shell model theory of alpha decay is evoked to explain the reduced width fluctuations of the even-odd N = 127 isotones. Theoretical and experimental results are also presented for the alpha decay of ^{215}Ra. The new isotopes ^{222}Th, ^{221}Th, ^{218}Ra, and ^{217}Ra are synthesized and studied. Precise atomic masses are calculated for several nuclei from the measurement of alpha decay Q-values.

ACKNOWLEDGEMENTS

It is a pleasure to thank Professor R. D. Macfarlane for his supervision and guidance of this work. The time spent by Drs. A. B. Volkov and A. J. Yarwood as members of my research committee is also gratefully acknowledged.

Conversations with several individuals have been fruitful and I have especially benefited from discussions with Drs. N. S. Oakey, M. C. Gupta, K. Beg, and Mr. R. A. Gough. In particular, I have enjoyed the monthly excursions to Yale with Mr. Gough.

Much valuable equipment has been fabricated in the Nuclear Research Shop and I express my gratitude to Messrs. T. Bryden and H. Howell and their staff for their cooperation. The staff of the Yale Heavy Ion Accelerator is also to be thanked for their assistance and for providing abundant quantities of beam.

A special acknowledgement is accorded to my wife, Dale, for her encouragement throughout this work.

Scholarships obtained from the National Research Council of Canada and from the Dow Chemical Company were very much appreciated.

TABLE OF CONTENTS

LIST OF TABLES

LIST OF ILLUSTRATIONS

CHAPTER I

INTRODUCTION

1.1 Nature of the Present Work

The greatest success of the nuclear shell model has been to explain the low energy properties of nuclei near doubly-closed shells. In general, it is possible to consider the motions of the extra-core particles or holes in a central field with the addition of certain residual forces to account for the extra-core interaction. The accumulation of detailed nuclear spectra in these regions contributes, therefore, to the basic understanding of nucleon-nucleon forces.

Investigations of the 125 and 127 isotones are particularly interesting since nuclear shell effects can be studied as one simultaneously moves away from the $^{208}_{126}Pb_{82}$ doubly-closed shell and the line of beta stability. Theoretical[1-4] and experimental[5-7] determinations of the energy levels of the odd-odd nuclei $^{208}_{125}Bi_{83}$ and $^{210}_{127}Bi_{83}$ have shown the importance of a residual neutron-proton tensor component in the shell model force. The qualitative features of this interaction are retained[8] if a proton pair is added to $^{210}_{127}Bi_{83}$ to form $^{212}_{127}At_{85}$. In both nuclei, isomerism is observed.

The present work has investigated the effect of

proton pairs on the 127 isotones $^{214}Fr_{87}$ and $^{216}Ac_{89}$ and on their alpha decay daughters, the 125 isotones $^{210}At_{85}$ and $^{212}Fr_{87}$ respectively[9,10]. In addition, the alpha decay of the even-odd 127 isotone $^{215}Ra_{88}$ has been studied and the low energy states of its daughter, $^{211}Rn_{86}$, have been determined. The results are discussed in terms of the shell model theory of alpha decay to be outlined in section 1.2-2. In conjunction with the above studies, the new isotopes ^{222}Th, ^{221}Th, ^{218}Ra, and ^{217}Ra have been observed and their alpha decay properties studied[11,12]. Atomic masses have been calculated from the careful measurement of alpha particle energies.

1.2 Alpha Decay

1.2-1 Conservation Laws and Barrier Penetrability

Alpha spectroscopy is a useful means of studying the low energy states of nuclei as decay rates are strongly energy dependent and are only mildly inhibited by angular momentum. Since it is the low energy states of a nucleus which generally reflect the most information with respect to nuclear structure, the contribution of such studies to nuclear models is of some importance.

Angular momentum J and parity π are good quantum numbers for alpha emission inasmuch as they are conserved in the strong interaction. Since the alpha particle has even parity and no intrinsic angular momentum, the selection rules

take on a relatively simple form. The orbital angular momentum of the alpha particle, L, is restricted by the limits

$$|J_i - J_f| \leq L \leq J_i + J_f \qquad 1.1$$

where the subscripts i and f refer to the initial and final states respectively. If the parities of the initial and final states are the same, then L is restricted to even values; if the parities are different, only odd L values are permitted.

The total energy released in the alpha decay process is the sum of the kinetic energies of the alpha particle and the daughter nucleus

$$Q = \frac{p^2}{2M_{He}} + \frac{p^2}{2M_D} = E_\alpha \left[1 + \frac{M_{He}}{M_D} \right] \qquad 1.2$$

where M_{He} and M_D are the masses of the alpha particle and daughter nucleus respectively, and E_α is the experimental decay energy.

Alpha transitions must conserve mass-energy and at infinite separations Q is a measure of the difference in atomic rest masses of the initial and final systems times the square of the velocity of light

$$Q = (M_p - M_D - M_{He})c^2 \ . \qquad 1.3$$

As the alpha particle leaves the nucleus, work must be done against the electron cloud. The "screening correc-

tion" energy is given by[13]

$$Q_{sc} = 65.3\ (Z)^{7/2} - 80\ (Z)^{2/5}\ \text{eV} \qquad 1.4$$

where Z is the atomic number of the parent nucleus. The effective decay energy for the bare nucleus is therefore

$$Q_e = E_a \left[1 + \frac{M_{He}}{M_D}\right] + Q_{sc} \quad . \qquad 1.5$$

The energy available to an alpha particle in the nucleus must be the binding energy of the alpha particle (28.3 MeV) less the binding energy of the last two neutrons and protons. Above A ~ 140 the nucleon binding energy has decreased to a point where the nuclear-alpha interaction energy is positive, and the decay becomes energetically possible. Alpha decay life-times, however, can vary from nanoseconds to longer than the age of the universe which is a result of the Coulomb barrier the alpha particle must penetrate. In this respect, it is convenient to express the experimental alpha decay constant as $\lambda = \lambda_o P$, where P is the penetrability factor for transitions through the barrier and λ_o is the reduced decay constant. The significance of λ_o is that it represents the probability of alpha decay in the absence of angular momentum and Coulomb barrier effects. This is usually expressed as a reduced width[14]

$$\delta^2 = h\lambda_o = \frac{h}{P}\lambda \quad . \qquad 1.6$$

The penetration factor P for transmissions through the barrier from r_i to r_o is taken from WKB theory[14]

$$P = \text{EXP} - \left(2\int_{r_i}^{r_o} K\,dx\right) , \qquad 1.7$$

$$K = 1/\hbar \sqrt{2m\,(V(r) - Q_e)} \qquad 1.8$$

where V(r) is the potential barrier and m is the alpha particle reduced mass. At the classical inner and outer turning points, r_i and r_o, the wave number must vanish. Solutions to equation 1.8 when K = 0 yields the typical values r_i - 9 fm and r_o - 28 fm for the heavy element region above lead.

The potential seen by the alpha particle consists of three terms

$$V(r) = \frac{2Ze^2}{r} + \frac{L(L+1)\hbar^2}{2mr^2} + V_N(r) \quad . \qquad 1.9$$

The first and second terms on the right of equation 1.9 represent the Coulomb potential and the angular momentum barrier respectively. The third term is the nuclear interaction potential. This has been determined from an optical model analysis of alpha particle scattering and is given by the real part of the optical potential[15]

$$V_N(r) = -1100\ \text{EXP}\left[\frac{1.17\,A^{1/3} - r}{0.574}\right] . \qquad 1.10$$

In this expression, A is the mass number of the daughter

nucleus.

Some comments should be made regarding the use of equation 1.7 to calculate experimental penetrabilities. The WKB approximation is generally applied only to a smoothly-varying potential. However, the potential seen by the alpha particle necessarily contains a relatively sharp cut-off due to the nuclear component, $V_N(r)$. The WKB integral, therefore, can be in error[16] by as much as a factor of 2. A second objection arises concerning the steep slope of the optical model potential, equation 1.10. Poggenburg[17] has advanced arguments in favor of using a Woods-Saxon[18] type potential having a more gradual slope. This has the effect of decreasing r_i and the penetrabilities are 34 to 48% lower. However, one obviates these objections if the reduced widths calculated from the penetrabilities are to be used only as a basis for comparison of relative alpha decay rates.

1.2-2 Shell Model Theory of Alpha Decay

Implicit in the discussion of barrier penetration in section 1.2-1 is the concept of an alpha particle oscillating against a potential barrier within the nucleus. In this respect, the reduced decay constant λ_o is to be interpreted as the alpha particle interaction frequency with the potential, and the penetrability P is literally the fraction of successful transmissions.

The nuclear environment, however, is clearly more

complex[19-21] than implied by this simple one-body model. The many-body concept of alpha decay, first described by Thomas[22], realistically takes into account the effects of nuclear structure. Specifically, it is the shell model theory of Mang[23-27] that has met with the greatest success in explaining alpha decay rates of spherical nuclei. The Mang theory explicitly takes into account alpha particle formation from constituent nucleons existing in shell model states.

A starting point of Mang's formulation is the assumption that the decaying system can be described in terms of a time-dependent wave function $\Psi_J^M(X_1X_2..X_A;t)$ involving the spin and space coordinates of all A nucleons in the system. The quantities J and M refer to the angular momentum of the parent nucleus and its z-projection. One further assumes that the wave function exists in a certain space-time region where the time dependence is known and can be factored out. Therefore, $\Psi_J^M(X_1X_2..X_A;t)$ is replaced by the shell model wave function of the parent nuclide, $\psi_J^M(X_1X_2..X_A)$.

The alpha particle internal wave function, χ_α, depends on the relative space and spin coordinates of 2 neutrons and 2 protons. It is possible to define a time-independent probability amplitude, $G_{Jj}^L(R)$, for the decaying system in terms of ψ_J^M, χ_α, and the shell model wave function of the daughter nucleus, ϕ_j^m.

$$G^{L}_{Jj}(R) = C\int \sum_{m}(jLmM-m|JM)Y_{L}^{M-m}\phi_{j}^{m}\chi_{a}\psi_{J}^{M}d\eta\, d\epsilon\, d\Omega \qquad 1.11$$

where C is a constant containing normalization and anti-symmetry terms,

η, ϵ are internal space and spin coordinates of the daughter nucleus and alpha particle respectively,

Ω represents the angular coordinates of the alpha particle with respect to the daughter nucleus,

R is the relative distance between the alpha particle and the daughter nucleus.

Essentially, $G^{L}_{Jj}(R)$ expresses the probability that the decaying system contains an alpha particle and a daughter nucleus having the specified quantum numbers.

A salient feature of Mang's theory is that there exists a radius R_o beyond which the alpha-nuclear interaction is independent of internal motion and can be completely described in terms of a two-body potential. For $R \leq R_o$, G^{L}_{Jj} is to be calculated from shell model wave functions. Mang then expresses the decay constant for all possible final angular momentum states in terms of a penetrability, $P_L(E,R_o)$, and a reduced width, γ^2_{JjL}, both calculated at the boundary R_o.

$$\lambda = \frac{1}{\hbar}\sum_{jL} P_L(E,R_o)\,\gamma^2_{JjL}(R_o), \qquad 1.12$$

$$\gamma^2_{JjL}(R_o) = \frac{\hbar^2}{2m}\frac{1}{R_o^2}\left|G^{L}_{Jj}(R_o)\right|^2 \qquad 1.13$$

where m is the alpha particle reduced mass. It is now apparent that the reduced width relates to the effect of nuclear structure on alpha decay.

Equation 1.13 can be solved by assuming that χ_a is a Gaussian type wave function and that there is no configurational mixing of the shell model states. The reduced width of an alpha particle emerging from neutron states $n_1l_1j_1$, $n_2l_2j_2$ and a paired proton state $n_3l_3j_3$ is

$$\gamma^2_{JjL} = 1/4N_1(j_1j_2 1/2\text{-}1/2|L0)^2 N_3(2j_3+3-N_3) \left[\mathcal{R}(n_1l_1n_2l_2n_3l_3n_3l_3;R_o)\right]^2 \qquad 1.14$$

where N is the number of particles in the specified state and $\mathcal{R}$ represents the radial dependence of G^L_{Jj}.

A simplified expression for the reduced width is obtained when the alpha wave function is approximated by a delta function. This eliminates the necessity of integrating over the relative space and spin coordinates of the alpha particle. Rasmussen[28] has successfully applied the delta function model to relative alpha decay rates near the ^{208}Pb closed shell. For decay to closed shells, but involving neutron states of non-zero seniority, the delta function reduced width is

$$\gamma^2_L = \text{const.} \frac{(2j_1+1)(2j_2+1)(2j_3+1)}{(2L+1)} \left[(j_1j_2 1/2\text{-}1/2|L0)(R_1R_2R_3^2 BpBn)\right]^2 \qquad 1.15$$

where the subscripts 1 and 2 refer to the neutron states, the subscript 3 refers to the paired proton state and R_1, R_2, R_3 are the radial wave functions evaluated at the connection radius. Rasmussen[28] has noted that the model overestimates the contribution to the reduced width of high-j orbitals. Fortunately, however, the deviations are systematic and a correction factor depending on the orbital angular momentum l can be applied. For equation 1.15, the appropriate correction formulae are

$$B_p = \mathrm{EXP}\left[-0.013\ l_3(l_3+1)\right] \qquad 1.16$$

and $$B_n = \mathrm{EXP}\left[-0.0065\ l_1(l_1+1)+l_2(l_2+1)-1/2L(L+1)\right] .$$

The inherent simplicity of the shell model theory is also its weakness. While the agreement between relative experimental and theoretical decay rates has been excellent, the calculation of absolute decay constants is not possible. Some impressive advances in this direction, however, have recently been made by Harada and Rauscher[29]. It would appear that more details of the alpha-nuclear interaction potential are required[30] as well as some consideration of nucleon clustering in the surface region[21,31].

1.3 The Mass Surface

1.3-1 The Semi-Empirical Mass Formula

The mass of a nuclide consists of the rest mass

energy of the constituent neutrons and protons less the total nuclear binding energy. It has long been recognized that the overall shape of the mass surface can be expressed in an analytical form based on the Weizacker liquid drop model[32]. The analytic expression contains binding energy terms for the volume, surface tension, and Coulomb repulsion of a charged liquid drop. In addition, a symmetry term is included which accounts for the extra stability associated with nuclei for which N = Z.

Deviations from the liquid drop description, however, can be as large as 10 MeV near magic number nuclei and might well be construed as direct evidence for the existence of shell structure. It follows, therefore, that terms relating to shell effects must be included in the mass formula. Indeed, a successful mass formula will attempt to contain virtually all of the important concepts of nuclear structure.

This imposes the restriction that only physically significant terms are to be included in the analytic expression if the mass law is to relate to nuclear properties. Over 30 nuclidic mass formulae have now been developed, not all of which fulfil this requirement[33-35]. For comparison to present results, the Myers-Swiatecki[35,36] equation has been chosen since it involves only 7 adjustable parameters and yet is capable of reproducing experimental masses to within a few hundred keV in the heavy element region.

1.3-2 Alpha-Beta Energy Systematics

A general characteristic of alpha decay is the high degree of regularity in the change of the total decay energy, Q, with mass number. In this respect, it is of interest to consider the alpha decay energy trends for a series of isotopes near the N = 126 closed shell. As one moves from the region of β-stability towards neutron deficient nuclei, there is a smooth increase in Q. This is accounted for in terms of the proton binding energies which are decreasing as more neutrons are removed. At the N = 126 closed shell, however, there is a pronounced increase in the neutron binding energies which offsets this trend. Accordingly, one observes a sharp decrease in the alpha decay energy. Thereafter, the Q-values once again increase as additional neutrons are removed.

From these considerations, unknown alpha transitions occurring in alpha decay chains are predicted with reasonable accuracy. The interrelation of parallel chains can be established by the beta decay process which thereby defines a lattice of nuclidic mass-energy differences. One may identify 4 such lattices of closed cycles connecting nuclides differing by 4 mass units: 4n, 4n+1, 4n+2, and 4n+3, where n is an integer. Predictions are made from empirical extrapolations of the cycles taking into account the systematics of alpha decay in a given mass region[37]. Thus, the mass-energy surface can be extended to unknown isotopes.

CHAPTER II

EXPERIMENTAL CONSIDERATIONS

2.1 The Helium Jet Recoil Transport Method

Nuclear reaction products were studied "on-line" using the helium jet recoil transport technique[38,39]. The essential characteristics of the method, illustrated in figure 1, are now considered.

The target is positioned before a copper hemisphere which is filled with helium at 1.9 atm. The incident beam, obtained from the Yale heavy ion accelerator, interacts with the target and is terminated in the hemisphere. Products recoiling from the target are thermalized in the helium and entrained in the gas flow through the metal capillary into an evacuated chamber.

At the time of the beam burst, the hemisphere is instantaneously filled with recoils but is completely emptied after 8 msec by the near-sonic gas flow through the capillary. The residual pressure is maintained at - 25 microns by means of a high speed diffusion pump having a capacity of 6000 l/sec. At the end of the capillary, the helium carrier gas expands rapidly into the chamber while the heavier reaction products are adsorbed onto a stainless steel collection assembly.

The alpha decay of the products was measured by means of 50 mm^2 annular Si(Au) surface barrier detectors obtained

FIGURE 1

Schematic of the helium jet recoil transport technique for the study of nuclear reaction products.

Hemisphere volume = 0.4 ml

Capillary diameter = 0.5 mm

Capillary length = 16 cm

Helium pressure = 1.9 atm

Gas flow rate = 50 ml/sec

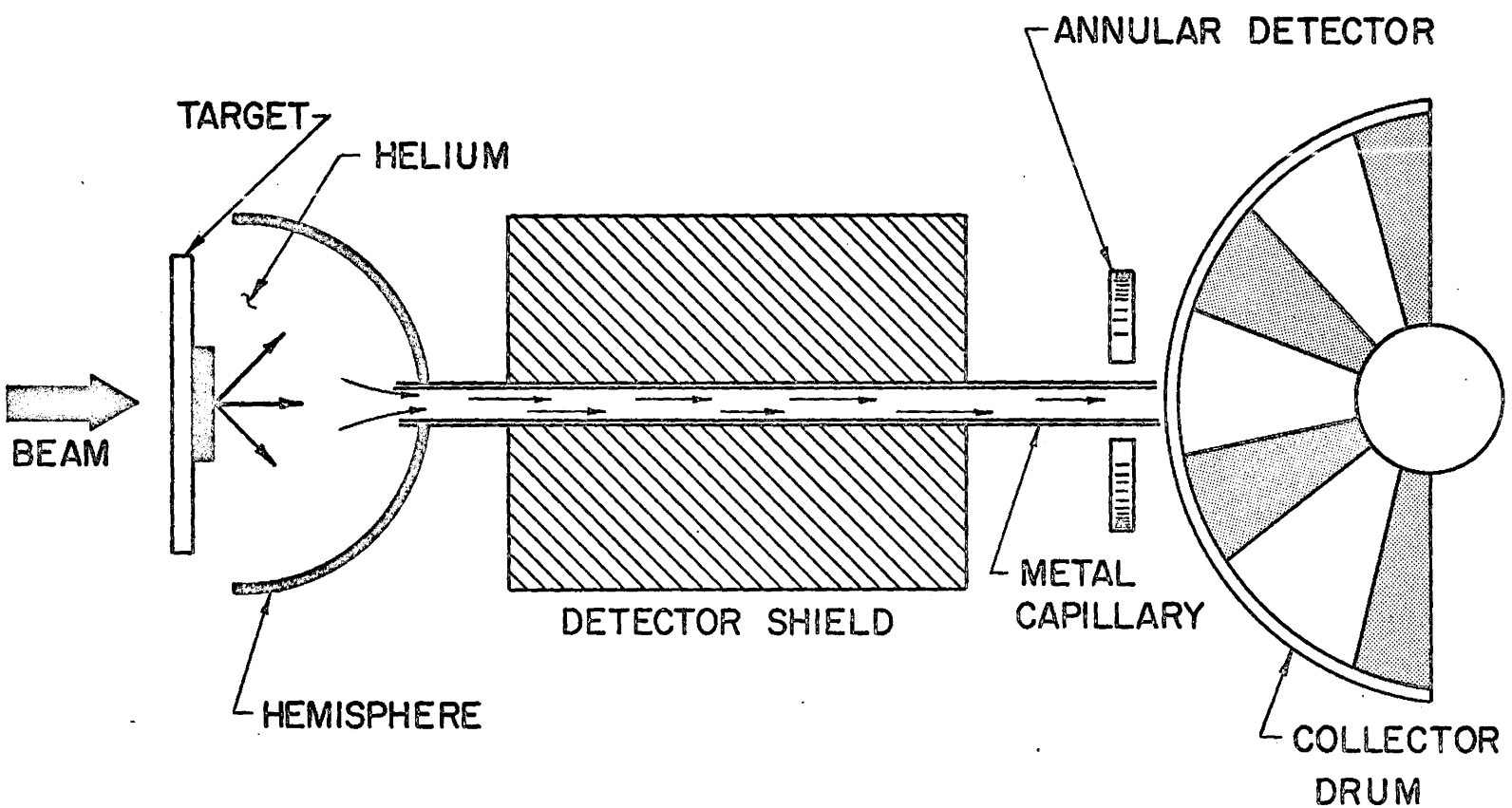
ANNULAR DETECTOR
TARGET
HELIUM
BEAM
DETECTOR SHIELD
METAL CAPILLARY
HEMISPHERE
COLLECTOR DRUM

from Oak Ridge National Laboratory. These detectors were observed to have a resolution of 25 - 30 keV (FWHM). Spectra were taken during and between beam bursts which came at a frequency of 10/sec, each burst lasting 2 msec. Shielding was provided by 13 cm of brass which effectively eliminated background due to the beam.

Much effort has been expended to optimize the helium jet recoil transport method with respect to collection efficiency for short-lived nuclei[39]. The conditions pertaining to the present work are summarized in the caption of figure 1. The collection efficiency of this system is dependent on three basic components: 1. loss of energetic recoils which become embedded in the hemisphere; 2. loss of products by adsorption on the capillary and hemisphere walls; 3. the effect of finite transportation time. The first effect is treated mathematically in section 2.3. It is found that this component of the efficiency is essentially constant with change in beam energy when thick targets are used (>2 mg/cm^2). The second factor is a function of gas flow turbulence and is discussed in detail in reference 39. Adsorption properties, however, are not expected to fluctuate with bombarding energy.

The final effect has been studied for some of the nuclear recoils formed in this work[39,43]. It is found, for example, that the collection time efficiency for ^{216}Ac (t1/2 = 0.33 msec) is only 4%. By contrast, the efficiency for the

longer-lived ^{214}Fr ($t_{1/2}$ = 5.0 msec) is 63%.

The collection time efficiency is observed to be essentially independent of incident beam energy for thick targets[43]. This result is not surprising since the recoil energy pattern from thick targets attains a uniform distribution. In terms of range, this indicates that the recoil distribution extends beyond the end of the hemisphere, corresponding to 1.2 cm of He at 1.9 atm. For thin targets, however, the recoil spectrum approaches a Gaussian distribution which moves towards the back of the hemisphere as the beam energy is increased. Since the recoil transport time in the capillary is only 0.25 msec compared to the overall collection time of 8 msec, it is apparent that any change in the position of the distribution will affect the collection time. These considerations are not trivial as fluctuation in yield must be independent of the experimental configuration and reflect only the energetics of the reaction being studied.

Many details of the helium jet recoil transport technique are not reproduced here but are treated in references 38-42. The method is in a state of constant evolution in order to improve its transport properties. In its present form, the system provides a means of rapid on-line target/product separation with correspondingly high spectroscopic resolution. It is now being modified in conjunction with a quadrupole mass filter to effect on-line chemical

separations. Besides the obvious use of such a system for the unambiguous detection of new elements and isotopes, the chemical environment of the nuclear recoils can be thoroughly studied.

2.2 Target Preparation

For reasons discussed in section 2.1, it was necessary to obtain targets infinitely thick with respect to recoil emission. Procedures have been developed to yield thick (~4 mg/cm^2), uniform targets of ^{209}Bi and ^{208}Pb by electrodeposition from non-aqueous solvents. Molecular plating from non-aqueous solutions has been described by Parker and Falk[44].

Milligram quantities of ^{208}Pb (99.5% enriched isotope) were obtained from Oak Ridge National Laboratory in the form of the nitrate. A sample was evaporated to dryness several times with concentrated HCl to form the chloride, $PbCl_2$. This was dissolved in the minimum amount of H_2O and placed in a 20 ml heated plating cell with a 50-50 mixture of hot methanol-isopropanol. This procedure was necessary to insure that the sample remained in solution. The ^{208}Pb was then deposited onto a 2.3 mg/cm^2 copper foil cathode at a constant current of 1 μamp (~6 volts). For a deposition efficiency of ~90%, several hours of careful plating was necessary. The resulting targets had the dark metallic color characteristic of the metal and were found to undergo

a minimum amount of evaporation when subjected to the beam.

Pellets of ^{209}Bi metal (99.99% pure) were obtained from Canadian Mining and Smelting Company. A sample of these was dissolved in HNO_3 and was evaporated to dryness several times with concentrated HBr. A plating cell solution was prepared by dissolving the $BiBr_3$ in ether to the saturation point. The ^{209}Bi was then deposited from the solution onto a 2.3 mg/cm^2 copper cathode at a fixed current of 1 μamp (-200 volts). In two hours of plating, a 4 mg/cm^2 target of bismuth could be prepared from a 20 ml sample of plating solution. These targets exhibited the same stability characteristic of the lead targets.

2.3 Thick Target Recoil Analysis

In order that excitation function data be meaningful, it is necessary to insure that the intensities of alpha groups measured at different incident beam energies correctly reflect the cross sections of formation. The problem is relatively simple in the case of thin targets (<1 mg/cm^2) since virtually all the products formed in the target have sufficient momentum to escape. For thick targets, however, the escape probability is a sensitive function of the position in the target where the recoil is formed.

For a heavy ion beam of energy E_{b_o} (lab) incident on a target of thickness t, the maximum kinetic energy transferred to the compound nucleus is $E_r = A_b E_b / A_r$, where

A_b and A_r are the masses of the incident ion and nuclear recoil respectively. If R_o is the mean range of the product in the target material, then the statistical distribution of range about R_o is assumed to be Gaussian:

$$P(R)dR = \frac{1}{\sqrt{2\pi}\,\sigma} \text{EXP} - \left[\frac{(R-R_o)}{\sqrt{2}\,\sigma}\right]^2 dR \qquad 2.1$$

A schematic of this function is shown in figure 2 for recoils ejected from a plane perpendicular to the beam axis and located x mg/cm^2 into the target material. If z is the mean range for recoils originating at x, and y is any point in the distribution, then the range probability is

$$P(y-x)d(y-x) = \frac{1}{\sqrt{2\pi}\,\sigma} \text{EXP}- \left[\frac{(y-x)-(z-x)}{\sqrt{2}\,\sigma}\right]^2 d(y-x) \qquad 2.2$$

where $(z-x) = R_o$ and $(y-x) = R$.

The fraction of recoils formed at x that escape the target is

$$F(x) = \int_{(t-x)}^{\infty} P(y-x)d(y-x) \qquad 2.3$$

If by definition $c = \left[(y-x)-(z-x)\right]/\sqrt{2}\,\sigma$, then $dc = d(y-x)/\sqrt{2}\,\sigma$. The lower limit of c is $c_L = \left[(t-x)-(z-x)\right]/\sqrt{2}\,\sigma$. Hence,

$$F(x) = 1/2 \left[2/\sqrt{\pi} \int_{c_L}^{\infty} \text{EXP}-(c)^2 dc\right]$$

$$= 1/2 \left[1-\text{ERF}\left[\frac{(t-x)-(z-x)}{\sqrt{2}\,\sigma}\right]\right] \qquad 2.4$$

FIGURE 2

The statistical range distribution of nuclear recoils formed at a point x in a target of thickness t.

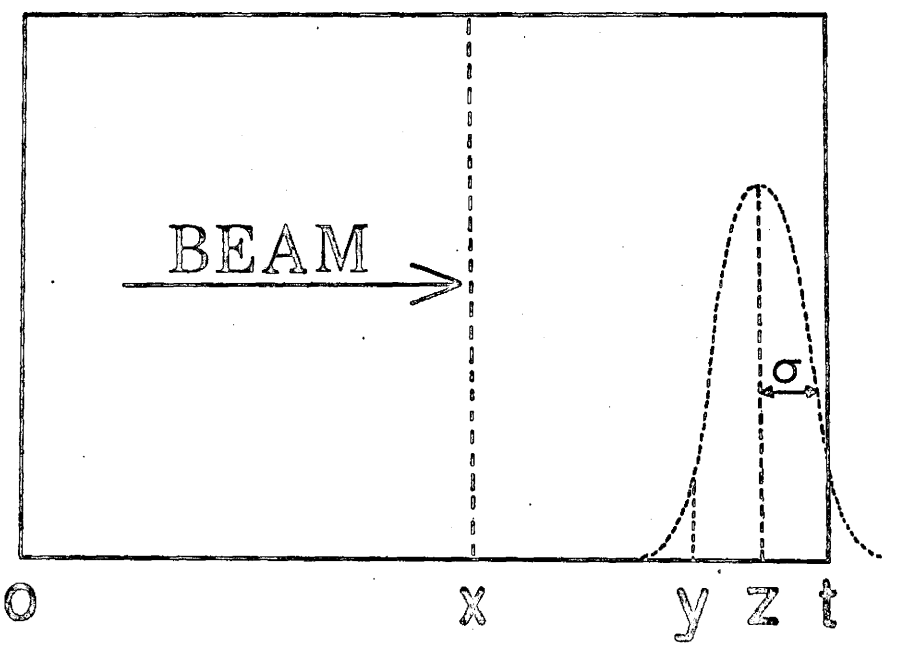
BEAM
σ
0
x
y
z
t

The beam energy at each point in the target, $E_b(x)$, is a function of the target thickness the beam has traversed. The degradation of the beam is $E_{b_o}-E_b(x)$. Since this is typically only a few MeV, the range-energy curve for the beam in the target material can be assumed to be linear over this region. Therefore, $E_b(x) = E_{b_o} - ax$, where a is the slope of the range-energy curve evaluated at E_{b_o}.

The mean deviation, σ, can be written $\sigma = R_o\rho$, where ρ is defined as the "straggling parameter" and is essentially independent of energy. Winsberg and Alexander[45] have experimentally determined the ranges and the straggling parameter of heavy ion astatine recoils in gold. Their data indicates that the relation between range and energy for astatine in gold is a linear function given by $R_o = 0.13\ E_o$, where R_o is in mg/cm^2 and E_o in MeV. The straggling parameter is 0.42. Assuming these values for slightly heavier recoils and targets, then $R_o = (z-x) \simeq 0.13(E_{b_o} - ax)\ A_b/A_r$ and $\sigma = 0.42R_o \simeq 0.055(E_{b_o} - ax)A_b/A_r$. The fraction of recoils formed at x that escape the target is therefore

$$F(x)dx = 1/2\left[1-ERF\left[\frac{t-x-0.13(E_{b_o} - ax)A_b/A_r}{0.077(E_{b_o} - ax)A_b/A_r}\right]\right]dx \qquad 2.5$$

This function is plotted in figure 3 for a 5 mg/cm^2 target of ^{208}Pb bombarded by ^{16}O at energies of 73 and 153.5 MeV. As the beam energy is decreased, the distribution is shifted towards the end of the target.

FIGURE 3

Recoil escape probabilities for ^{224}Th recoils formed in a 5 mg/cm^2 ^{208}Pb target at ^{16}O beam energies of 153.5 and 73 MeV (lab). The curves were calculated from equation 2.5.

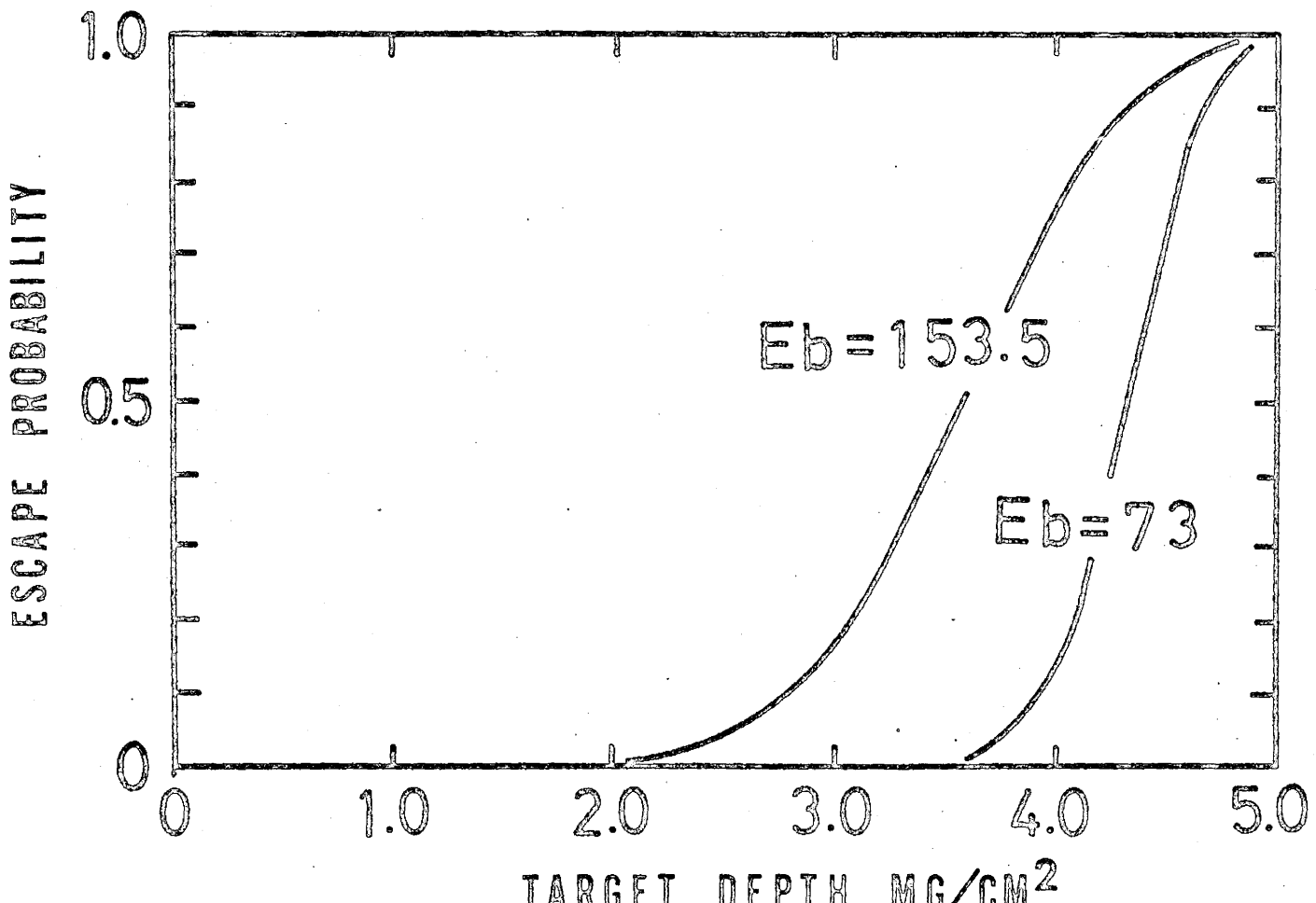
1.0
0.5
0
ESCAPE PROBABILITY
Eb=153.5
Eb=73
0
1.0
2.0
3.0
4.0
5.0
TARGET DEPTH MG/CM2

The total escape probability for a particular incident beam energy is

$$P(E_{b_o}) = \frac{1}{t}\int_o^t F(x)dx \qquad 2.6$$

The experimental configuration is such that recoils having sufficient energy to traverse 1.2 cm of helium at 1.9 atm become imbedded in the hemisphere and are not detected. From the range theory of Lindhard, Scharff, and Schiott[68] it is possible to calculate this energy (see appendix). For ^{224}Th this corresponds to a 2.8 MeV recoil. A maximum target thickness, x_m, is defined such that recoils originating from the plane of x_m have a mean range of 1.2 cm in helium: $x_m = 1/a(E_{b_o} - 2.8A_r/A_b)$. The effective escape probability is therefore

$$P_e(E_{b_o}) = 1/t\int_o^{x_m} F(x)dx \qquad 2.7$$

Equations 2.6 and 2.7 were integrated numerically by computer for various recoils in ^{208}Pb and ^{209}Bi targets. The results for ^{224}Th recoils in a 5.0 mg/cm^2 ^{208}Pb target are plotted in figure 4. The effective escape probability is reasonably flat over a wide range of incident beam energies. For an experiment designed to collect the total activity recoiling from a thick target, however, it is clear that a correction factor is necessary in order that yield be proportional to cross section.

FIGURE 4

Graph of the probability integrals $P(\overline{E}_b)$ and $P_e(\overline{E}_b)$ for ^{224}Th recoils in a 5.0 mg/cm^2 ^{208}Pb target. Beam energies have been corrected according to equation 2.9.

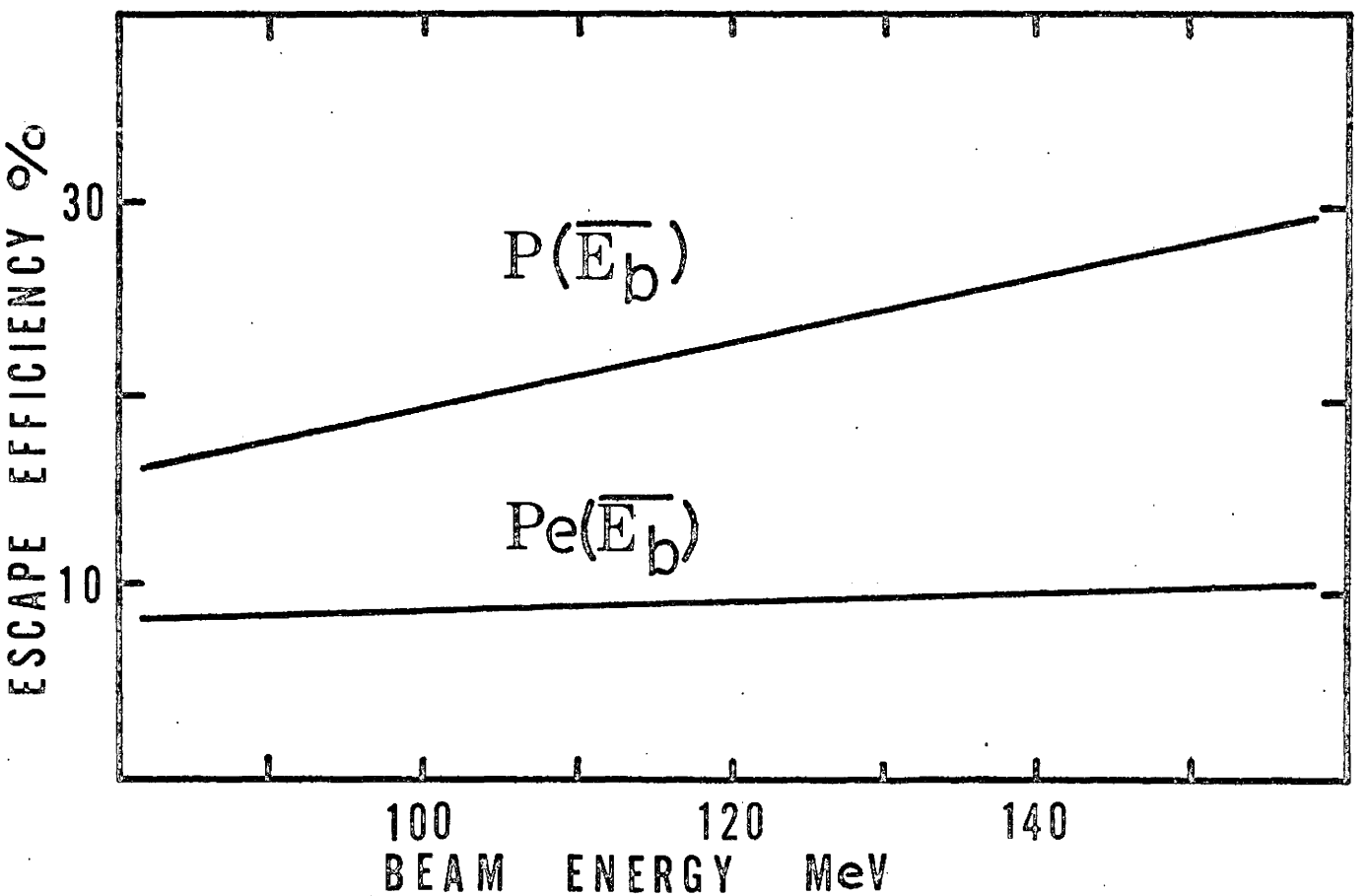
ESCAPE EFFICIENCY %
30
10
$P(\overline{E_b})$
$Pe(\overline{E_b})$
100
120
140
BEAM ENERGY MeV

As the beam sees a finite target thickness, it is important to correct for the energy loss in the target. It is possible to define an average target thickness, $\bar{x}$:

$$\bar{x} = \frac{\int_o^{x_m} xF(x)dx}{\int_o^{x_m} F(x)dx} \qquad 2.8$$

Since the correction is only of the order of a few MeV, the corrected beam energy, $\bar{E_b}$, is

$$\bar{E_b} = E_{b_o} - a\bar{x} \qquad 2.9$$

2.4 Analysis of Data and Experimental Technique

Alpha particle groups were analysed for energy, intensity, and half-life. This data was used to determine experimental reduced widths, excitation functions, energy level diagrams, and nuclear masses.

As the counting took place from thin sources deposited on the collection assembly, the peak shapes were essentially Gaussian. Deviations were caused by the acceptance cone of the detector, the attenuation effect of the helium gas impinging on the source, and the effect of adsorption of organic impurities on the collection surface. For these reasons, some straggling on the low energy side of the peaks was observed. In addition, a non-Gaussian high energy tail was observed due to alpha/gamma or alpha/beta coincidences. Peak positions were therefore determined by fitting the experimental points near the centroid of the peak to a Gaussian

distribution using the non-linear least squares technique. Energy analysis was completed by fitting a quadratic function to the peak positions of known alpha group standards in the spectrum, thus taking into account any inherent non-linearity of the electronics. In the case of ^{214}Fr, alpha energies were assigned relative to the ^{228}Th decay chain[46]. For subsequent spectra, the prominent ^{214}Fr groups[9] were used as internal standards along with other established groups in the spectrum.

The above procedure was implemented using the FORTRAN computer program ALSPAN. A zeroth order analysis was carried out by the program MINIPLOT which scanned each spectrum for the alpha groups, assigned approximate energies and intensities, and then plotted the spectrum. The plots were internally scaled and could be linear or logarithmic.

For excitation function measurements, alpha group intensities were obtained by numerically integrating over the peaks once background had been removed. Beam energies were chosen by degrading the incident ions (10.5 MeV/nucleon) using nickel foils. The range-energy data of Northcliffe[47], Roll and Steigert[48], and Walton[49] were used to determine the resulting energies. These were subsequently corrected for target thickness by the procedure outlined in section 2.3.

Half-lives were measured between beam bursts which were 2 msec in duration at a frequency of 10/sec. Two experimental procedures were used. In the first instance, an

alpha particle group was electronically gated to drive a single channel analyser. The output was routed into a pulse height analyser which could be time scaled in a number of different modes. A machine pulse coming 1 msec before the beam burst was used as a start pulse on the analyser. In this way, both the build-up of activity and its subsequent decay could be followed. The schematic of this operation is shown in figure 5A.

In the second method, a delayed gate generator triggered on the machine pulse was used to enable a linear gate. The linear gate would accept pulses from the detector only during the time pulse of the generator. By varying the delay time of the generator, the decay curves of all the short-lived alpha groups in the spectrum could be obtained. The schematic of this procedure is shown in figure 5B.

Decay curves falling within the 8 msec limit required to empty the hemisphere contain a component due to activity being deposited on the collection drum. Hence the decay law is

$$N(t) = N_s(t)e^{-\lambda t} \qquad 2.10$$

where $N_s(t) = \int_0^t D(t)dt$, and $D(t)$ is the rate of product deposition on the collection drum. This function has been determined by Gough[43] for the experimental configuration used in this work. For the region 2-4.5 msec, where t=0 is the start of the machine pulse, the function is

$$D(t) = 1510t^2 - 1395t. \qquad 2.11$$

FIGURE 5

Schematic of electronic system used for half-life measurements.

A

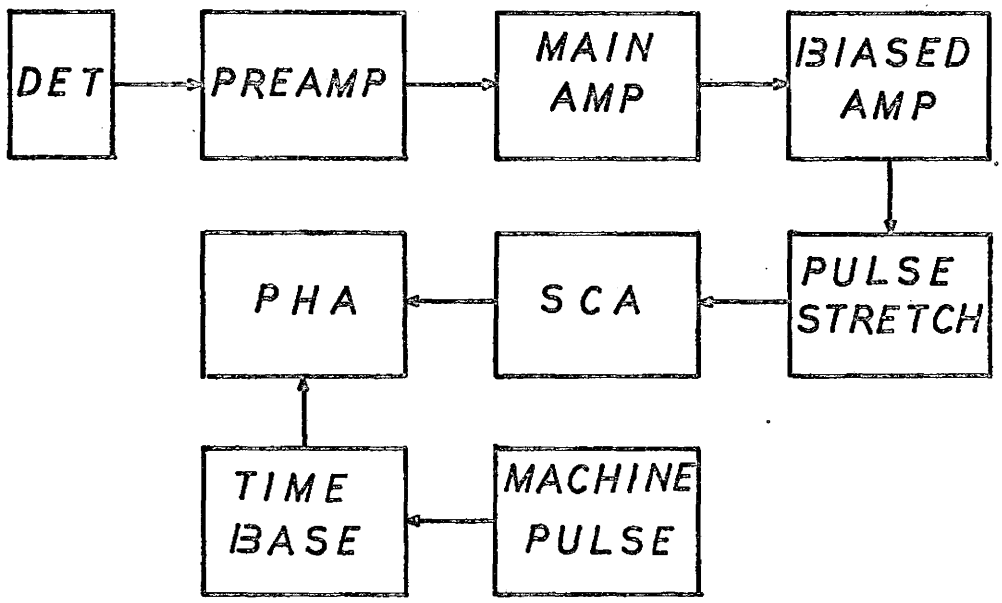
DET
PREAMP
MAIN AMP
BIASED AMP
PULSE STRETCH
SCA
PHA
TIME BASE
MACHINE PULSE

B

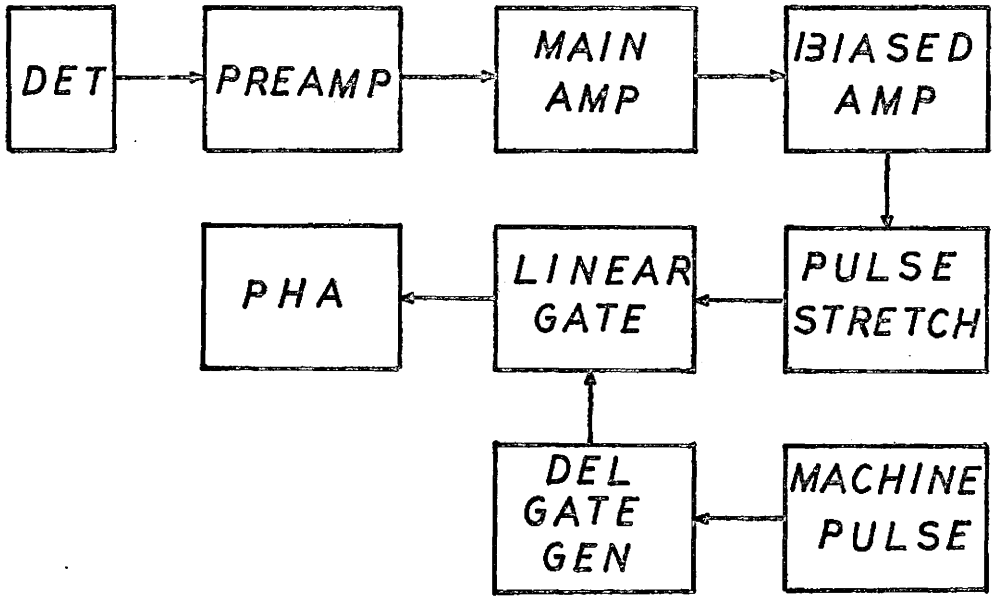
DET
PREAMP
MAIN AMP
BIASED AMP
PULSE STRETCH
LINEAR GATE
PHA
DEL GATE GEN
MACHINE PULSE

CHAPTER III

FRANCIUM 214 RESULTS

3.1 Introduction

As mentioned previously, the energy level structure of ^{214}Fr and of its alpha decay daughter, ^{210}At, are expected to be governed by the neutron-proton force in the presence of proton pairs and the ^{208}Pb core. Of particular interest in ^{214}Fr are the 10 levels arising from the coupling of a $g_{9/2}$ neutron and an $h_{9/2}$ proton. The strong coupling rule[50] predicts the existence of low-lying (0-) and (9-) states for this configuration and the occurrence of isomerism in ^{214}Fr is possible. It is noted at this point that "isomerism" used in the present context will mean that an excited state is sufficiently hindered with respect to gamma transitions such that alpha particle emission is the unique mode of decay. This avoids placing an arbitrary lower limit on the life-time of an excited level to classify it as an isomer.

The alpha particle emitter ^{214}Fr was first observed by Griffioen and Macfarlane[51], having $E_\alpha = 8.55$ MeV and $t_{1/2} = 3.9$ msec. These results were substantiated by Rotter *et al.*[52], but Valli *et al.*[53] have obtained a significantly different alpha decay energy (8.430 MeV) by producing ^{214}Fr as an electron capture (EC) daughter of ^{214}Ra.

An alpha particle spectrum resulting from the irrad-

iation of ^{208}Pb with 70 MeV ^{11}B ions is shown in figure 6. Several transitions are observed between 7.4 and 8.6 MeV which are assigned to ^{214}Fr and two distinct groupings of the data are possible on the basis of excitation function and half-life measurements. In addition to Fr isotopes, formed by neutron emission from the compound nucleus ($^{219}Fr^*$), and their alpha decay At daughters, the spectrum contains activity due to ^{213}Rn and ^{211}Po. The ^{213}Rn is the EC daughter of ^{213}Fr [54], while most of the ^{211}Po is likely formed by direct reaction mechanisms.

3.2 Metastable State Transitions

The resolution maintained in these experiments (30 keV, FWHM) was sufficient to resolve the previously reported single peak for ^{214}Fr into two intense groups at 8.477 and 8.546 MeV. Decay curves for these two groups have been measured along with the weaker activities at 8.046, 7.963, 7.708, and 7.594 MeV. A least squares fit to this data, summarized in figure 7, has yielded a half-life of 3.35 ± 0.05 msec for these transitions.

Excitation functions, measured at several different beam energies, for some of the products of the $^{208}Pb + ^{11}B$ reaction are shown in figure 8. The excitation function of the ^{213}Fr group at 6.772 MeV, corresponding to the $^{208}Pb(^{11}B,6n)^{213}Fr$ reaction, is observed to peak at a ^{11}B energy of 80 MeV (lab). For the ^{214}Fr activities, however, the relative cross

FIGURE 6

Alpha particle spectrum of the products resulting from the bombardment of ^{208}Pb with 70 MeV ^{11}B ions.

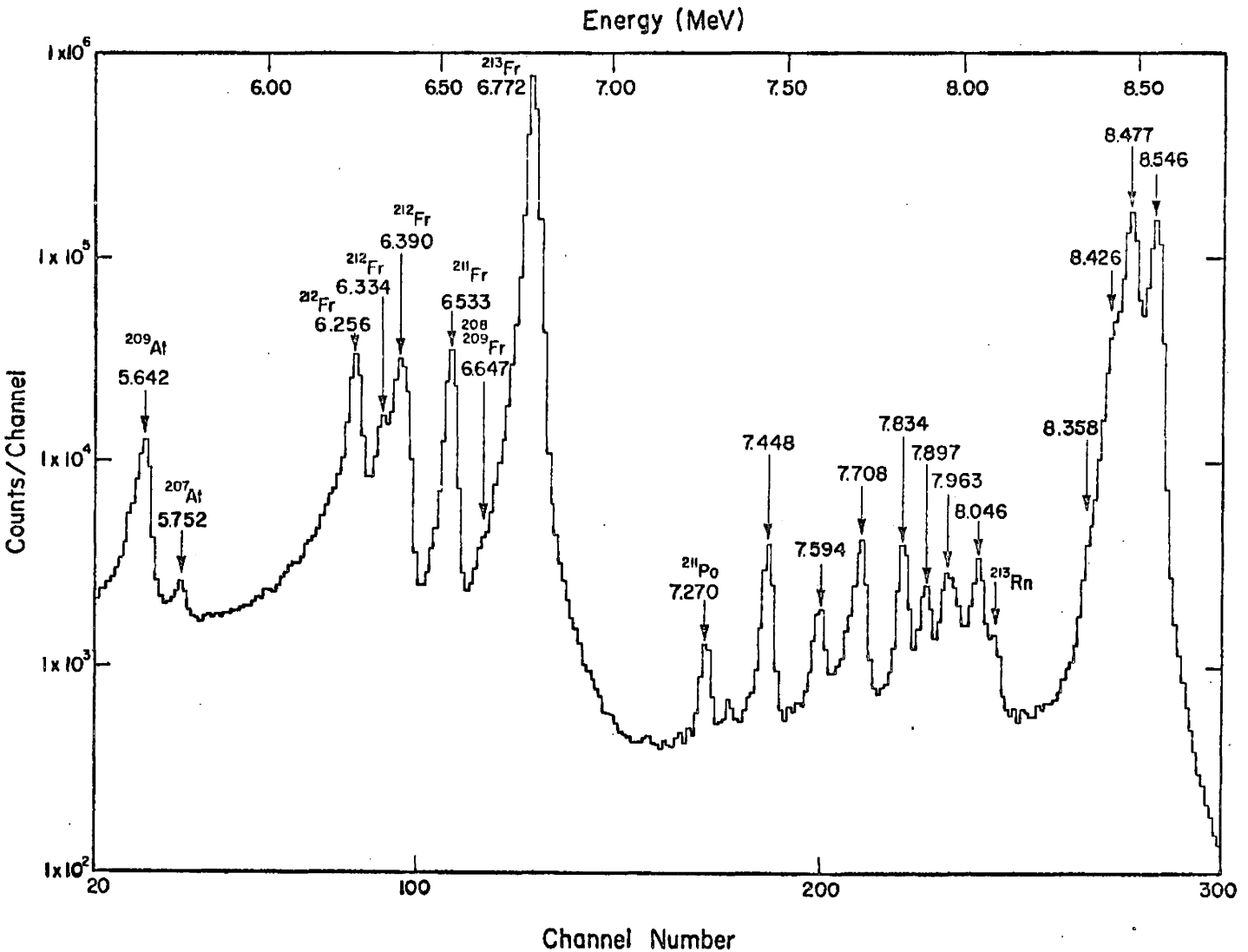
Energy (MeV)
1x10^6
1 x 10^5
1 x 10^4
1 x 10^3
1x10^2
Counts/Channel
6.00
6.50
7.00
7.50
8.00
8.50
20
100
200
300
Channel Number
213Fr 6.772
212Fr 6.390
212Fr 6.334
212Fr 6.256
211Fr 6.533
208 209Fr 6.647
209At 5.642
207At 5.752
211Po 7.270
7.448
7.594
7.708
7.834
7.897
7.963
8.046
213Rn
8.358
8.426
8.477
8.546

FIGURE 7

Decay curves for alpha transitions from the metastable state of ^{214}Fr. The half-life of these groups, determined by a non-linear least squares fit to the data, is 3.35 ± 0.05 msec.

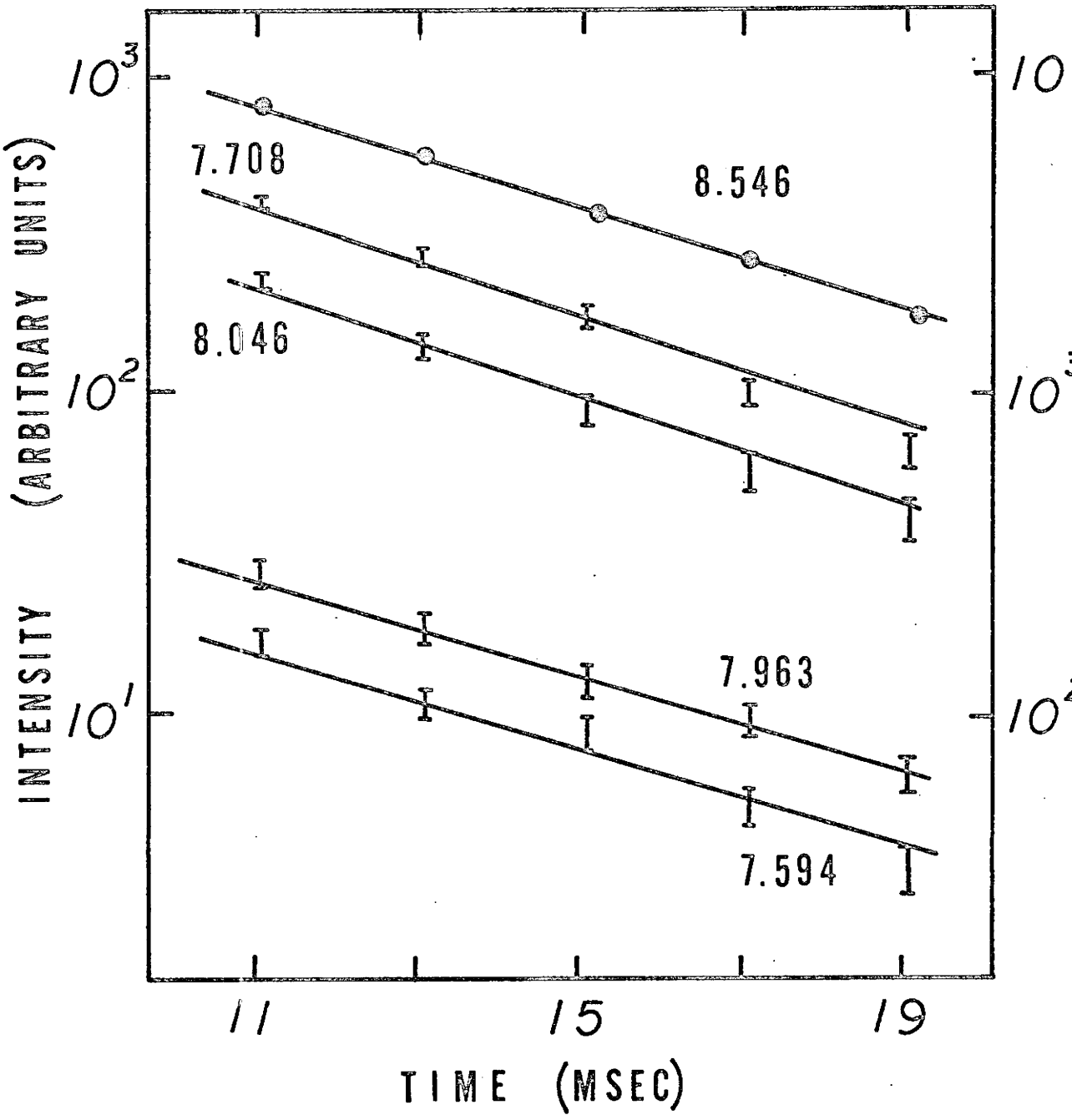
INTENSITY (ARBITRARY UNITS)
10^3
10^2
10^1
7.708
8.546
8.046
7.963
7.594
11
15
19
TIME (MSEC)

FIGURE 8

Excitation functions for some of the products of the $^{208}Pb + ^{11}B$ reaction.

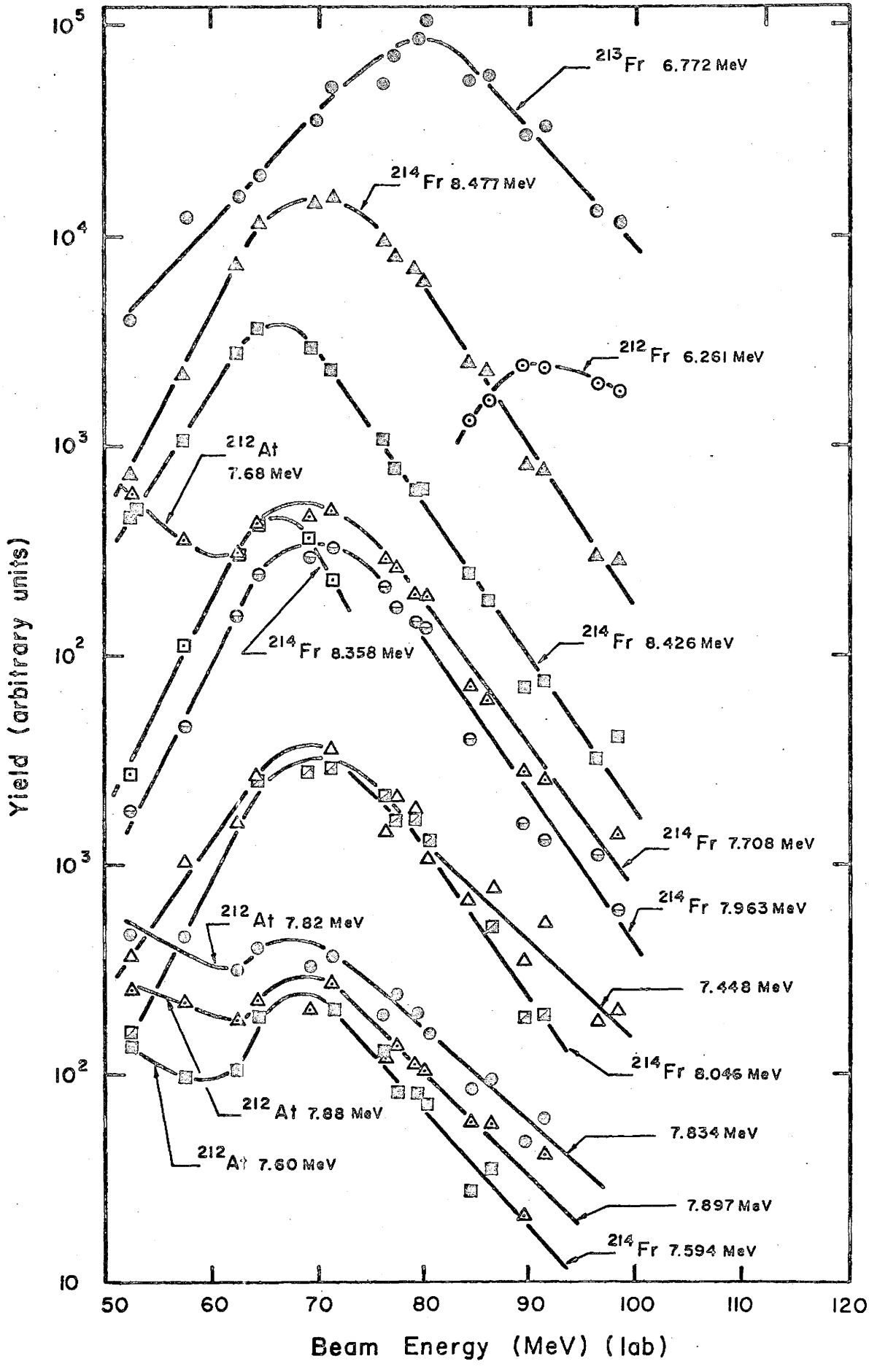
10^5
10^4
10^3
10^2
10^3
10^2
10
Yield (arbitrary units)
^{213}Fr 6.772 MeV
^{214}Fr 8.477 MeV
^{212}Fr 6.261 MeV
^{212}At 7.68 MeV
^{214}Fr 8.358 MeV
^{214}Fr 8.426 MeV
^{214}Fr 7.708 MeV
^{214}Fr 7.963 MeV
^{212}At 7.82 MeV
7.448 MeV
^{214}Fr 8.046 MeV
^{212}At 7.88 MeV
7.834 MeV
^{212}At 7.60 MeV
7.897 MeV
^{214}Fr 7.594 MeV
50
60
70
80
90
100
110
120
Beam Energy (MeV) (lab)

sections maximize at 9 MeV less excitation. The work of Macfarlane and Griffioen[55] in this region has shown that this is the expected excitation energy difference for the (^{11}B,6n) reaction relative to the (^{11}B,5n) reaction. Assigning these groups to an alpha decaying state of ^{214}Fr is therefore consistent with their results.

The 6 alpha particle transitions discussed in this section are assigned to a metastable state in ^{214}Fr. The reasons for this assignment will be made clear in the following section.

3.3 Ground State Transitions

At lower ^{11}B bombarding energies, 2 alpha particle groups at 8.426 and 8.358 MeV are clearly observed on the low-energy side of the 8.477 MeV peak. These activities are shown in figure 9 for an incident ^{11}B energy of 60 MeV. The solid line represents the Gaussian line shape calculated from the experimental points using the computer program ALSPAN.

The excitation functions of the 8.426 and 8.358 MeV groups shown in figure 8 are interesting in that they are shifted 4 MeV lower in ^{11}B bombarding energy relative to the 3.35 msec activities. This shift is somewhat smaller than that expected for the (^{11}B,4n) reaction leading to ^{215}Fr formation. However, a similar shift involving the low spin member of an isomer pair produced in heavy-ion reactions has been observed, and is a result of the angular momentum dependence

FIGURE 9

Detail of the ^{214}Fr groups between 8.3 and 8.6 MeV produced at an incident ^{11}B energy of 60 MeV. The solid line is the Gaussian distribution calculated from the experimental data.

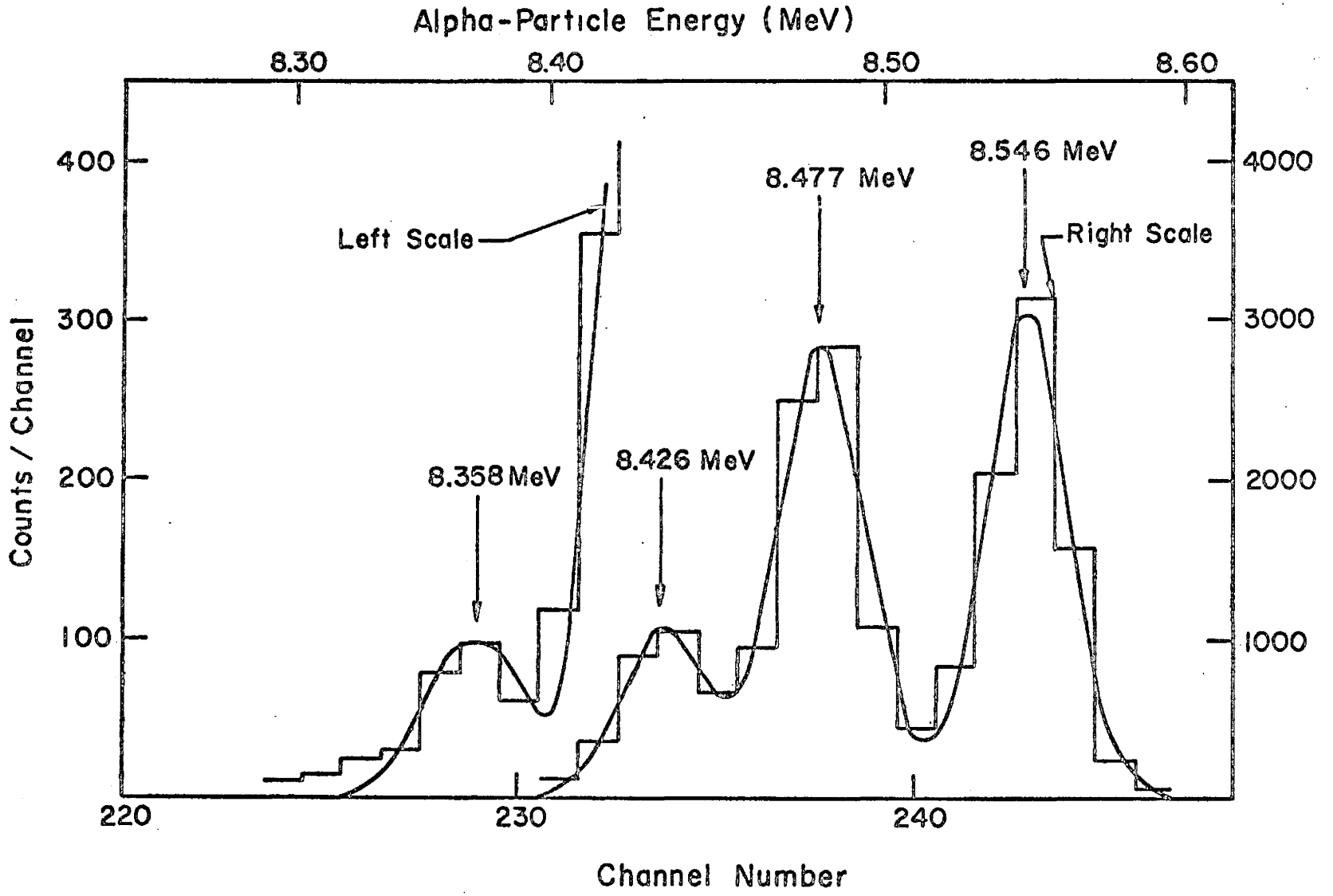
Alpha-Particle Energy (MeV)
8.30
8.40
8.50
8.60
400
300
200
100
4000
3000
2000
1000
Counts / Channel
Left Scale
Right Scale
8.358 MeV
8.426 MeV
8.477 MeV
8.546 MeV
220
230
240
Channel Number

of neutron and gamma emission widths of compound nuclear states[56]. It is apparent, therefore, that this activity arises from a low spin state of ^{214}Fr and that the 3.35 msec activity corresponds to a high spin state of ^{214}Fr.

Further information is obtained from the study of the ^{214}Fr activity formed by the electron capture decay of ^{214}Ra. These transitions should favor the low spin state since the ground state of the even-even ^{214}Ra has $J^{\pi} = (0^+)$. The half-life of ^{214}Ra is 2.6 sec[53]. Figure 10A is an alpha particle spectrum of the reaction ^{209}Bi(^{11}B,6n)^{214}Ra which is delayed 50 msec from the beam burst to allow for the decay of any ^{214}Fr formed by (p,5n) emission from the ^{220}Ra* compound nucleus. The existence of the ^{214}Fr groups at 8.426 and 8.358 MeV in this spectrum is additional evidence for the low spin assignment. From these results, the EC branching of ^{214}Ra is 0.06 ± 0.01%. This experiment also explains the results of Valli *et al.*[53] for the alpha energy of ^{214}Fr.

In the analysis of the ^{208}Pb(^{11}B,xn)$^{219-x}$Fr spectrum it is observed that the peaks at 7.448, 7.834, and 7.897 MeV all exhibit the same apparent excitation function dependence as the low spin isomer (figure 8). However, these energies correspond to known groups: ^{211}Po at 7.448 MeV[46] and the recently re-determined ^{212m}At at 7.837 and 7.899 MeV[57].

It is found that the low spin state of ^{214}Fr is populated in high yield from the alpha decay of ^{218}Ac.

FIGURE 10

Alpha particle groups associated with the low spin isomer of ^{214}Fr.

A. $^{209}Bi + ^{11}B$

Groups at 8.358 and 8.426 MeV produced from the EC decay of ^{214}Ra. The spectrum was delayed 50 msec from the beam burst to allow for the decay of ^{214}Fr produced directly.

B. $^{209}Bi + ^{12}C$

Low spin isomer groups produced with good intensity from the alpha decay of ^{218}Ac.

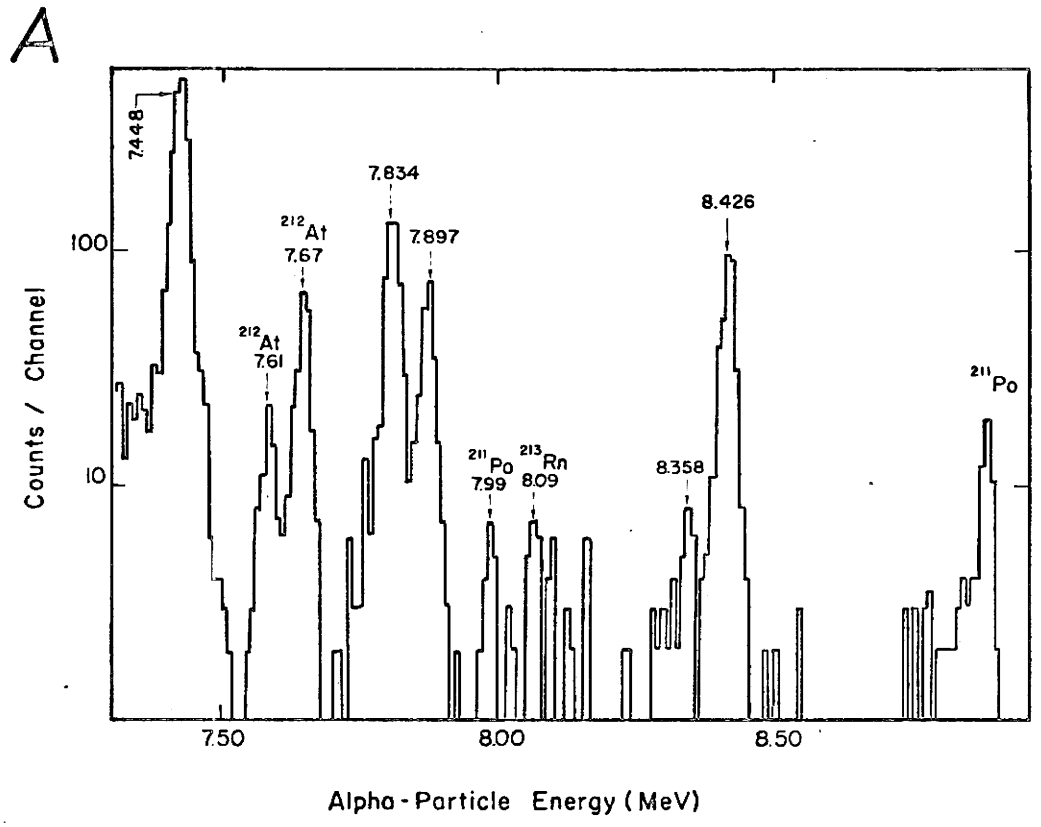
A
7.448
7.834
8.426
212At
7.67
7.897
212At
7.61
211Po
7.99
213Rn
8.09
8.358
211Po
100
10
Counts / Channel
7.50
8.00
8.50
Alpha-Particle Energy (MeV)

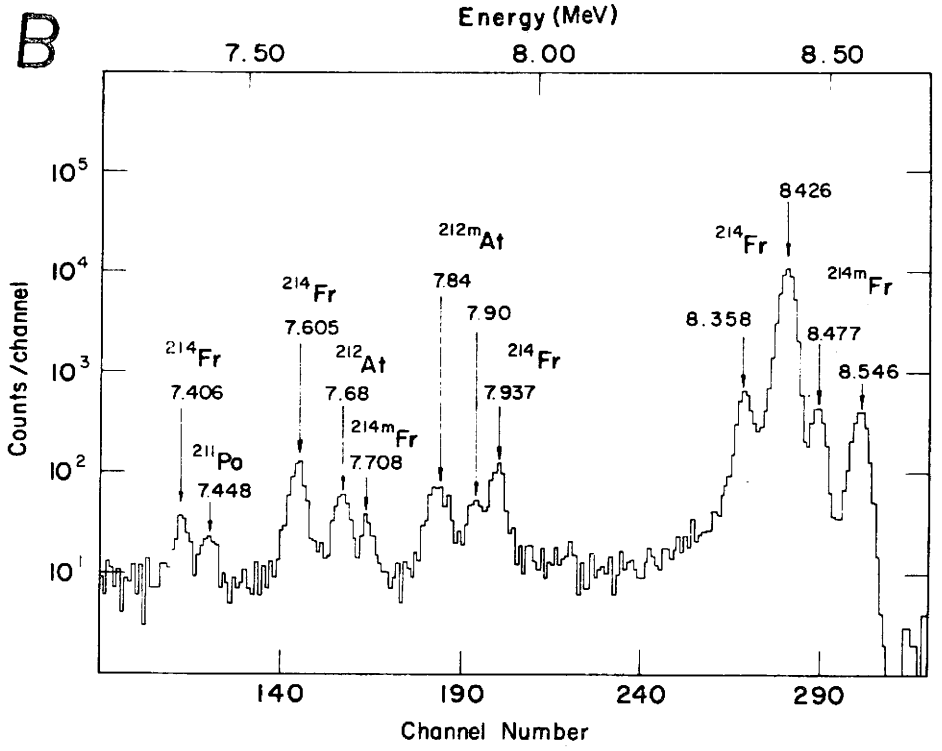
B
Energy (MeV)
7.50
8.00
8.50
10^5
10^4
10^3
10^2
10^1
Counts/channel
214Fr
7.406
211Po
7.448
214Fr
7.605
212At
7.68
214mFr
7.708
212mAt
7.84
7.90
214Fr
7.937
214Fr
8.358
8426
214Fr
214mFr
8.477
8.546
140
190
240
290
Channel Number

This is due to the fact that the ground state of the unknown isotope ^{218}Ac is undoubtably low-J. Using the reaction $^{209}Bi(^{12}C,3n)^{218}Ac$, therefore, it is possible to produce abundant quantities of the ground state groups of ^{214}Fr.

The spectrum of this reaction obtained for 72 MeV ^{12}C ions is shown in figure 10B. In addition to the 2 main ground state transitions, groups at 7.406, 7.605, and 7.937 MeV are observed to have the same excitation function dependence (figure 11) and decay curve chacteristics (figure 12). The half-life of these activities is measured to be 5.0 ± 0.2 msec. It is evident that the 7.406 and 7.937 groups are present with sufficient intensity in the $^{208}Pb(^{11}B,xn)^{219-x}Fr$ spectrum to affect the ^{211}Po and ^{212m}At peaks, but remain unresolved. Furthermore, the slight broadening of the 7.837 MeV ^{212m}At group observed in figure 10B is characteristic of all the $^{209}Bi(^{12}C,3n)^{218}Ac$ spectra studied and is likely due to a ^{214}Fr group of about the same energy. However, it was not possible to resolve this activity in the present work.

3.4 Levels of Francium 214

The alpha particle decay scheme derived from Q - values is shown in figure 13. These results indicate that the decay of ^{214}Fr involves the ground state and an isomeric state at 123 keV excitation. The theoretical work of Kim and Rasmussen[4] on the energy levels of ^{210}Bi, an isotone

FIGURE 11

Excitation functions for the weak ^{214}Fr ground state transitions at 7.406, 7.603, and 7.957 MeV produced in the bombardment of ^{209}Bi with ^{12}C compared to the main ^{214}Fr group at 8.426 MeV. The excitation function for the metastable state transition at 8.546 MeV produced in this reaction is also shown.

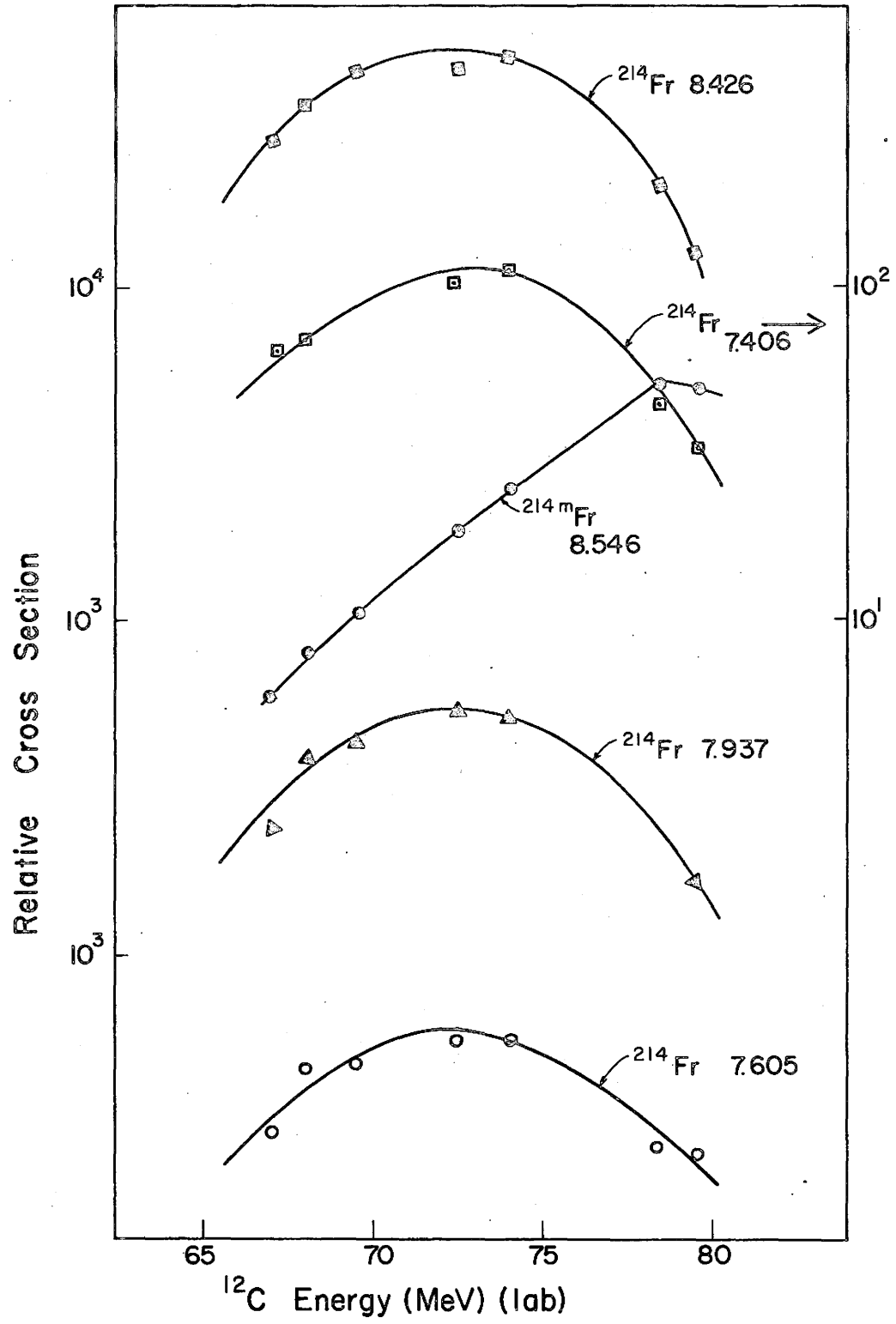
214Fr 8.426
214Fr 7.406
214mFr 8.546
214Fr 7.937
214Fr 7.605
Relative Cross Section
10^4
10^3
10^3
10^2
10^1
65
70
75
80
12C Energy (MeV) (lab)

FIGURE 12

Decay curves measured for the 8.426, 8.358, 7.937, and 7.605 MeV groups associated with the ground state decay of ^{214}Fr. The half-life is 5.0 ± 0.2 msec.

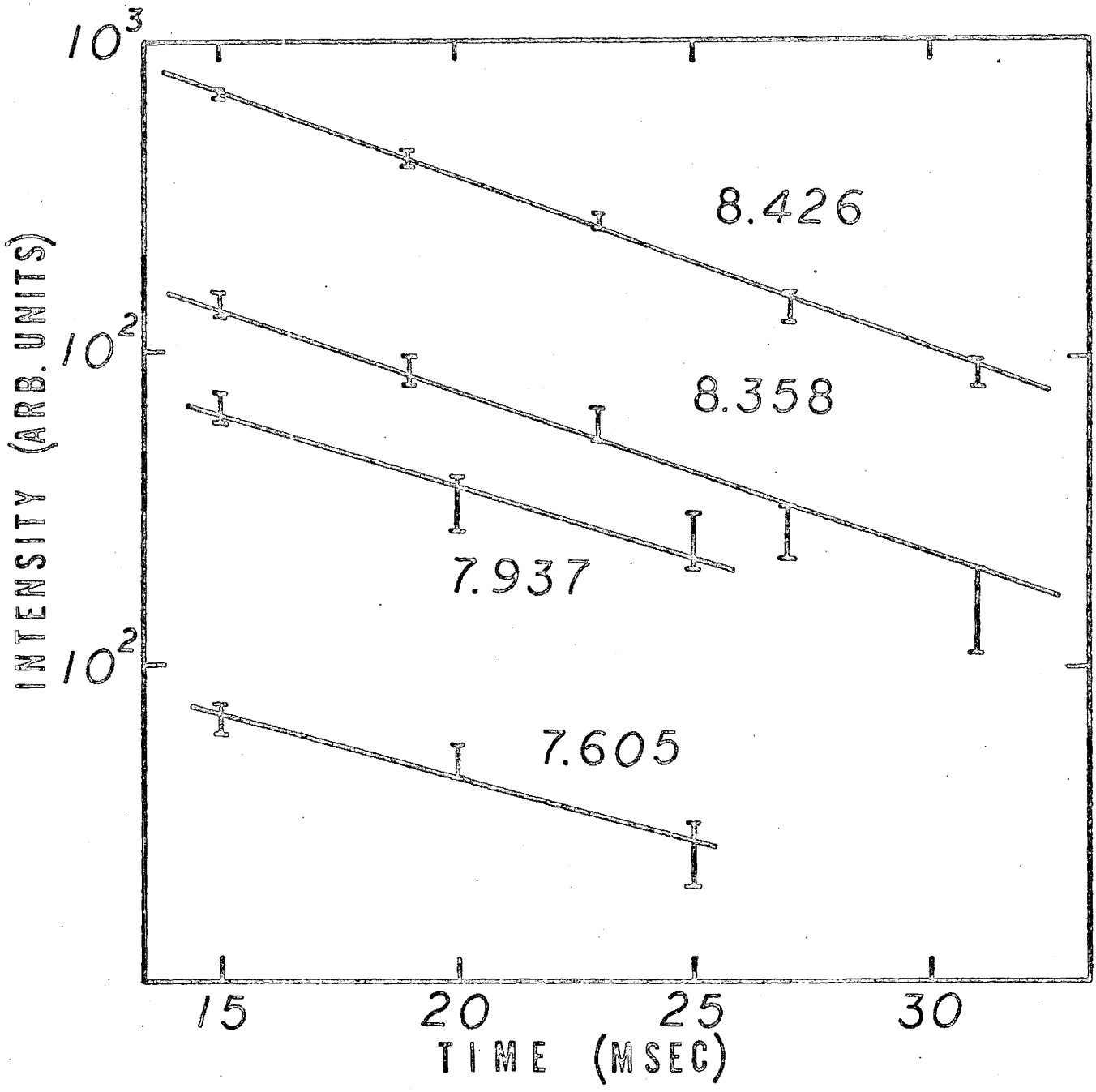
10^3
10^2
10^2
INTENSITY (ARB. UNITS)
8.426
8.358
7.937
7.605
15
20
25
30
TIME (MSEC)

FIGURE 13

Alpha particle decay scheme of the isomers of ^{214}Fr.

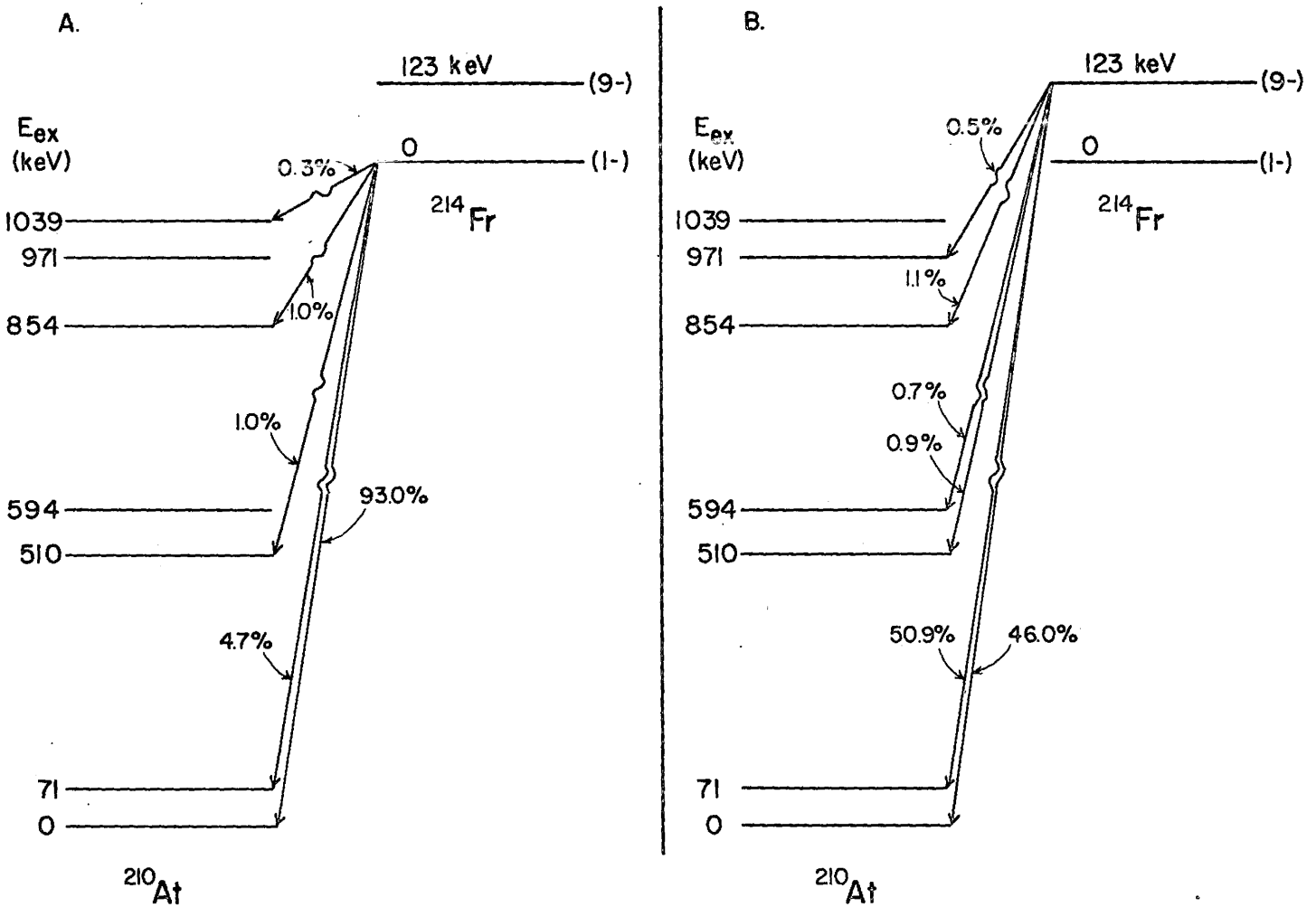
A.
123 keV
(9-)
Eex
(keV)
0
(1-)
0.3%
214Fr
1039
971
1.0%
854
1.0%
594
93.0%
510
4.7%
71
0
210At
B.
123 keV
(9-)
Eex
(keV)
0.5%
0
(1-)
214Fr
1039
971
1.1%
854
0.7%
0.9%
594
510
50.9%
46.0%
71
0
210At

of ^{214}Fr, is particularly relevant in this case. The 2 lowest levels of ^{210}Bi have angular momentum and parity (1-) and (0-) at 0 and 47 keV respectively. Their relative ordering is a consequence of the tensor component in the shell model force. The next level at 268 keV is (9-) and is a long-lived isomeric state. As mentioned earlier, these levels are part of a multiplet arising from the coupling of a $(g_{9/2})(h_{9/2})$ neutron-proton configuration.

The work of Jones[8] on ^{212}At has shown that the essential nature of the neutron-proton force remains when a proton pair is added to ^{210}Bi. Thus, the (1-) level is the ground state in ^{212}At and the (9-) level is lowered to 220 keV.

The present work indicates that the (1-) level is retained as the ground state in ^{214}Fr. Alpha transitions are observed to both the ground and first excited levels of ^{210}At. In the following section it is shown that these states are expected to be (5+) and (4+) respectively. Hence, to conserve parity, the ground state of ^{214}Fr cannot be (0-). It is probable, therefore, that the ground state angular momentum and parity is (1-) and the isomeric state (9-) in analogy with ^{208}Bi and ^{212}At.

3.5 Levels of Astatine 210

The energy levels of ^{210}At are observed to cluster into 3 groups in a manner quite similar to those of its isotone, ^{208}Bi. The levels of this nuclide have been

experimentally characterized by Erskine[5] using (d,t) reaction spectroscopy and theoretically by Kim and Rasmussen[1]. These investigations have some relevance to the levels of ^{210}At.

The neutron-hole, proton-particle configuration of the ground state of ^{208}Bi is predominantly $(p_{1/2})^{-1}(h_{9/2})$ and results in 2 levels coupled to angular momenta (5+) and (4+). The next configuration, $(f_{5/2})^{-1}(h_{9/2})$, produces a quintet of levels having J = 3 - 7 centered around 600 keV plus a J = 2 state at ~950 keV. A quartet of levels, predominantly $(p_{3/2})^{-1}(h_{9/2})$ coupled to J = 3 - 6, is centered about 1.1 MeV.

Figure 14 is a comparison between the levels of ^{208}Bi and the levels of ^{210}At populated in this work. The similarity of the levels is remarkable and indicative of the correlations to be found near the ^{208}Pb closed shell. Included in figure 14 are the states of ^{212}Fr to be discussed in chapter IV.

Spins and parities of the levels of ^{210}At have not been measured, but some information might be deduced from the correspondence between ^{210}At and ^{208}Bi. It is stressed that these assignments are speculative and are not meant to be construed as experimental results.

It is reasonable to assign the ground and first excited states of ^{210}At to spins and parities of (5+) and

FIGURE 14

Energy level structures of the N = 125 isotones. The theoretical and experimental work on ^{208}Bi is compared to the present results for ^{210}At and ^{212}Fr.

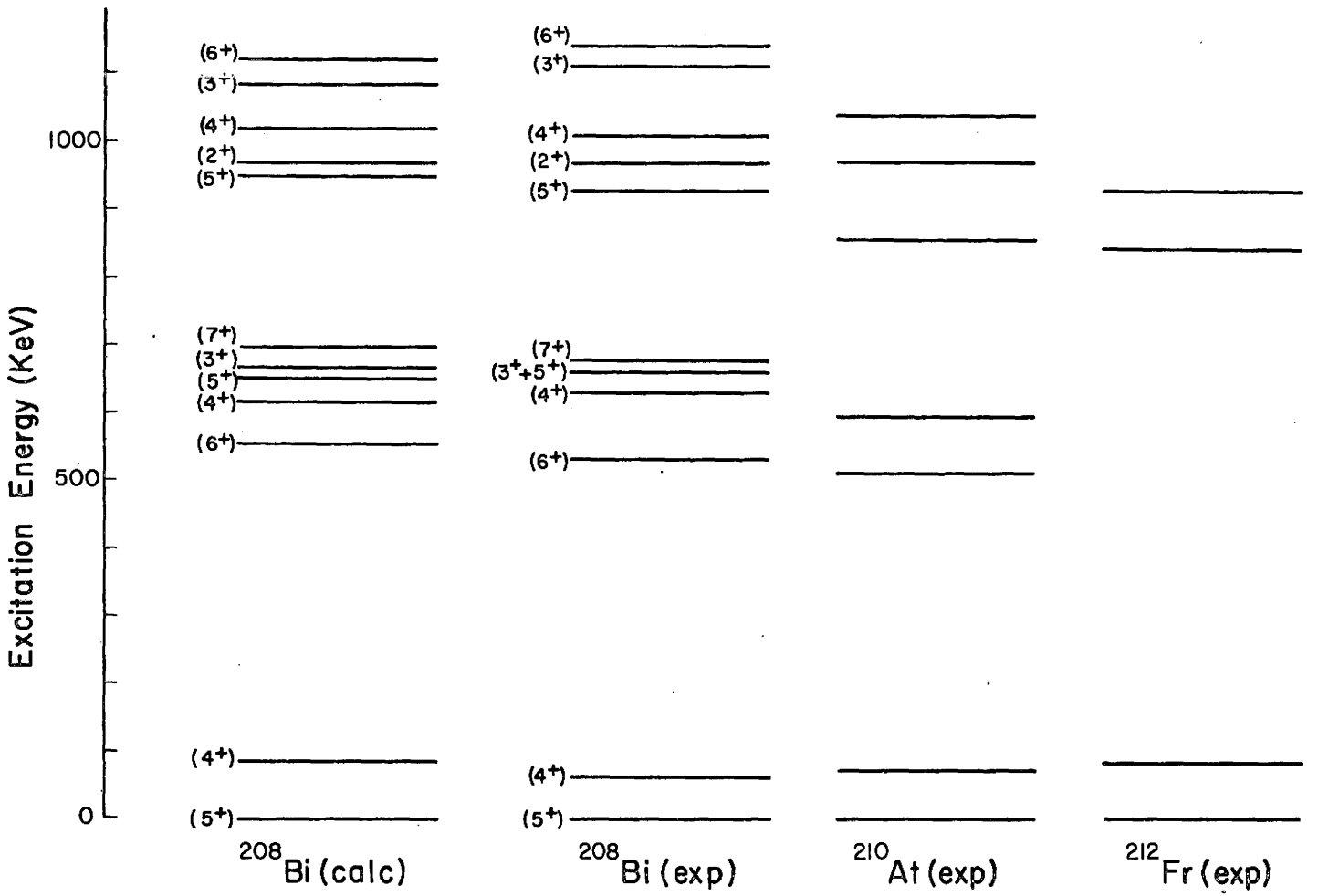
Excitation Energy (KeV)
1000
500
0
(6+)
(3+)
(4+)
(2+)
(5+)
(7+)
(3+)
(5+)
(4+)
(6+)
(4+)
(5+)
208Bi (calc)
(6+)
(3+)
(4+)
(2+)
(5+)
(7+)
(3+ + 5+)
(4+)
(6+)
(4+)
(5+)
208Bi (exp)
210At (exp)
212Fr (exp)

(4+) respectively in direct analogy with ^{208}Bi. Both alpha decaying levels of ^{214}Fr populate these states and L = 3 or 5 transitions will be predominant in both cases.

For the following configuration, both ^{214}Fr states populate the lowest level which is (6+) in ^{208}Bi. The next level in ^{208}Bi is (4+). If the analogous state exists in ^{210}At at 594 keV, one would expect it to be populated by both isomers. It is suspected that the slight broadening observed for the 7.84 MeV ^{212}At group may correspond to a transition from the (1-) state of ^{214}Fr to the 594 level in ^{210}At.

A distinct pattern emerges for the next set of levels arising from the $(p_{3/2})^{-1}(h_{9/2})$ configuration. Both isomers have transitions to the lowest level which would involve L = 5 alpha particles if the state were (5+). The (9-) level appears to exclusively populate the ^{210}At level at 971 keV, while the (1-) isomer exclusively populates the 1039 keV level. It is possible, however, that the (1-) isomer does populate the 971 keV level, since the transition would fall below the ^{211}Po group at 7.45 MeV. This would help to explain the excitation function behavior of the 7.45 MeV peak in the ^{208}Pb + ^{11}B reaction. There is no similar evidence, however, for a (9-) isomer transition to the 1039 keV level.

The above spin and parity considerations for the levels of ^{210}At are useful for the calculation of penetra-

TABLE I

Alpha Groups of Francium 214

^{214}Fr $J\pi$	Energy (MeV)	^{210}At $J\pi$	Level (keV)	%	L	Penetrability	δ^2 (keV)
(1-)	8.426 ± 0.005	(5+)	0	93.0	5	1.03×10^{-15}	5.15
(1-)	8.358 ± 0.005	(4+)	71	4.7	3	2.98×10^{-16}	0.091
(1-)	7.937 ± 0.008	(6+)	510	1.0	5	4.13×10^{-18}	1.39
(1-)	7.605 ± 0.008	(5+)	854	1.0	5	3.87×10^{-19}	14.8
(1-)	7.406 ± 0.008	-	1039	0.3	5	8.63×10^{-20}	19.9
(9-)	8.546 ± 0.005	(5+)	0	46.0	5	2.17×10^{-16}	1.82
(9-)	8.477 ± 0.005	(4+)	71	50.9	5	1.42×10^{-16}	3.08
(9-)	8.046 ± 0.008	(6+)	510	0.9	3	3.92×10^{-17}	0.197
(9-)	7.963 ± 0.008	(4+)	594	0.7	5	4.94×10^{-18}	1.21
(9-)	7.708 ± 0.008	(5+)	854	1.1	5	8.20×10^{-19}	11.5
(9-)	7.594 ± 0.008	-	971	0.5	5	3.56×10^{-19}	12.0

bilities and reduced widths. These are determined from the experimental data using the appropriate equations given in section 1.2-1. A summary of the results obtained for ^{214}Fr is contained in table I, using the lowest allowed alpha particle L-wave in each instance. For those levels for which possible spin and parity assignments could not be made, an L = 5 alpha particle is assumed.

The reduced widths for the alpha decay of ^{214}Fr are a factor of 10 - 1000 smaller than those for neighboring even-even nuclei[14]. This is to be expected since alpha particle formation in nuclei having an odd number of neutrons or protons often involves the splitting of nucleon pairs. The extra energy required for this process decreases the probability of alpha particle clustering, and it has long been recognized that alpha decay involving unpaired nucleons is hindered[58].

CHAPTER IV

ACTINIUM 216 RESULTS

4.1 Introduction

The study of ^{216}Ac and ^{212}Fr is interesting since these nuclei differ from ^{214}Fr and ^{210}At respectively by an additional proton pair in the $h_{9/2}$ shell. It is expected, therefore, that some analogies will exist with the results obtained in chapter III if the extra protons do not significantly alter the neutron-proton force.

Rotter et al.[52] first reported the existence of the alpha particle emitter ^{216}Ac with $E_\alpha = 9.14$ MeV and $t_{1/2} = 0.39$ msec. These results have been extended by Valli and Hyde[57] who have observed 4 alpha groups belonging to ^{216}Ac, produced by bombardment of ^{209}Bi with ^{12}C. This reaction has also been studied in the present work but with improved resolution and counting statistics.

A typical spectrum obtained in this investigation is shown in figure 15. In order to discriminate against the longer-lived ^{214}Fr, data accumulation began at the start of the beam burst and continued for only 3 msec thereafter. The origin of the ^{214}Fr peaks in the $^{209}Bi + ^{12}C$ alpha particle spectrum has been explained in section 3.3. Activity arising from ^{215}Ra is also observed and is due to charged particle emission from the compound nucleus[43].

FIGURE 15

Alpha particle spectrum of ^{216}Ac groups produced by irradiation of ^{209}Bi with 84.5 MeV ^{12}C ions. Data accumulation took place 0 - 3 msec, where time 0 is the beginning of the beam pulse.

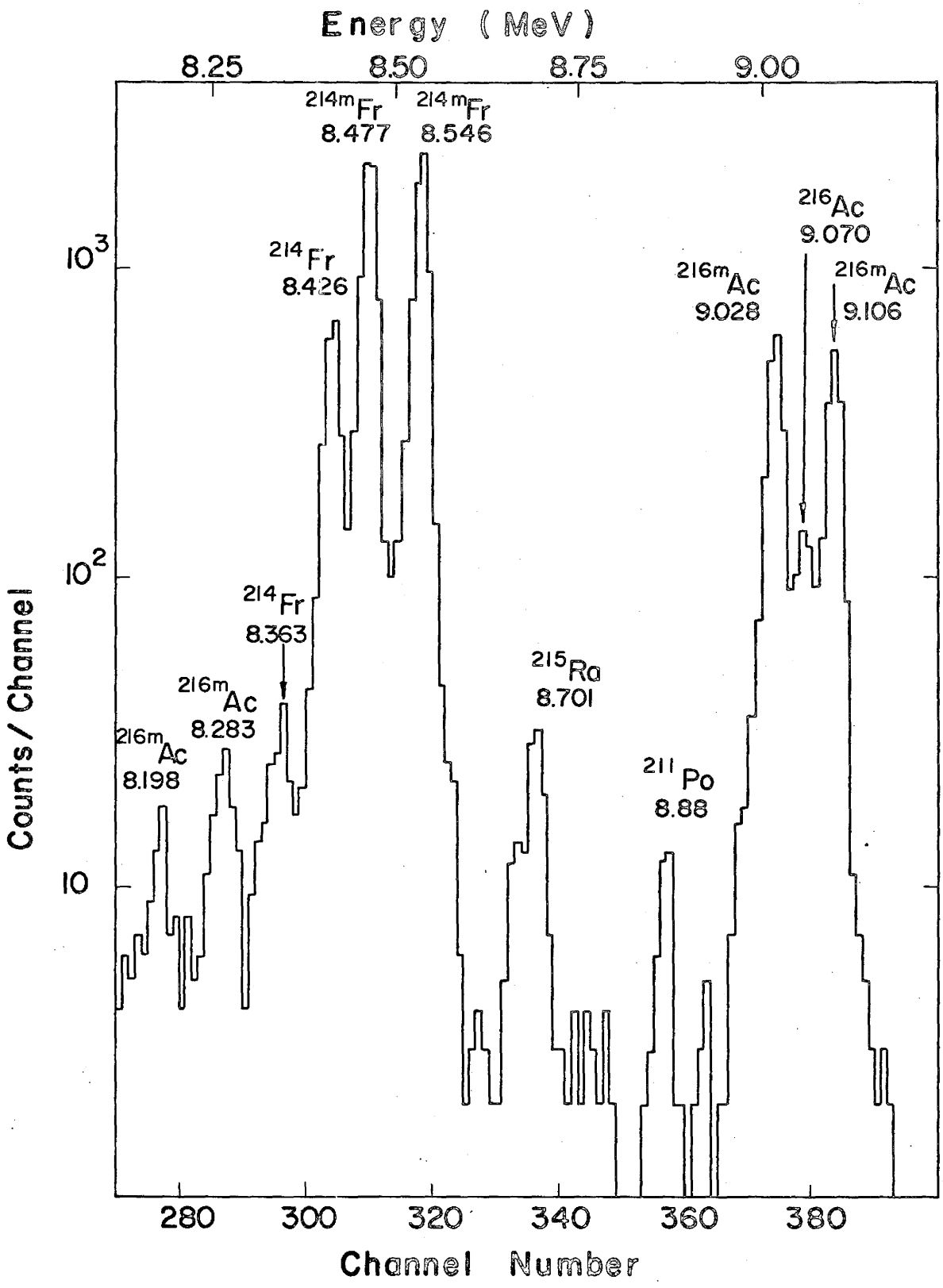
Energy (MeV)
8.25
8.50
8.75
9.00
214m Fr 8.477
214m Fr 8.546
214 Fr 8.426
214 Fr 8.363
216m Ac 8.283
216m Ac 8.198
215 Ra 8.701
211 Po 8.88
216m Ac 9.028
216 Ac 9.070
216m Ac 9.106
10^3
10^2
10
Counts / Channel
280
300
320
340
360
380
Channel Number

This nuclide is to be discussed in chapter V.

As in the case of ^{214}Fr, the alpha groups of ^{216}Ac are observed to originate from 2 different states.

4.2 Metastable State Transitions

Excitation functions measured for the ^{216}Ac alpha transitions are shown in figure 16. The excitation functions of the two main groups at 9.028 and 9.106 MeV are well characterized and are observed to attain a maximum at a ^{12}C energy 12 MeV less than the maximum for ^{215}Ac at 7.602 MeV[59]. Two very weak groups at 8.198 and 8.283 MeV are also observed but comprise less than 5% of the total alpha decay of ^{216}Ac. The relative cross sections for these groups could not be measured at all beam energies due to the domination of the ^{214}Fr peaks. However, the excitation functions appear to follow those of the 9.028 and 9.106 MeV peaks.

Decay curves for the 2 main groups are plotted in figure 17. The half-life of ^{216}Ac is 0.33 ± 0.02 msec. This value has been corrected for the collection time effect since the ^{216}Ac decay curves are within the 8 msec limit described in section 2.4.

4.3 Ground State Transitions

The resolution attained in this work (25 keV, FWHM) was sufficient for the observation of a group at 9.070 ± 0.008 MeV which is assigned to the ground state of ^{216}Ac. The excitation function of this group was measured after meticulously subtracting off the line shape of the 2 main

FIGURE 16

Excitation functions of ^{216}Ac and ^{215}Ac produced in bombardments of ^{209}Bi with ^{12}C.

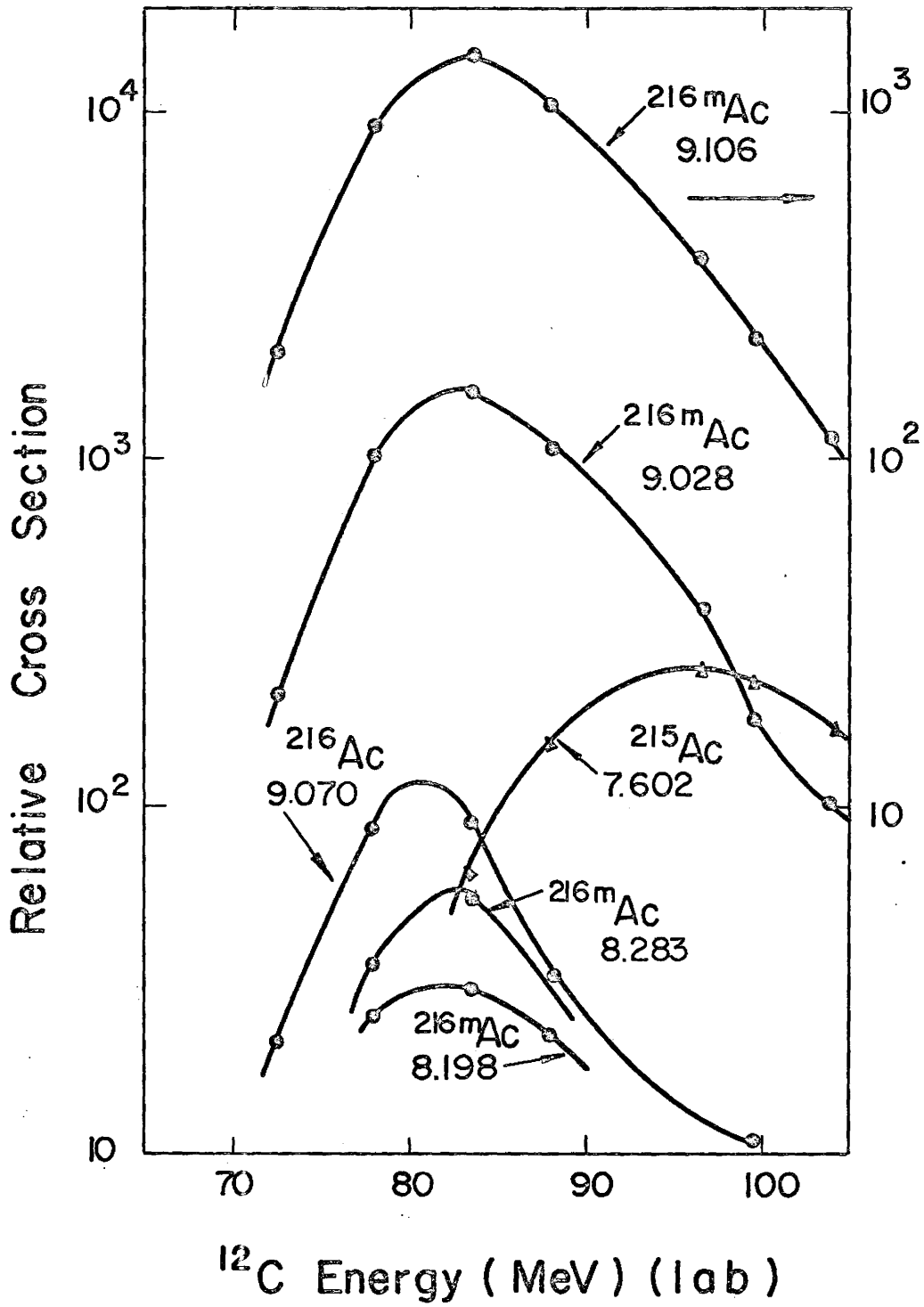
Relative Cross Section
10^4
10^3
10^2
10
10^3
10^2
10
70
80
90
100
^{12}C Energy (MeV) (lab)
^{216m}Ac
9.106
^{216m}Ac
9.028
^{216}Ac
9.070
^{215}Ac
7.602
^{216m}Ac
8.283
^{216m}Ac
8.198

FIGURE 17

Decay curves for the 9.106, 9.028, and 9.070 groups of ^{216}Ac. The half-life is 0.33 ± 0.02 msec.

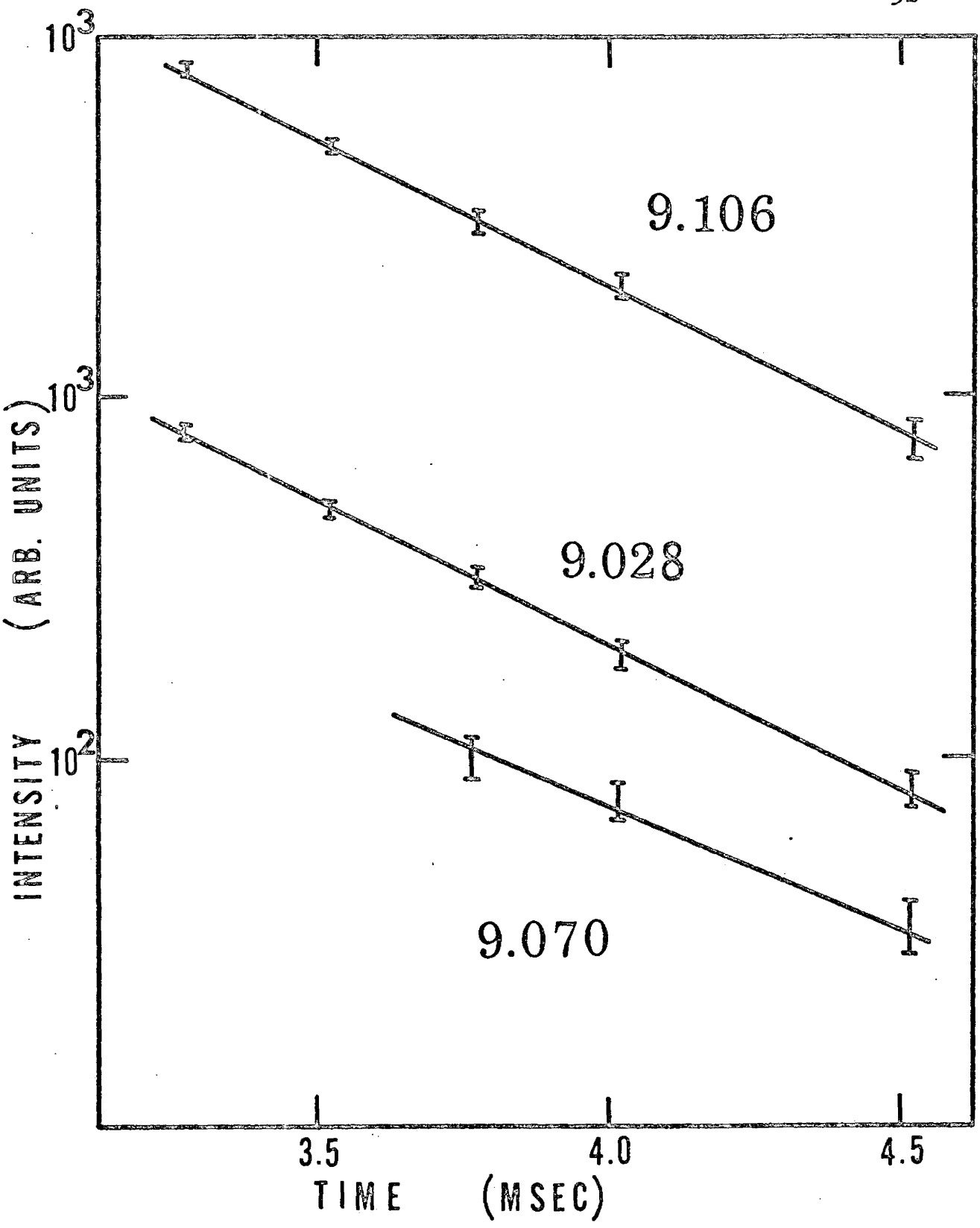
10^3
10^3
10^2
INTENSITY (ARB. UNITS)
9.106
9.028
9.070
3.5
4.0
4.5
TIME (MSEC)

^{216}Ac peaks, and the results are shown in figure 16. It is clear that the relative cross section for the production of this group is displaced to 3 MeV lower excitation relative to the metastable state transitions.

The half-life of the 9.070 MeV group is experimentally the same as that measured for the metastable state transitions. This might be expected, however, since the transition is only 36 keV removed from the 9.106 MeV group; energy change is the dominating factor affecting alpha decay rates.

A weak group at 8.99 $\pm$ 0.02 MeV is observed on the low energy tail of the 9.028 MeV peak, but could not be sufficiently resolved for a meaningful excitation function measurement. Details of the ^{216}Ac transitions between 8.9 and 9.2 MeV are shown in figure 18 for 3 different ^{12}C incident beam energies. On the basis of the alpha decay systematics of the metastable state decay, a group at this energy corresponding to a transition from the ground state is expected. Since no other known alpha transitions at this energy can result from the products formed in this reaction, the 8.99 MeV group is tentatively assigned to the ground state of ^{216}Ac.

4.4 Levels of Actinium 216

Alpha transitions observed in this work for ^{216}Ac are compared to the results of Valli and Hyde[57] in table II. Their assignments, which were tentative, are not consistent

FIGURE 18

Detail of the ^{216}Ac groups between 8.9 and 9.2 MeV at 3 incident ^{12}C energies. The solid line represents the Gaussian line shape calculated from the experimental points.

A. E_b = 88 MeV

B. E_b = 78 MeV

C. E_b = 72.5 MeV

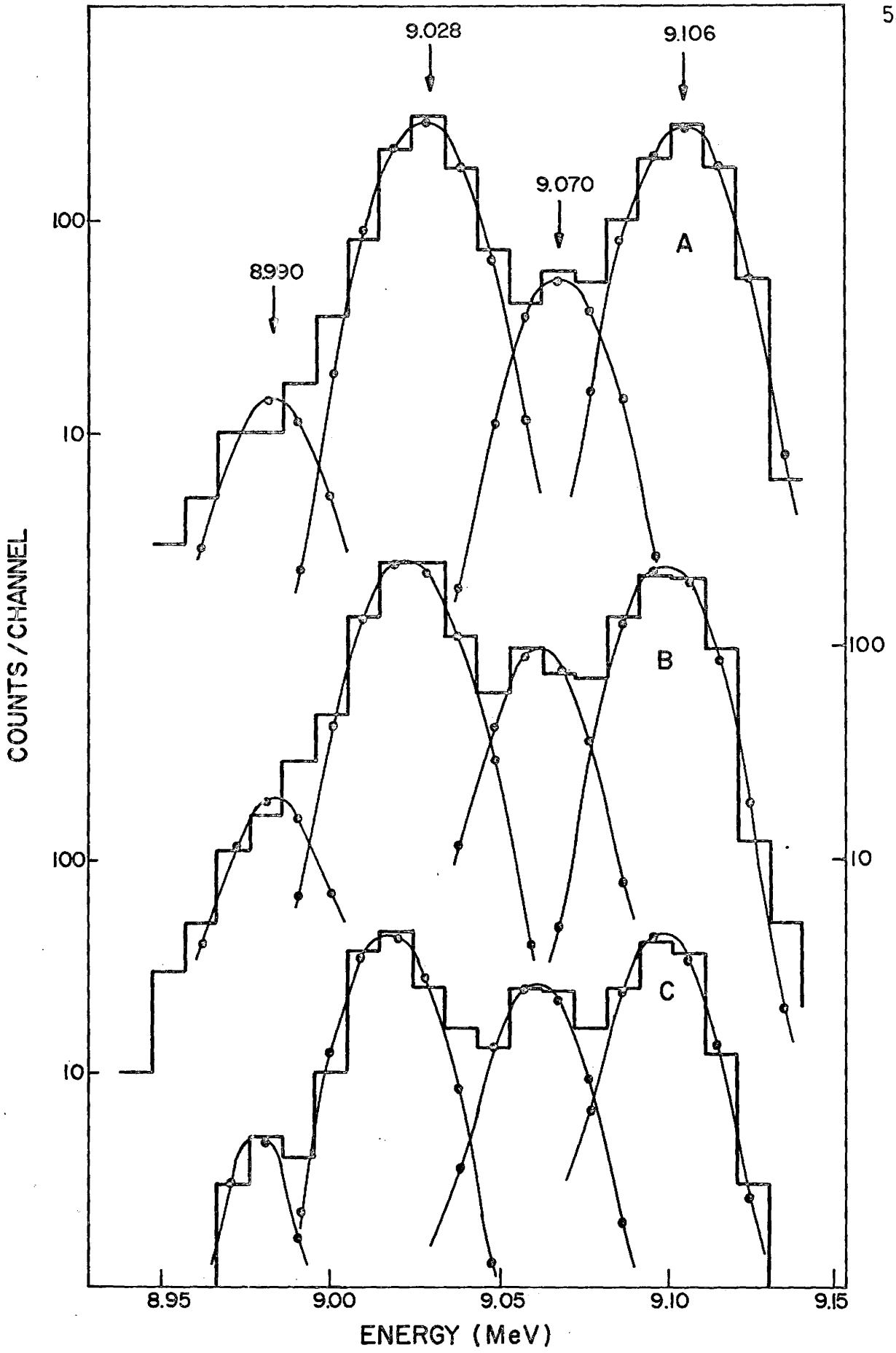
9.028
9.106
9.070
8.930
A
B
C
100
10
100
10
100
10
COUNTS / CHANNEL
8.95
9.00
9.05
9.10
9.15
ENERGY (MeV)

TABLE II

Alpha Groups of Actinium 216

This Work			Valli and Hyde	
Energy (MeV)	%	Assignment*	Energy (MeV)	Assignment*
9.106 ± 0.005	46.2	M	9.105	M
9.028 ± 0.005	49.6	M	9.020	G
8.283 ± 0.008	2.5	M	8.283	M
8.198 ± 0.008	1.7	M	8.198	G
9.070 ± 0.008	~90	G	-	-
(8.99 ± 0.02)	~10	G	-	-

* M = metastable transitions

G = ground state transitions

with the present results. The essential reasons for the discrepancies are as follows. The Valli and Hyde interpretation is based on energy differences only without additional experimental evidence. However, the energy obtained in the present work for the 9.028 MeV group is inconsistent with this conclusion. Furthermore, the definitive result in the present work is the observation of the 9.070 MeV group and the measurement of its excitation function shift. The absence of this effect might cast serious doubt as to the occurrence of isomerism in ^{216}Ac.

It is therefore concluded that the alpha decay of ^{216}Ac is qualitatively similar to that of ^{214}Fr and ^{212}At. Applying the same arguments as in the case of ^{214}Fr, a spin and parity (1-) is assigned to the ground state of ^{216}Ac, and (9-) to a metastable state at 37 keV excitation. A decay scheme consistent with the experimental information is presented in figure 19.

4.5 Levels of Francium 212

The decay of ^{216}Ac populates 4 levels in ^{212}Fr. From these results, it can be argued that the levels of ^{212}Fr exhibit the same characteristics observed in ^{208}Bi and ^{210}At. A comparison of the levels of the 125 isotones is made in figure 14. The first 2 states of ^{212}Fr likely arise from the $(p_{1/2})^{-1}(h_{9/2})$ configuration coupled to angular momenta (5+) and (4+).

FIGURE 19

Alpha particle decay scheme of the isomers of ^{216}Ac.

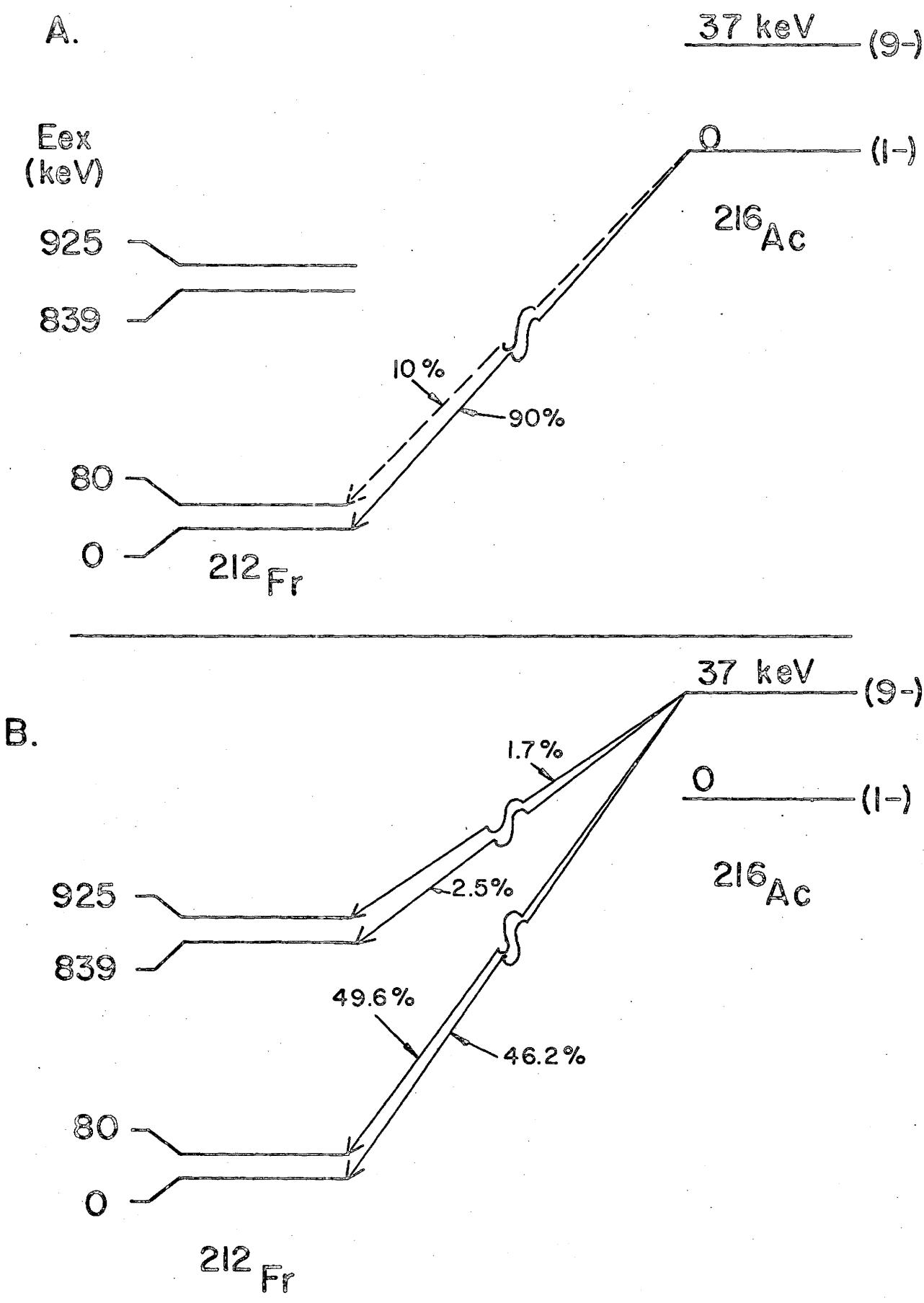
A.
37 keV
(9-)
Eex
(keV)
0
(1-)
925
839
216Ac
10%
90%
80
0
212Fr
B.
37 keV
(9-)
1.7%
0
(1-)
216Ac
925
2.5%
839
49.6%
46.2%
80
0
212Fr

The states arising from the $(f_{5/2})^{-1}(h_{9/2})$ configuration are notably absent in the level scheme of ^{212}Fr. Transitions to these levels would correspond to alpha particle energies of approximately 8.5 MeV. The presence of the relatively intense ^{214}Fr groups in this region, however, would effectively prevent the detection of these transitions.

The next configuration, predominantly $(p_{3/2})^{-1}(h_{9/2})$, would yield levels from roughly 800 to 1200 keV. It is felt that the levels at 839 and 925 keV constitute members of this multiplet. This interpretation is consistent with the alpha decay of ^{214}Fr in which it is found that the high spin isomer populates 2 levels of the $(p_{3/2})^{-1}(h_{9/2})$ configuration at 854 and 971 keV in ^{210}At. To the degree that similarities exist between ^{210}At and ^{212}Fr, it is expected that the metastable state of ^{216}Ac would populate the same members of this multiplet.

These considerations are summarized in table III. The predicted angular momentum assignments for the levels of ^{212}Fr are used to calculate WKB penetrabilities and experimental reduced widths. For these calculations, the lowest L-wave alpha particle transition is used in each case. An examination of table III reveals that the reduced widths exhibit fluctuations similar to those observed for ^{214}Fr. This point will be further considered in chapter VII.

TABLE III

Reduced Widths and Penetrabilities of Actinium 216

^{216}Ac $J\pi$	Energy (MeV)	^{212}Fr $J\pi$	L	Level (keV)	Penetrability	δ^2 (keV)
(9-)	9.106	(5+)	5	0	1.37×10^{-15}	2.54
(9-)	9.028	(4+)	5	80	8.77×10^{-16}	4.27
(9-)	8.283	(5+)	5	839	8.86×10^{-18}	21.3
(9-)	8.198	—	5	925	5.03×10^{-18}	25.4
(1-)	9.070	(5+)	5	0	1.03×10^{-15}	6.42
(1-)	(8.99)	(4+)	3	80	2.80×10^{-15}	0.263

CHAPTER V

RADIUM 215 RESULTS

5.1 Introduction

The even-odd 127 isotone ^{215}Ra was first reported by Griffioen and Macfarlane[51] to have an alpha-energy of 8.7 MeV and a half-life of 1.6 msec.

The ground state of ^{215}Ra involves a single $2g_{9/2}$ neutron in the presence of 3 proton pairs and the inert ^{208}Pb core. Isomerism is not expected in this case since the low energy states are thought to be perturbed shell model levels, which in this region do not involve spin changes great enough to hinder gamma emission. The even-odd 127 isotone ^{211}Po, however, emits alpha particles from its ground state (9/2+) and from a metastable level (25/2+) at about 1.5 MeV excitation[60]. Since there is reason to believe that some regularity exists in the energy levels of this region, a metastable state in ^{215}Ra at about the same excitation is possible. However, the decay energy involved in this instance would be approximately 10 MeV. A state emitting an alpha particle of this energy is expected to have a half-life of only a few microseconds, which is well beyond the capability of the helium jet recoil method at this time.

The alpha decay daughter of ^{215}Ra is ^{211}Rn. In terms of the shell model, the ground state of this nuclide consists of a $3p_{1/2}$ neutron hole plus 2 proton pairs. The low-lying energy levels of ^{211}Rn, therefore, are expected to exhibit the properties of a single neutron hole state in ^{208}Pb perturbed by proton pairs.

Subsequent studies of ^{215}Ra have reproduced the results of Griffioen and Macfarlane, but have not revealed the more detailed nature of its decay[52,59]. New data has recently been reported by Valli and Hyde[57], however, that parallels the results presented here.

An alpha particle spectrum (for 7-9 MeV alpha groups) of the products resulting from the bombardment of a 4 mg/cm^2 target of ^{209}Bi with 68 MeV ^{11}B ions is shown in figure 20. The compound nucleus for this reaction is ^{220}Ra*. In addition to radium groups, alpha activity from ^{211}Po, ^{212}At, ^{214}Fr, and ^{213}Rn is observed in the spectrum.

As in the case of the ^{208}Pb(^{11}B,xn) $^{219-x}$Fr reaction, most of the Po and At groups originated from multi-nucleon transfer processes or by charged particle emission from the compound nucleus. Much of the ground state ^{214}Fr, however, resulted from the electron capture decay of ^{214}Ra, which has been discussed in chapter III.

The ^{213}Rn group at 8.090 MeV[54] is produced as the alpha decay daughter of ^{217}Ra which decayed before reaching the detector. This nuclide has been detected[10,11], however,

FIGURE 20

Alpha particle spectrum of the products resulting from the bombardment of ^{209}Bi with 68 MeV ^{11}B ions.

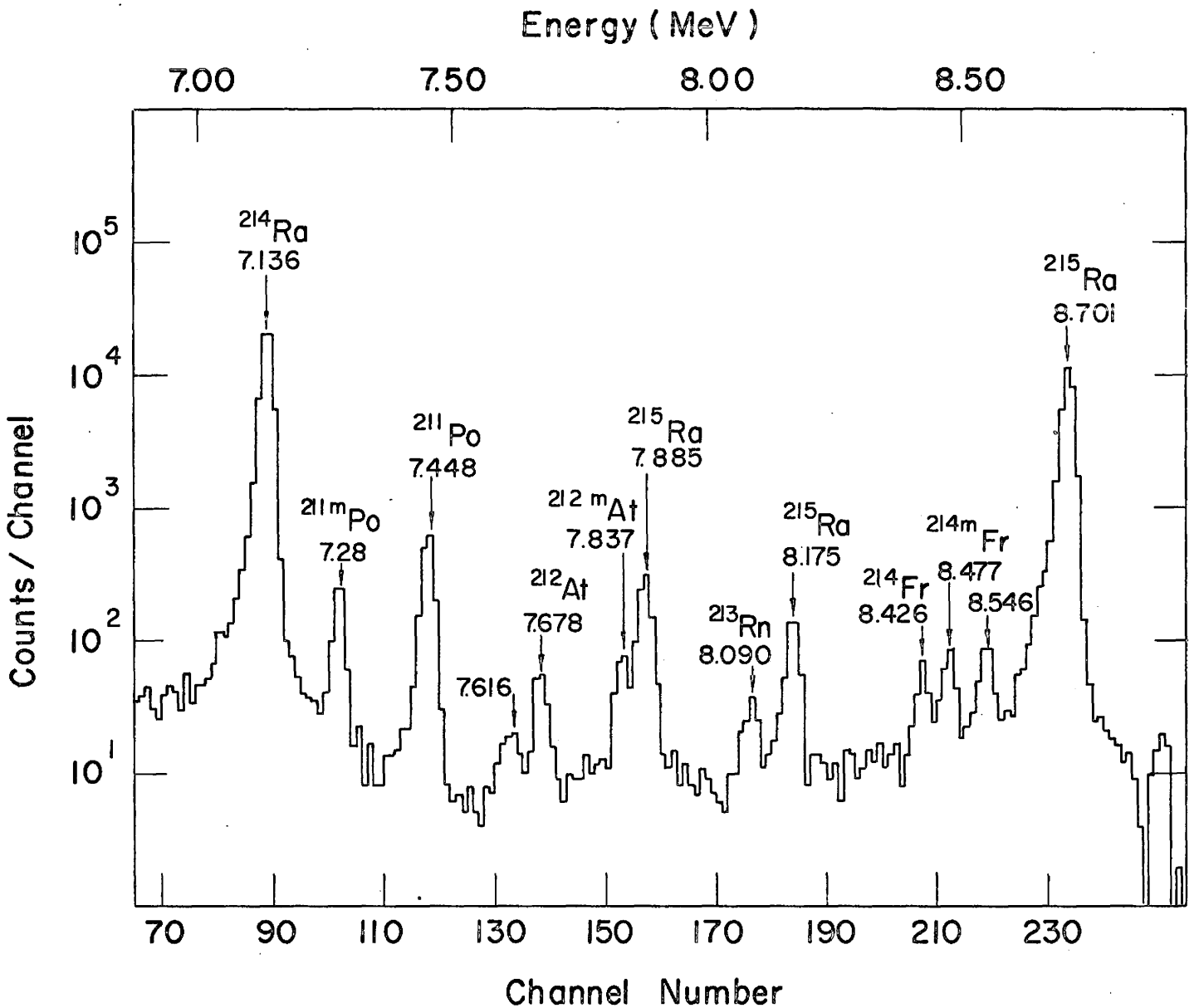
Energy (MeV)
7.00
7.50
8.00
8.50
Counts / Channel
10^5
10^4
10^3
10^2
10^1
^{214}Ra
7.136
^{211m}Po
7.28
^{211}Po
7.448
7.616
^{212}At
7.678
^{212m}At
7.837
^{215}Ra
7.885
^{213}Rn
8.090
^{215}Ra
8.175
^{214}Fr
8.426
^{214m}Fr
8.477
8.546
^{215}Ra
8.701
70
90
110
130
150
170
190
210
230
Channel Number

in bombardments of ^{208}Pb targets with ^{16}O. These results are discussed in section 6.1.

5.2 Radium 215 Alpha Transitions

Three ^{215}Ra alpha groups are observed at energies of 8.701, 8.175, and 7.885 MeV. Excitation functions of the ^{215}Ra activities and of ^{214}Ra have been measured and are summarized in figure 21. The ^{215}Ra groups peaked at an excitation energy 11 MeV lower then ^{214}Ra, which was consistent with their assignment.

The measured decay curves for ^{215}Ra are shown in figure 22. From these determinations, the half-life of ^{215}Ra is 1.56 ± 0.10 msec. The group at 7.885 MeV appeared to have a half-life closer to 1.3 ± 0.2 msec, but this result was in experimental agreement with the other ^{215}Ra activities.

Valli and Hyde[57] have also observed 3 alpha activities belonging to ^{215}Ra. Their results are compared to the energies measured in the present work in table IV. Slight discrepancies exist, possibly due to the larger counting statistics attained in the present work.

5.3 Levels of Radon 211

The ^{211}Rn states populated in this work are shown in figure 23 and are compared to the first 3 levels in ^{207}Pb which correspond to neutron hole states in the ^{208}Pb core. From these results it is apparent that the lowest states of

FIGURE 21

Excitation functions for ^{215}Ra and ^{214}Ra produced from the reaction $^{209}Bi + ^{11}B$.

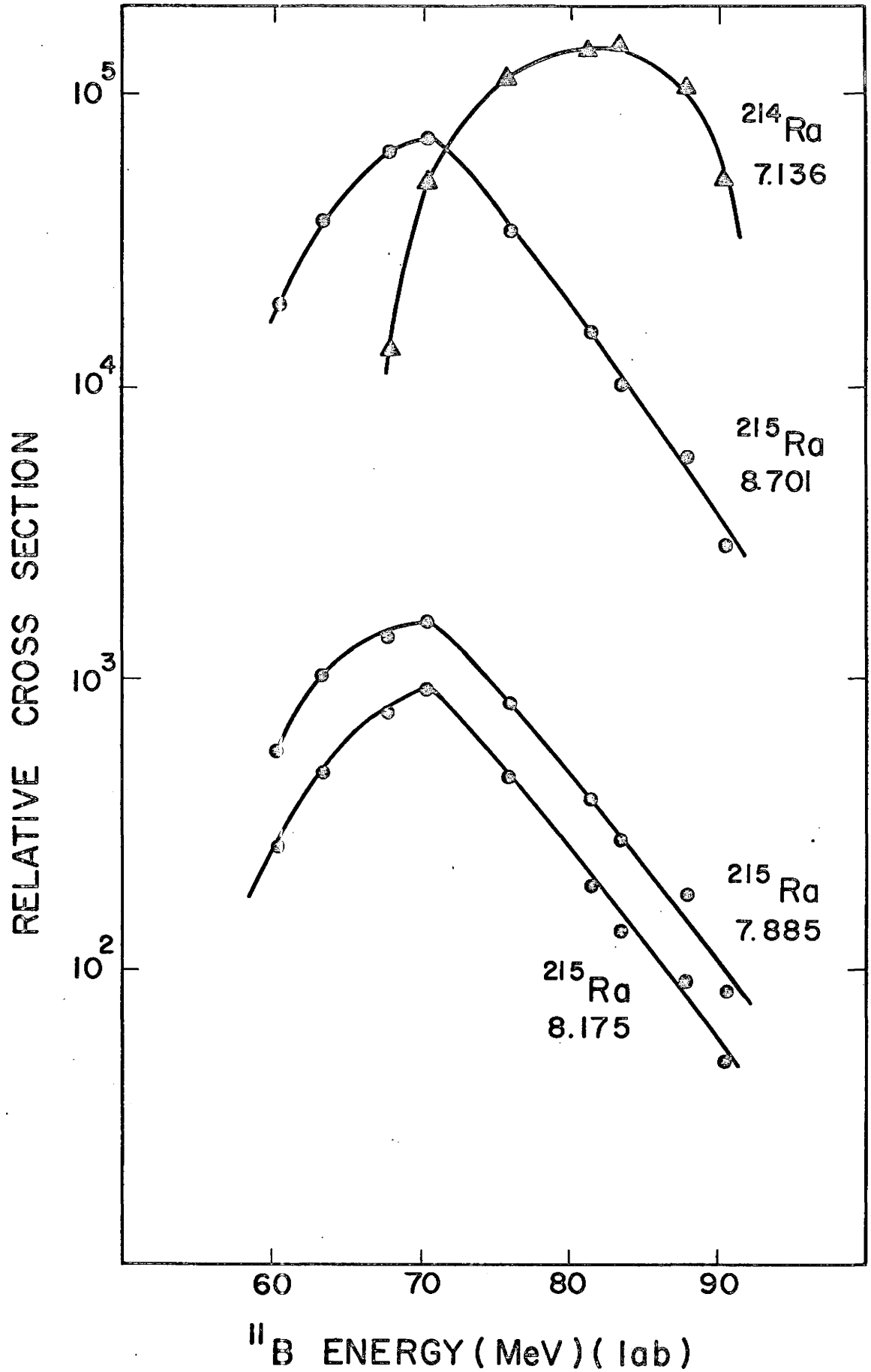
RELATIVE CROSS SECTION
10^5
10^4
10^3
10^2
^{214}Ra
7.136
^{215}Ra
8.701
^{215}Ra
7.885
^{215}Ra
8.175
60
70
80
90
^{11}B ENERGY (MeV) (lab)

FIGURE 22

Decay curves for ^{215}Ra activities. Half-life = 1.56 ± 0.03 msec.

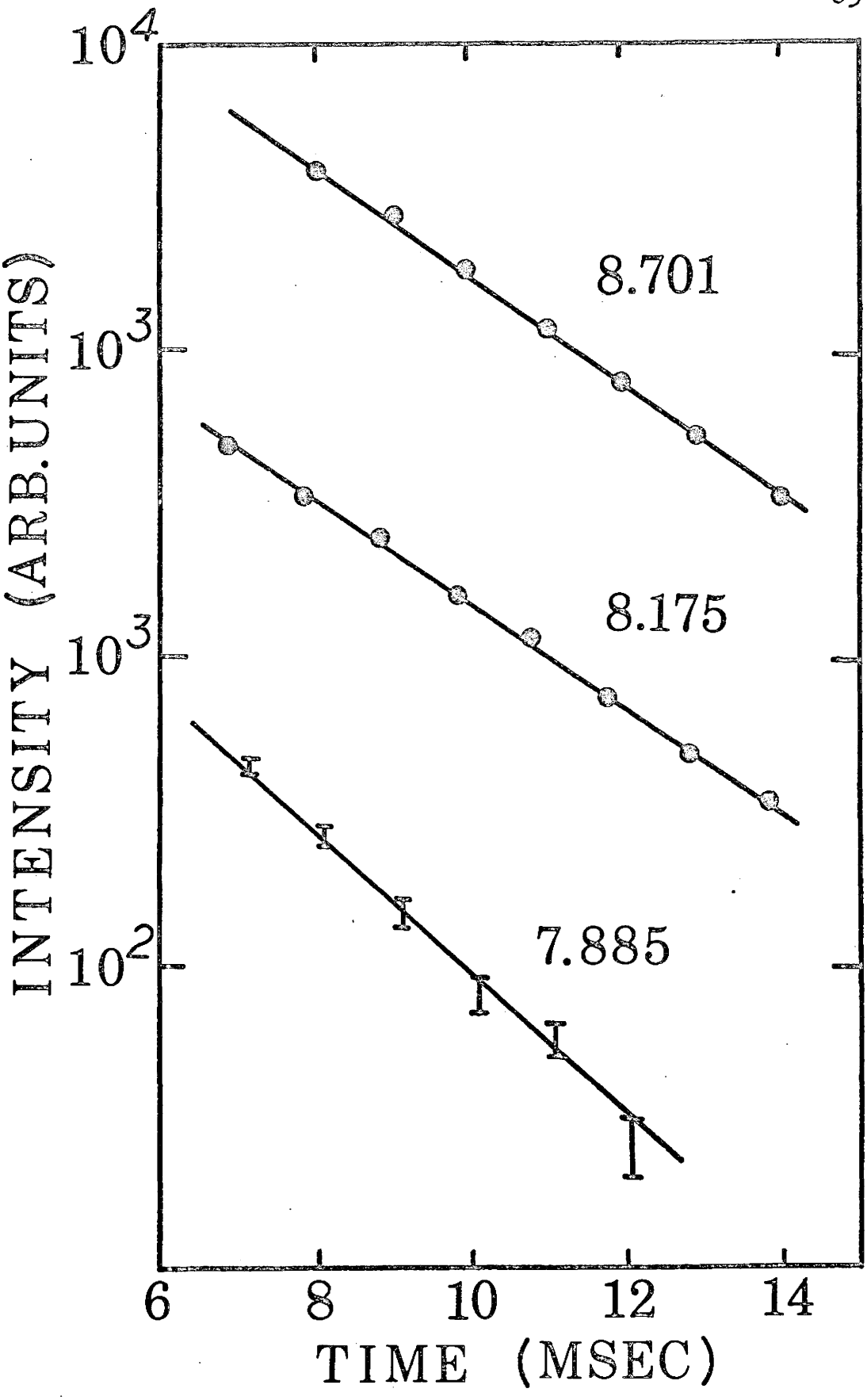
10^4
10^3
10^3
10^2
INTENSITY (ARB.UNITS)
8.701
8.175
7.885
6
8
10
12
14
TIME (MSEC)

FIGURE 23

Alpha decay scheme of ^{215}Ra. The low-lying levels of ^{211}Rn are compared to those of ^{207}Pb.

TABLE IV

Alpha Groups of Radium 215

This Work					Valli and Hyde
E_α MeV	Int %	Level in ^{211}Rn (keV)	Probable $J\pi$	δ^2 (keV)	E_α (MeV)
8.701 ± 0.005	96.0	0	(1/2-)	6.9	8.698 ± 0.005
8.175 ± 0.008	1.4	536	(5/2-)	0.63	8.168 ± 0.008
7.885 ± 0.008	2.6	832	(3/2-)	8.6	7.880 ± 0.008

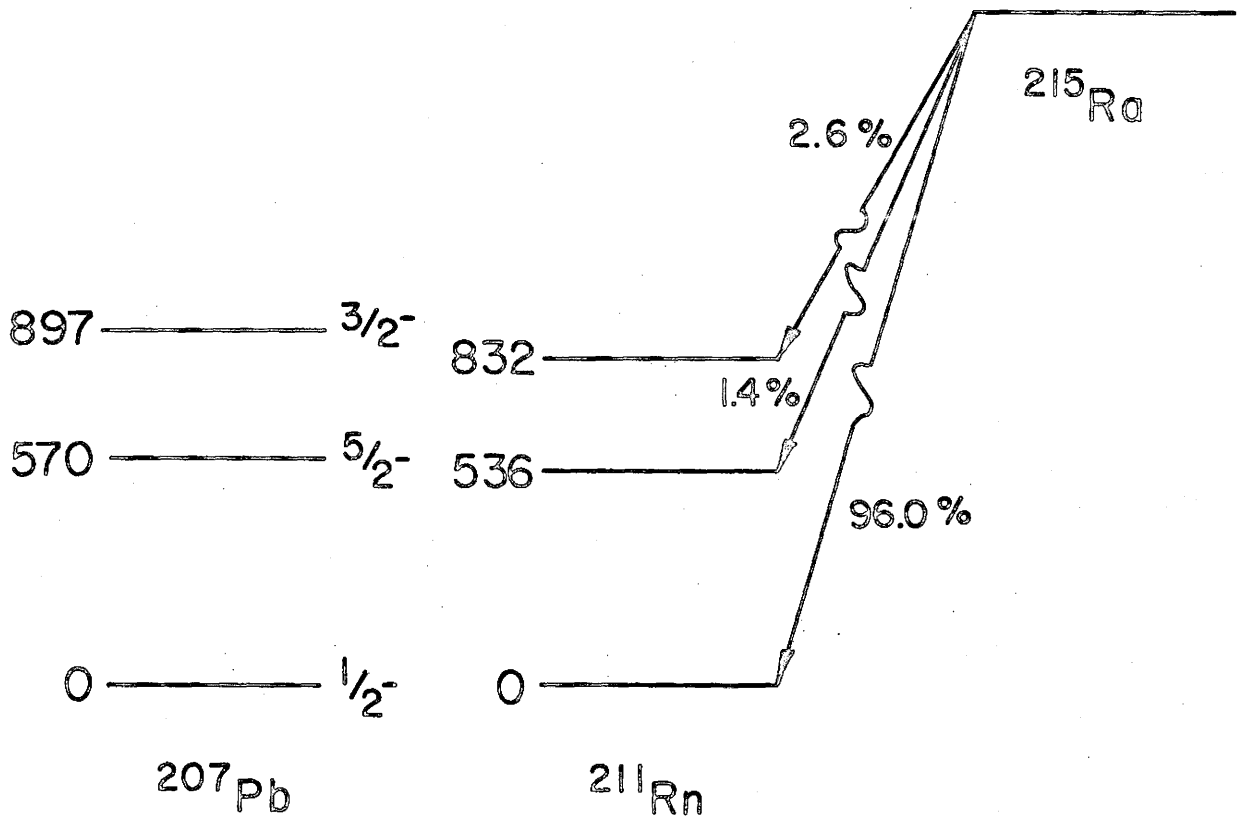
897
3/2-
570
5/2-
0
1/2-
207Pb
832
536
0
211Rn
215Ra
2.6%
1.4%
96.0%

^{211}Rn retain much of their single particle character. The effect of the 4 protons in the $h_{9/2}$ shell is to perturb the energy spacings to lower values, and could be a consequence of core polarization.

The transition to the ground state of ^{211}Rn accounts for 96% of the total decay of ^{215}Ra. The large branching ratio is an example of the importance of the energy factor on alpha decay rates since the single particle spacings are relatively large in this region. The branching to the 0.83 MeV level, however, is 2.6% compared with the 1.4% branching to the 0.54 MeV state. The reason for this apparent reversal must be due to the size of the relative matrix elements for alpha decay, since L = 3 transitions are involved in both cases.

Experimental alpha reduced widths, δ^2, have been calculated for the observed transitions using angular momentum values for the levels of ^{211}Rn in analogy with those of ^{207}Pb. For these calculations, it was assumed that the ground state of ^{215}Ra was (9/2+) as predicted by the shell model. The results are presented in table IV.

The reduced width represents the nuclear effect on alpha decay and depends on the size of the matrix element between the two states. It is clear from these calculations, therefore, that the branching to the 0.54 MeV level is hindered with respect to the other two transitions.

Since the levels of ^{211}Rn appear to be predominantly single particle states, one expects the shell model theory of alpha decay to be applicable to the observed transitions. These results will be discussed in section 7.2.

CHAPTER VI

NEW ISOTOPE RESULTS

6.1 Introduction

It is estimated that less than 50% of the isotopes existing between the limits of nucleon stability have been synthesized and studied. Investigations of unknown nuclides, therefore, are both inherently interesting and necessary to further the understanding of nuclear structure.

There are few experimental techniques capable of directly detecting new isotopes having half-lives in the millisecond region; there are virtually no methods for the satisfactory detection of microsecond activity. The latter problem can be circumvented, however, by the careful study of alpha decay chains in which a relatively long-lived parent nuclide is used to populate the levels of a relatively short-lived daughter. The parent-daughter relationship can then be established on the basis of excitation function and decay curve data.

An alpha particle spectrum for the products resulting from the irradiation of ^{208}Pb targets with ^{16}O ions is shown in figure 24. Four new isotopes are identified from the study of this reaction: ^{222}Th, ^{221}Th, ^{218}Ra and ^{217}Ra. Unpublished results of Macfarlane and Griffioen[67] suggest that ^{217}Ra may be an alpha emitter of energy ~9.0 MeV.

FIGURE 24

Alpha particle spectrum of the products resulting from the irradiation of ^{208}Pb with 84.5 MeV ^{16}O ions.

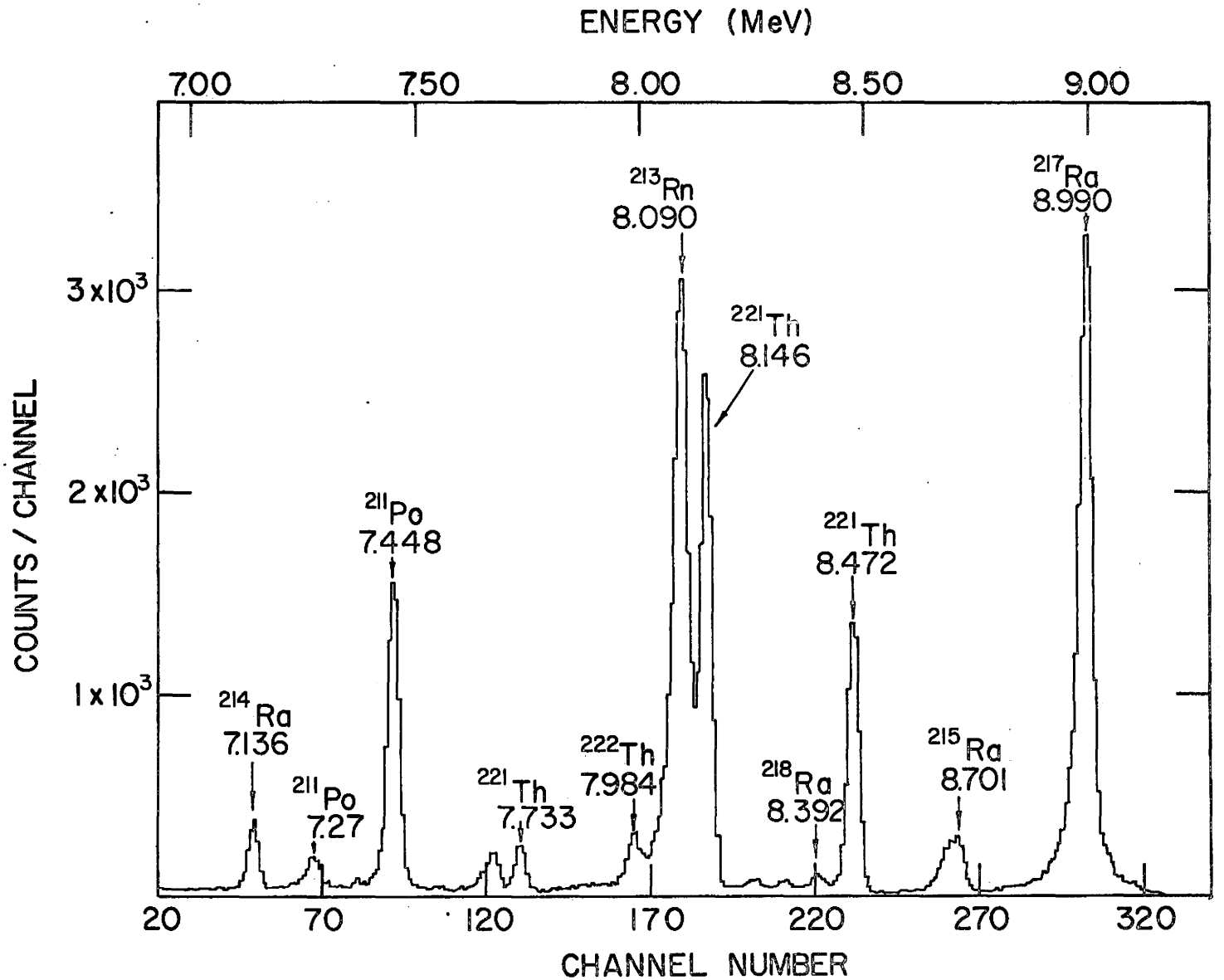
ENERGY (MeV)
7.00
7.50
8.00
8.50
9.00
COUNTS / CHANNEL
3x10³
2x10³
1x10³
214 Ra 7.136
211 Po 7.27
211 Po 7.448
221 Th 7.733
222 Th 7.984
213 Rn 8.090
221 Th 8.146
218 Ra 8.392
221 Th 8.472
215 Ra 8.701
217 Ra 8.990
20
70
120
170
220
270
320
CHANNEL NUMBER

6.2 Thorium 221 and Radium 217

The most prominant groups in the spectrum shown in figure 24 are those belonging to the ^{221}Th alpha decay chain:

$$^{208}Pb(^{16}O,3n)^{221}Th \longrightarrow ^{217}Ra \longrightarrow ^{213}Rn \longrightarrow ^{209}Po$$

Identification of the new isotopes ^{221}Th and ^{217}Ra is based on predicted energies from alpha decay systematics[37], decay curve data, and by the correlation of relative cross section data.

Excitation functions for the products of interest resulting from the $^{208}Pb + ^{16}O$ reaction are plotted in figure 25. Activities at 8.990, 8.472, 8.146, and 7.733 MeV are observed to have the same yield-energy dependence as the known alpha group of ^{213}Rn (E_α = 8.090 MeV, $t_{1/2}$ = 19 msec)[54] and can therefore be assigned to the ^{221}Th decay chain.

Decay curves for these groups have been measured by the procedures outlined in section 2.4 and are shown in figure 26. All 4 groups exhibit the same apparent half-life which must be that of the parent ^{221}Th, 1.7 $\pm$ 0.2 msec. However, ^{217}Ra, predicted from alpha decay trends to have $E_\alpha \sim 9$ MeV and $t_{1/2} < 10$ μsec, is expected to be in the spectrum. This is the 8.990 $\pm$ 0.008 MeV group whose decay curve relative to the machine pulse (described in section 2.4) follows that of the much longer-lived parent ^{221}Th.

In principle, one or more of the groups at 8.472, 8.146, and 7.733 MeV could correspond to an alpha transition

FIGURE 25

Excitation functions measured for ^{222}Th, ^{221}Th, ^{218}Ra and ^{217}Ra groups produced in the reaction $^{208}Pb + ^{16}O$.

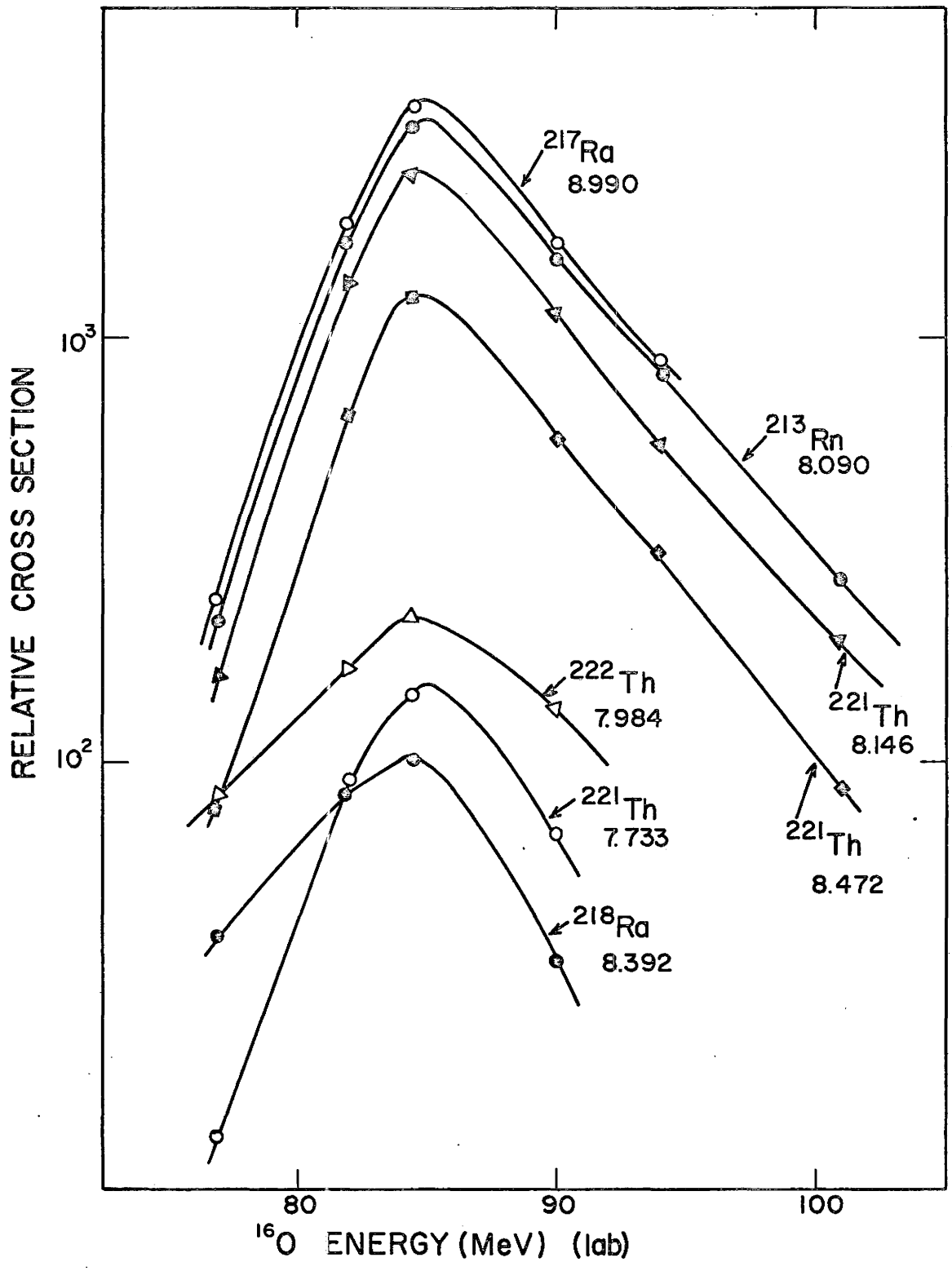
RELATIVE CROSS SECTION
10^3
10^2
^{217}Ra
8.990
^{213}Rn
8.090
^{221}Th
8.146
^{222}Th
7.984
^{221}Th
7.733
^{221}Th
8.472
^{218}Ra
8.392
80
90
100
^{16}O ENERGY (MeV) (lab)

FIGURE 26

Decay curves of ^{222}Th and ^{221}Th. The short-lived ^{217}Ra at 8.990 MeV Decays away with the same half-life of the parent ^{221}Th

$^{222}Th\ t_{1/2} = 4.0 \pm 0.6$ msec

$^{221}Th\ t_{1/2} = 1.7 \pm 0.2$ msec

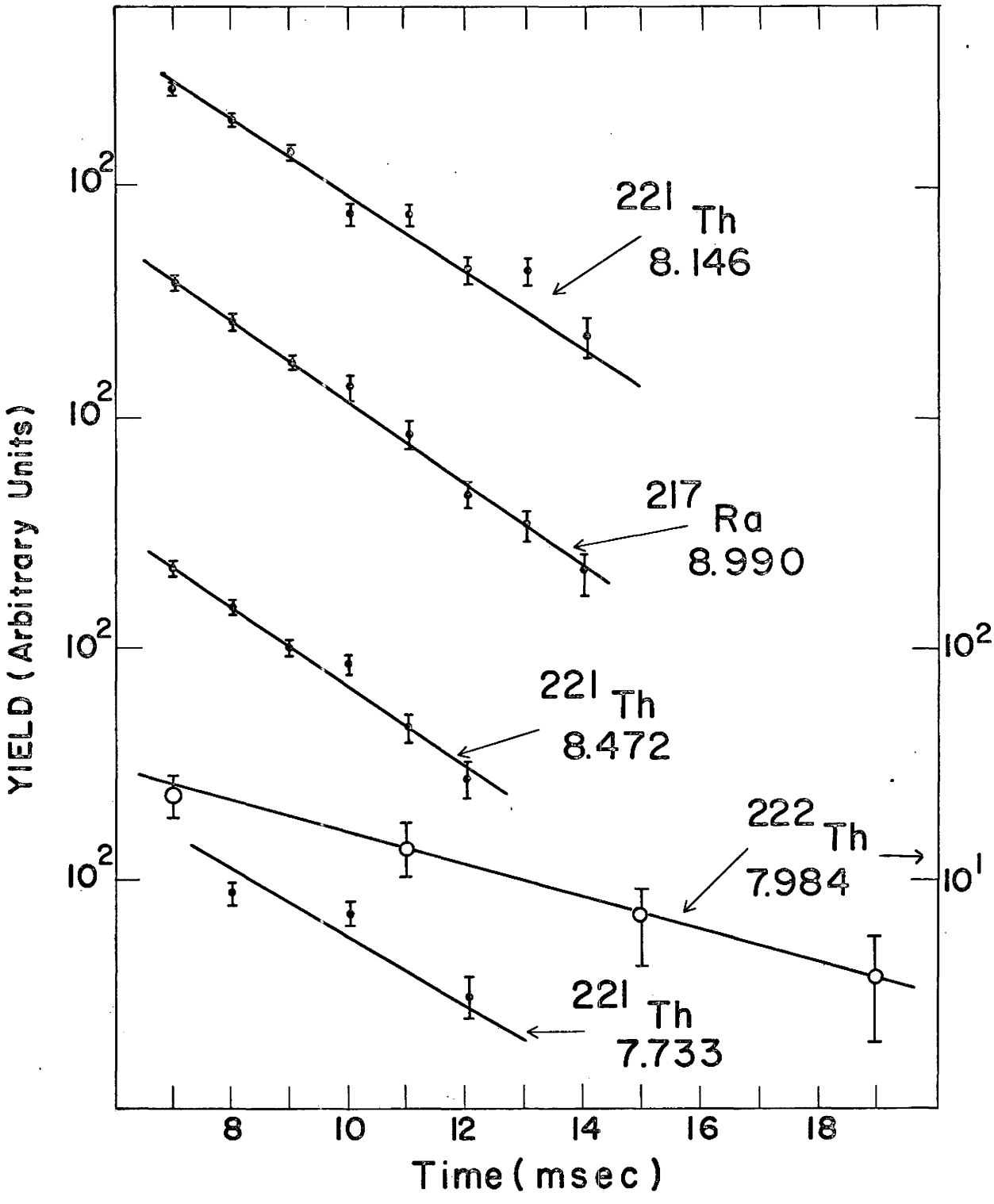
YIELD (Arbitrary Units)
10^2
10^2
10^2
10^2
10^1
221 Th
8.146
217 Ra
8.990
221 Th
8.472
222 Th
7.984
221 Th
7.733
8
10
12
14
16
18
Time (msec)

of ^{217}Ra to an excited state of ^{213}Rn. However, these groups are assigned to ^{221}Th for the following reasons. The predicted ground state alpha decay energy of ^{221}Th is ~8.5 MeV which agrees well with the group at 8.472 MeV. The intensity of the ^{221}Th parent groups must be at least equal to the intensity of the daughter ^{217}Ra. Hence, the 8.146 MeV group belongs to ^{221}Th and not ^{217} Ra. Finally, the 7.733 MeV group would relate to an alpha transition to a 1.3 MeV excited state in ^{213}Rn if it were assigned to ^{217}Ra. This state would not be expected to be populated with measurable intensity for the counting statistics obtained in this work, since alpha decay rates are exponentially dependent on energy. It is highly probable, therefore, that the 7.733 MeV group belongs to ^{221}Th.

To consolidate these results, the true half-life of ^{217}Ra was measured relative to the parent ^{221}Th using a time-to-amplitude converter (TAC). The 2 prominant ^{221}Th peaks (8.146 and 8.472 MeV) and the ^{217}Ra peak were electronically gated to produce a start and stop pulse respectively on the TAC. The TAC produced a bipolar signal, proportional to the time difference between the start and stop, which was routed into a pulse height analyser. The analyser was calibrated using a pulse generator whose output was divided into a prompt signal, used as the start pulse on the TAC, and a delayed signal, used as the stop pulse. By varying the delay, a calibration curve could be obtained. The

results of this measurement are shown in figure 27, and the half-life of ^{217}Ra is determined to be 4 ± 1 μsec.

The decay schemes of ^{221}Th and ^{217}Ra are illustrated in figure 28. A discussion of the reduced widths for the alpha decay of these nuclei is to be found in section 6.4.

6.3 Thorium 222 and Radium 218

Alpha particle transitions at 7.984 and 8.392 MeV are assigned to ^{222}Th and ^{218}Ra respectively. The excitation functions for these groups, plotted in figure 25, appear to maximize at the same incident ^{16}O beam energy as the ^{221}Th groups, but decrease much less rapidly at lower energies. This is a result of the retarding Coulomb barrier for the ^{208}Pb + ^{16}O $\longrightarrow$ ^{224}Th* reaction at 80 MeV. It is evident that the optimum excitation energy for ^{222}Th formation lies below the classical barrier. This explains the low intensity of the ^{222}Th group in the spectrum.

The half-life of ^{222}Th, determined from the decay curve in figure 26, is 4.0 ± 0.6 msec. Due to poor counting statistics, however, the half-life of the ^{218}Ra daughter at 8.392 MeV could not be measured.

Table V summarizes the results obtained for the new isotopes discussed in this chapter. For comparative purposes, the predicted or calculated alpha decay Q-values of Viola and Seaborg[37] are tabulated along with those obtained experimentally. It is noted that the predicted values for ^{218}Ra and ^{217}Ra are in excellent agreement with experiment

FIGURE 27

True decay curve of ^{217}Ra. The method of determining this curve is described in the text.

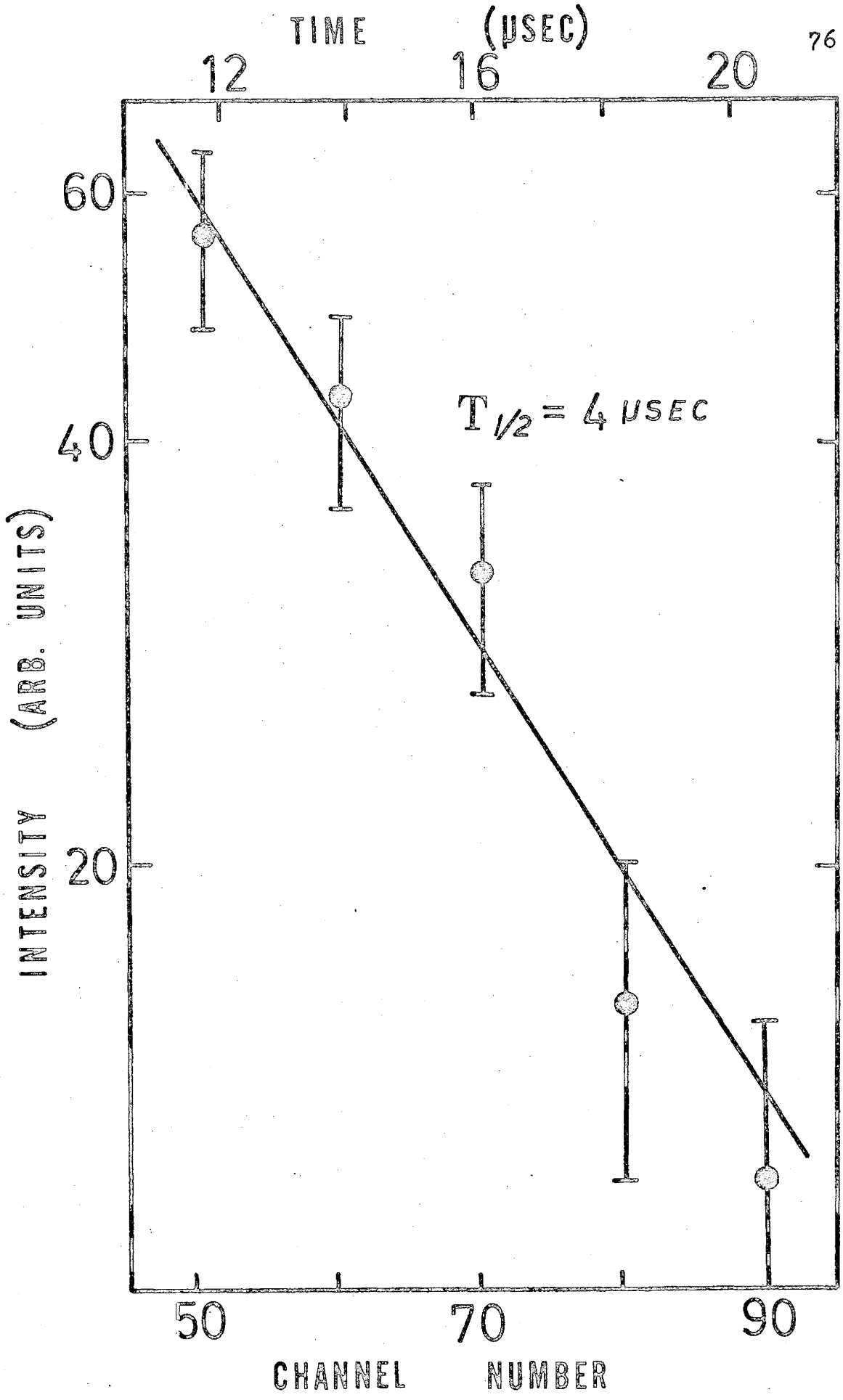
TIME (μSEC)
12
16
20
60
40
20
INTENSITY (ARB. UNITS)
$T_{1/2} = 4$ μSEC
50
70
90
CHANNEL NUMBER

FIGURE 28

Alpha decay scheme of ^{221}Th and ^{217}Ra.

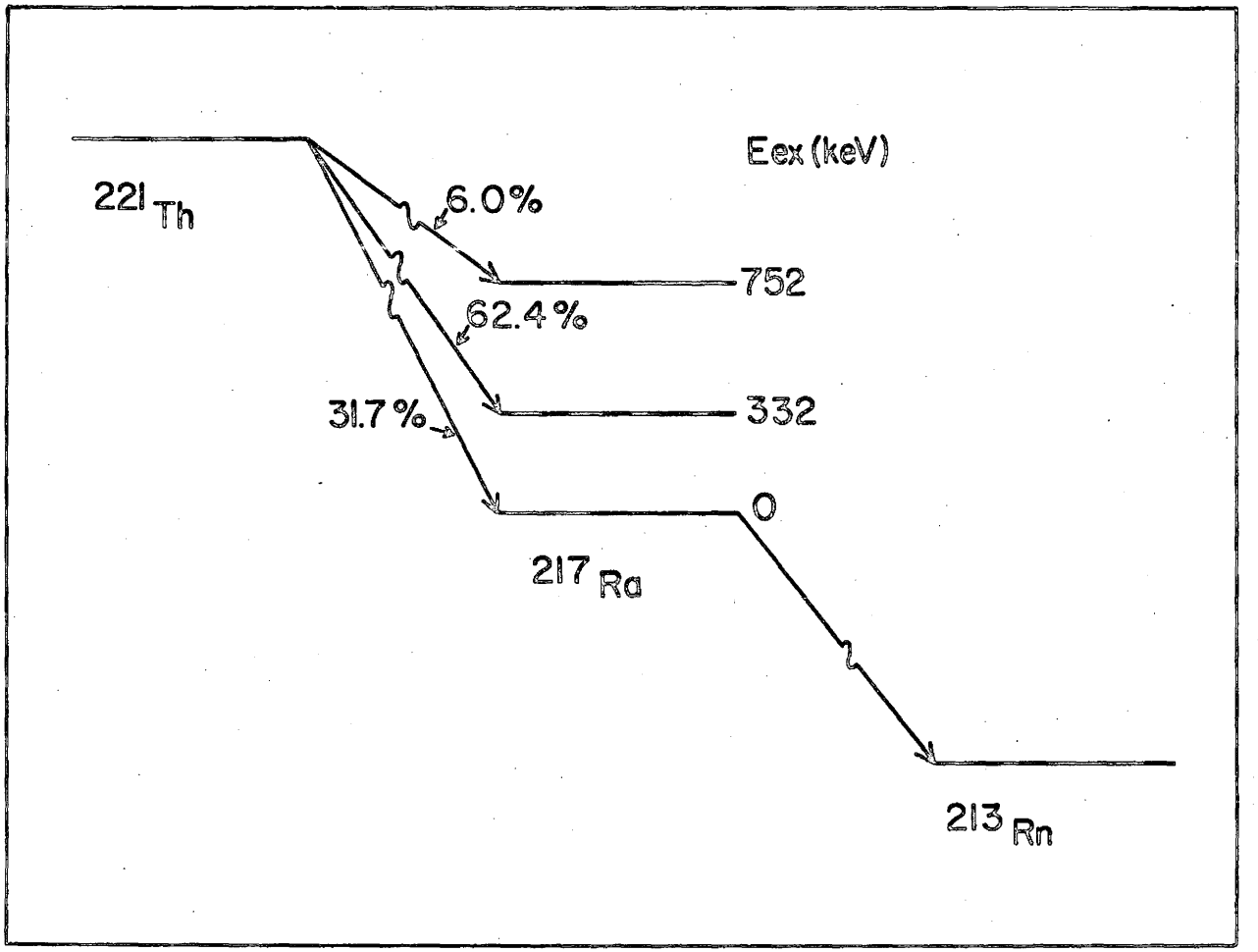
Eex (keV)
221 Th
6.0%
752
62.4%
332
31.7%
0
217 Ra
213 Rn

TABLE V

New Isotope Results

Isotope	E_α (MeV)	$t_{1/2}$ (msec)	Q (MeV) exp	Q* (MeV) VS	δ^2 (keV) L = 0	E_D** (keV)	Int %
^{222}Th	7.984 ± 0.008	4.0 ± 0.6	8.130	8.230	106	0	100
^{221}Th	8.472 ± 0.005	1.7 ± 0.2	8.628	8.710	3.10	0	31.6
	8.146 ± 0.005		8.296		53.2	332	62.4
	7.733 ± 0.008		7.876		95.2	752	6.0
^{218}Ra	8.392 ± 0.008	-	8.549	8.560	-	0	100
^{217}Ra	8.990 ± 0.008	0.004 ± 0.001	9.159	9.176	41.5	0	100

* Predicted or calculated value of Viola and Seaborg

** Daughter level populated

and are somewhat better than those predicted for ^{222}Th and ^{221}Th. This is not surprising as the latter results were obtained by extrapolation of experimental data, while the former results were obtained by interpolation. The correspondence of the experimental and predicted Q-values indicates the value of Viola and Seaborg's work for the determination of new isotopes from alpha decay studies.

6.4 Reduced Widths

Reduced widths calculated for L = 0 alpha particles are listed in table V. The transition from the even-even ^{222}Th to the even-even ^{218}Ra represents the most favored case of alpha decay. Alpha particle formation takes place from paired nucleons and only S-wave transitions are involved since $J\pi$ = (0+) for both parent and daughter. Accordingly, the reduced width for ^{222}Th is 106 keV which is a factor of 30 greater than the reduced width for the ground state decay of the even-odd ^{221}Th.

The reduced widths of ^{221}Th are interesting in that transitions to excited states in ^{217}Ra are favored over the ground state transition and the reduced widths approach the values obtained for neighboring even-even nuclei. To understand this effect, however, much more information must be obtained with respect to the nature of the states involved in these transitions.

The region of discussion, however, is close to the

point where the spherical shell model has validity. The reduced width for the ^{217}Ra to ^{213}Rn ground state alpha transition is 41.5 keV which suggests that paired nucleons are involved in alpha particle formation. It is reasonable to assume that paired protons take part in alpha particle clustering in the even-odd ^{217}Ra nucleus. If 3 neutrons fall into the $2g_{9/2}$ shell model state, then the ground state decay can also involve a neutron pair. This would explain the large reduced width value for ^{217}Ra.

CHAPTER VII

DISCUSSION OF RESULTS

7.1 Isomerism in the Odd-Odd 127 Isotones

The systematic occurrence of isomerism in the odd-odd- N = 127 isotones is now established and arises from the coupling of a $g_{9/2}$ neutron and an $h_{9/2}$ proton. It is experimentally observed that the addition of proton pairs to the $h_{9/2}$ shell does not affect the qualitative nature of this coupling. Hence, these nuclei are characterized by a (1-) ground state and a (9-) metastable state.

An examination of the energy levels of ^{210}Po reveals that the energy required to uncouple a proton pair from $(h_{9/2})^2_{J=0}$ to $(h_{9/2})^2_{J=2}$ is 1.18 MeV[60]. Assuming that the pairing energy does not radically change in the presence of additional pairs, then levels below 1.18 MeV excitation are expected to retain the J=0 proton-proton coupling.

This is clearly the situation for the ground and metastable states of ^{212}At, ^{214}Fr, and ^{216}Ac, whose (1-) to (9-) energy level spacings are 220, 123, and 37 keV respectively. Since the excitation energy does not exceed the proton pairing energy, the core can be increased in size to include the inert protons. In addition to the increase in size, one would expect a larger degree of core polarization

as extra nucleon pairs are added. This might qualitatively explain the decreasing energy separation of the (1-) and (9-) states between ^{210}Bi and ^{216}Ac. By taking these effects into account, one might anticipate that a short-range tensor force such as that used by Kim and Rasmussen[1] could be utilized to theoretically determine the levels of these isotones

7.2 Reduced Widths of Francium 214 and Actinium 216

A comparison of the reduced widths of ^{214}Fr (table I) and ^{216}Ac (table III) reveals two salient points: a) the reduced widths of ^{216}Ac are all slightly enhanced with respect to ^{214}Fr and b) the fluctuations in the relative reduced widths for transitions to daughter levels show the same trends. The latter observation can be illustrated by normalizing the reduced widths to the ground state to ground state transitions:

Configuration	Transition	^{214}Fr	^{216}Ac
$(p_{1/2}, g_{9/2})$	(1-) - (5+)	1	1
	(1-) - (4+)	0.02	0.02
	(9-) - (5+)	0.35	0.40
	(9-) - (4+)	0.60	0.66
$(p_{3/2}, g_{9/2})$	(9-) - (5+)	2.2	3.3
	(9-) - (4+)	2.3	4.0

The first point is easily explained, since the extra proton pair in ^{216}Ac is expected to enhance alpha particle

formation. The second point indicates that it is the neutron single particle states that have the greatest influence on the decay rate. Again, this is not surprising since alpha particle formation will involve paired protons in the $h_{9/2}$ shell, leaving the odd proton undisturbed.

A quantitative discussion of the reduced width fluctuations of ^{214}Fr or ^{216}Ac would require detailed knowledge of the neutron and proton wave functions involved. Calculation of theoretical reduced widths for an odd-odd nucleus is beyond the scope and purpose of the present work. However, in the next two sections, theoretical reduced widths calculated from the Mang shell model theory will be presented for much simpler cases of alpha decay, the even-odd 127 isotones.

7.3 Reduced Widths of the Even-Odd 127 Isotones

It is of interest to determine how well the shell model theory of alpha decay can simulate experimental trends. The alpha decay of the even-odd 127 isotones represents a particularly simple mode of alpha decay, since the protons are all paired and the neutron orbitals involved are particle or hole states in the N = 126 core. Therefore, equation 1.14 can be directly applied.

In order to evaluate equation 1.14, a form for the radial wave functions must be chosen. For the present case, pure shell model configurations are assumed and are described by harmonic oscillator wave functions. The radial dependence

of the reduced width is then approximated by [24]

$$R(n_1 l_1 n_2 l_2 n_3 l_3 n_4 l_4; R_o) \sim \mathrm{Exp}(-2R_o^2)(\alpha^{1/2}R_o)^{l_1+l_2+l_3+l_4} \times \left[\frac{n_1! n_2! n_3! n_4!}{(n_1+l_1+1/2)!(n_2+l_2+1/2)!(n_3+l_3+1/2)!(n_4+l_4+1/2)!}\right]^{1/2} \times Ln_1^{l_1+1/2}(\alpha R_o^2) Ln_2^{l_2+1/2}(\alpha R_o^2) Ln_3^{l_3+1/2}(\alpha R_o^2) Ln_4^{l_4+1/2}(\alpha R_o^2) \qquad 7.1$$

where $\alpha = 0.175 \times 10^{26}\,\mathrm{cm}^{-2}$ and $L_n^{l+1/2}$ is the generalized Laguerre Polynomial

$$L_n^{l+1/2} = \sum_{k=0}^{n} \binom{n+l+1/2}{n-k} \frac{(-1)^k}{k!} (\alpha R_o^2)^k \qquad 7.2$$

The connection radius R_o is chosen at 9 fm.

It is found that the theoretical values calculated from the Mang theory differ from the experimental values by a factor of 10^4 for a connection radius of 9 fm. This is consistent with the work of Zeh[61] who calculated reduced widths for ^{211}Po using several different radii. Moreover, the experimental and theoretical reduced widths are not defined in exactly the same manner and the values are expected to differ by a factor of ~6. This point is discussed in reference 13.

To facilitate comparison, therefore, ^{211}Po is taken as a standard and the theoretical reduced width is set equal to the experimental value. These results are summarized in table VI. By using this procedure, it is hoped to minimize any ambiguities introduced by the choice of the radial wave functions and the parameters α and R_o.

To clearly present the theoretical and experimental trends, the ratio of the reduced widths to ^{211}Po are plotted in figure 29. It is observed that the Mang theory reproduces the sharp rise in reduced width on going from ^{211}Po to ^{213}Rn and allows for the smaller difference between ^{213}Rn and ^{215}Ra.

However, the experimental and theoretical trends at ^{217}Th become divergent. The experimental data for ^{217}Th is not complete since only an upper limit is known for the half-life. By extrapolating the half-lives of the other 127 isotones, the half-life of ^{217}Th is predicted to be ~100 μsec. Using this value would increase the reduced width by a factor of 3.

It is clear, therefore, that the theory breaks down at ^{217}Th. It is probable that the nuclear wave function can no longer be described in terms of pure configuration shell model orbitals. Nevertheless, the results of these calculations show that some of the simple concepts of the shell model have validity well beyond the ^{208}Pb core.

TABLE VI

Reduced Widths of the Even-Odd 127 Isotones

Nuclide	E (MeV)	$t_{1/2}$ (msec)	Ref	δ^2 exp (keV)(L=5)	γ^2 theoret (keV)(L=5)
^{211}Po	7.448	520	60	3.29	3.29
^{213}Rn	8.090	19	54	5.67	5.15
^{215}Ra	8.701	1.56	-	7.00	5.90
^{217}Th	9.250	<0.3	57	>7.07	5.15

TABLE VII

Radium 215 Reduced Widths and Intensities

^{211}Rn Level	L	P/P_{gs} x10^{-2}	γ^2/γ^2_{gs}	Int (theoret)	Int (exp)
$3p_{1/2}$	5	100	1	100	100
$2f_{5/2}$	3	15.9	0.08	1.3	
	5	3.56	0.30	1.1	
	7	0.43	1.26	0.5	
				2.9	1.5
$3p_{3/2}$	3	2.20	1.19	2.6	
	5	0.49	0.66	0.3	
				2.9	2.7

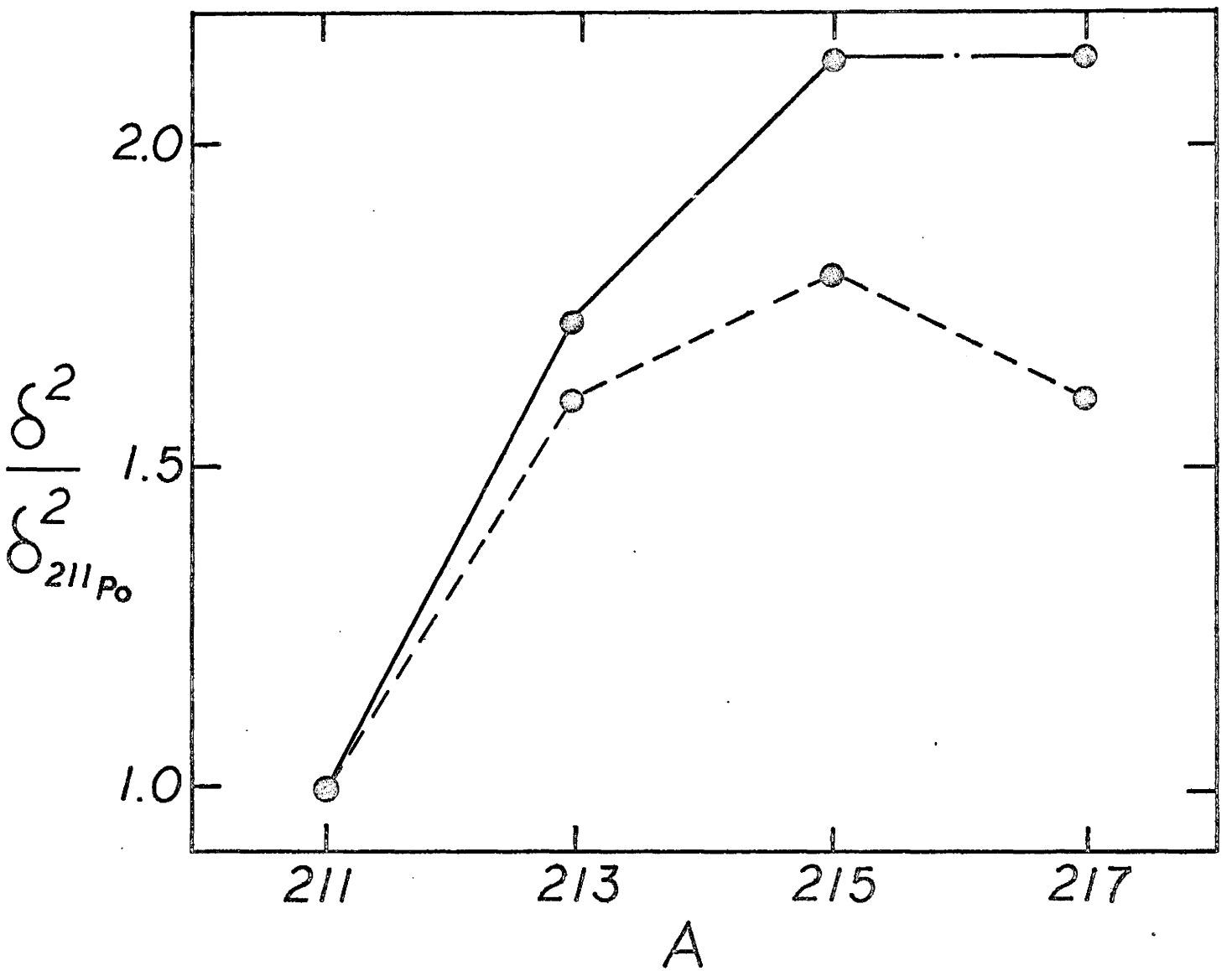
2.0
1.5
1.0
$\frac{\delta^2}{\delta^2_{211_{Po}}}$
211
213
215
217
A

7.4 Delta-Function Model Applied to Radium 215

The experimental results obtained for ^{215}Ra suggest that relatively pure shell model states are involved in the alpha decay process. Therefore, Rasmussen's equation 1.15 for decay involving unpaired nucleons is thought to be applicable.

It is the purpose of the δ-function model to reproduce relative decay rates only. Therefore, only the ratio of reduced widths to the ground state decay will be considered.

Alpha particle formation involves one of the 2 sets of paired protons from the $h_{9/2}$ shell. Since only ratios are being calculated, the proton factors cancel out. The ratio then depends on one of the final state neutron orbitals of angular momentum j ($p_{1/2}$, $f_{5/2}$, or $p_{3/2}$). The appropriate expression is

$$\frac{\gamma^2_{Lj}}{\gamma^2_{5p_{1/2}}} = \left[\frac{2j+1}{2}\right]\left[\frac{(j\ 9/2\ 1/2\text{-}1/2|L0)}{(1/2\ 9/2\ 1/2\text{-}1/2|50)} \times \frac{R_j}{R_{p_{1/2}}} \times \frac{B(l_f l_i L)}{B(115)}\right]^2 \qquad 7.3$$

where the coefficients B are defined in equation 1.16.

For the radial neutron wave functions R_j, harmonic oscillator functions might be used. However, a more realistic approach is to use the wave functions of Blomqvist and Walhborn[62] calculated for a diffuse Woods-Saxon type potential at ^{208}Pb.

The solutions to equation 7.3 for ^{215}Ra, using Blomqvist and Walhborn wave functions, are shown in table VII. Relative reduced widths are calculated for all allowed L-waves.

Relative penetrability factors, calculated from equation 1.7, are also tabulated and are multiplied by the relative reduced widths to yield theoretical intensities. The theoretical intensities are added for each transition and are compared to the experimental result, which includes contributions from all allowed L-waves. The correspondence between theory and experiment is very reasonable.

It is gratifying that the shell model theory can be used to simulate the alpha intensity pattern of ^{215}Ra. The experimental and theoretical results both imply that relatively pure shell model configurations adequately describe the ground state of ^{215}Ra and some of the low-lying levels of ^{211}Rn. It would be of great interest, therefore, to extend these calculations to some of the other 127 isotones once additional experimental data becomes available.

7.5 Atomic Masses

The experimental measurement of ground state alpha decay energies provides a useful and extremely accurate means of determining atomic masses. The alpha decay Q-value is related to atomic mass through the following expression

$$Q = (m_p - m_d - m_{He})c^2 \qquad 7.4$$

where m_p, and m_d are atomic masses of the parent and daughter nuclei respectively.

It is noted that the quantity relating to nuclear mass is Q_e which is equal to the Q-value plus the electron screening correction. Thus, Q_e represents the energy released if the alpha decay process were to take place from a bare nucleus.

It is customary to express the atomic mass as the "mass decrement" which is equal to the total mass less the mass number.

$$\Delta m(Z,A) = {}_Z m^A - A \qquad 7.5$$

The mass decrement is usually tabulated in terms of its energy equivalent.

Atomic mass decrements calculated for most of the nuclei studied in this work are presented in table VIII. Included in the table are alpha groups corresponding to the $^{221}Ac \longrightarrow {}^{217}Fr \longrightarrow {}^{213}At$ alpha decay chain for which improved alpha decay energies have been obtained. For completeness, the new isotope ^{214}Rn, belonging to the ^{222}Th decay chain, is also listed in table VIII. Results for this nuclide are preliminary and additional data is presently being acquired.

The masses determined in this work ultimately depend on a standard mass to which the alpha decay chain is

TABLE VIII

Experimental Atomic Masses

Isotope	E_α (MeV) This Work	E_α (MeV) Previous Results	Ref.	Mass Decrement (keV) This Work	Mass Decrement (keV) 1964 Mass Table	Mass Decrement (keV) Swiatecki-Meyers
^{213}At	9.089 ± 0.015	9.06	64	-6574 ± 17	-6460 ± 200	-7760
^{213}Rn	8.090 ± 0.008	8.090	54	-5700 ± 14	-5652 ± 23	-6941
^{214}Rn	9.040 ± 0.020	-		-4313 ± 21	-4310 ± 1000	-5579
^{214}Fr	8.426 ± 0.005	8.430	53	-1065 ± 26	-930 ± 33	-2596
^{217}Fr	8.320 ± 0.008	8.31	64	4327 ± 19	4430 ± 280	2618
^{215}Ra	8.701 ± 0.005	8.698	57	2504 ± 12	2529 ± 23	668
^{217}Ra	8.990 ± 0.008	(9.0)	67	5884 ± 16	5949 ± 38	4077
^{218}Ra	8.392 ± 0.008	-		6661 ± 22	6680 ± 1410	5198
^{221}Ac	7.640 ± 0.008	7.64	64	14533 ± 21	14600 ± 300	13284
^{221}Th	8.472 ± 0.005	-		16937 ± 17	-	15369
^{222}Th	7.984 ± 0.008	-		17315 ± 23	-	16135

related. These are as follows

$$^{222}\text{Th} \longrightarrow {}^{218}\text{Ra} \longrightarrow {}^{214}\text{Rn} \longrightarrow {}^{211}\text{Po} \quad (-15950 \pm 6)$$

$$^{221}\text{Th} \longrightarrow {}^{217}\text{Ra} \longrightarrow {}^{213}\text{Rn} \longrightarrow {}^{209}\text{Po} \quad (-16370 \pm 12)$$

$$^{221}\text{Ac} \longrightarrow {}^{217}\text{Fr} \longrightarrow {}^{213}\text{At} \longrightarrow {}^{209}\text{Bi} \quad (-18262 \pm 7)$$

$$^{215}\text{Ra} \longrightarrow {}^{211}\text{Rn} \quad (-8787 \pm 11)$$

$$^{214}\text{Fr} \longrightarrow {}^{210}\text{At} \quad (-12075 \pm 26)$$

where the last isotope in each case is chosen as the standard and the quantity in parentheses is the published mass decrement in keV[63]. For the ^{221}Th decay chain, it was necessary to correct the published mass decrement of ^{213}Rn as indicated in table VIII.

An examination of table VIII reveals that the mass decrements measured in this work are somewhat improved relative to those listed in the 1964 mass table of Mattauch et al.[63] The 1964 mass table also includes some masses for unknown nuclei calculated from the predicted alpha decay Q-values of Viola and Seaborg[37].

Mass decrements calculated from the Swiatecki-Meyers mass formula[35] were taken from reference 36. It is observed that the calculated masses are systematically smaller than the experimental values. Mass formulae are not expected to reproduce accurate masses in the neutron-deficient region since formulae parameters are obtained from a fit to all known experimental data. Since relatively few experimental masses have been measured in neutron deficient regions, mass

FIGURE 30

Alpha-beta mass-energy cycles for some of the nuclides studied in this work. The numbers associated with the diagonal lines are the neutron binding energies calculated from experimental mass differences, and link the 4n+2 with the 4n+1 series. All units are in keV.

formulae heavily favor the region of beta-stability.

7.6 Alpha-Beta Energy Systematics

Alpha decay Q-values are useful for extending alpha-beta closed cycles. Figure 30 is a presentation of some of the Q-values measured in this work incorporated into the 4n+1 and 4n+2 mass-energy lattices.

The horizontal lines in figure 30 represent the alpha transitions, while the numbers associated with the vertical lines are the electon capture decay energies calculated from mass differences. All quantities are given for the process taking place in the direction of the arrow. The sum of the energies in any cycle must necessarily be zero to conserve mass-energy.

The diagonal lines in figure 30 connect the 4n+2 with the 4n+1 series. The numbers associated with these lines are the neutron binding energies calculated from

$$(BE)_n = (m(Z,N)-m(Z,N-1)-m_n)c^2 \qquad 7.6$$

where m_n is the mass of the neutron.

It is clear that much invaluable information about the neutron-deficient region can be derived from careful atomic mass measurements. It is anticipated that as experimental techniques improve, the investigation of more of these nuclei will become feasible.

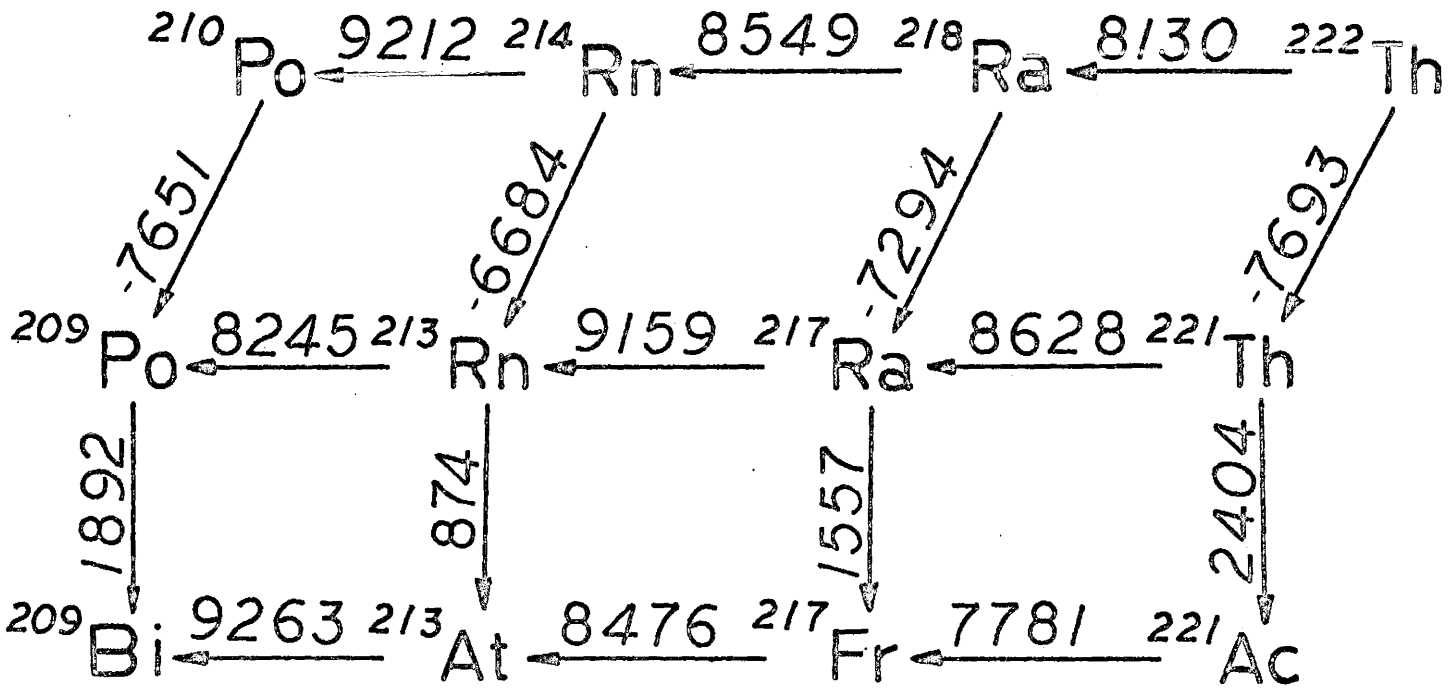
210 Po 9212 214 Rn 8549 218 Ra 8130 222 Th
.7651
.6684
.7294
.7693
209 Po 8245 213 Rn 9159 217 Ra 8628 221 Th
1892
874
1557
2404
209 Bi 9263 213 At 8476 217 Fr 7781 221 Ac

CHAPTER VIII

CONCLUSIONS

Several nuclei in the neutron-deficient region have been studied using the helium jet recoil transport method. The prominent features of these studies are as follows.

Investigations of the alpha decay of ^{214}Fr and ^{216}Ac have revealed a systematic occurrence of isomerism in the odd-odd N = 127 isotones. The nature of the isomeric states can likely be explained using a short range tensor neutron-proton residual force and expanding the inert core to include paired protons. Similar trends are observed in the reduced width fluctuations of ^{214}Fr and ^{216}Ac.

Levels of ^{210}At and ^{212}Fr up to ~1 MeV excitation populated by alpha decay have been studied and a striking correspondence was found to exist between these nuclei and ^{208}Bi. On the basis of this correspondence, some information about spins and parities of these levels was deduced.

The alpha decay of ^{215}Ra was studied experimentally, and theoretically using the δ-function approximation. It was found that the theory reproduced the experimental results well when pure shell model configurations were used for the ground state of ^{215}Ra and the first 3 levels of ^{211}Rn. Experimentally it was observed that the low-lying energy levels of ^{211}Rn greatly resembled those of ^{207}Pb.

The ground state alpha decay of the even-odd 127 isotones ^{211}Po, ^{213}Rn, ^{215}Ra, and ^{217}Th has been studied theoretically using the Mang shell model theory. It was observed that the theory adequately reproduced the relative alpha decay rates up to ^{215}Ra. At ^{217}Th, theory and experiment became divergent. This was probably a consequence of approximating the nucleon wave functions by pure shell model orbitals.

The new isotopes ^{222}Th, ^{221}Th, ^{218}Ra, and ^{217}Ra were discovered and their alpha decay properties measured. Reduced width fluctuations were understood in terms of simple nucleon pairing considerations.

Atomic masses for several nuclei were calculated from the ground state alpha decay Q-values measured in this work. New information concerning neutron binding energies and electron-capture decay energies was obtained.

APPENDIX

LSS RANGE THEORY

Some of the concepts of the Lindhard Scharff and Schiott[65] range theory are summarized with special emphasis on the ranges in helium of recoils studied in this work.

Lindhard *et al.* have formulated a "unified theory" of atomic stopping in terms of the 2 dimensionless parameters ρ and ϵ. These are defined in the following expressions where subscript 1 refers to the recoil and subscript 2 refers to the He gas.

$$\rho = 4\, a^2 R N M_2 \frac{M_1}{(M_1+M_2)^2} \quad , \qquad \text{A.1}$$

$$\epsilon = E \frac{aM_2}{Z_1 Z_2 e^2 (M_1 + M_2)} \qquad \text{A.2}$$

Here, R is the range (cm), E is the energy (ergs), and N is the number of He atoms/cc. The parameter a is defined as

$$a = 0.8853\, a_o\, (Z_1^{2/3}+Z_2^{2/3})^{-1/2} \qquad \text{A.3}$$

where a_o is the Bohr radius. Essentially, ρ and ϵ represent generalized range and energy respectively.

For the recoil energies encountered in this work, both electronic and nuclear stopping processes are important.

In terms of the generalized parameters ρ and ϵ, the electronic stopping power is

$$\left(\frac{d\epsilon}{d\rho}\right)_e = k \cdot \epsilon^{1/2} \qquad \text{A.3}$$

where

$$k = Z^{1/6}\left\{\frac{0.0793\ Z_1^{1/2} Z_2^{1/2} (A_1+A_2)^{3/2}}{(Z_1^{2/3}+Z_2^{2/3})^{3/4} A_1^{3/2} A_2^{1/2}}\right\} \qquad \text{A.4}$$

The nuclear stopping power is derived assuming that the interaction between the colliding atoms can be described by the screened potential $(Z_1 Z_2 e^2/r)U(r/a)$, where $U(r/a)$ is the Fermi distribution. Further details are contained in reference 65.

Several generalized range-energy curves have been calculated for various values of k, taking into account both nuclear and electronic stopping. The parameter k is quite insensitive to mass number, and for recoils in the region of A = 220, k = 0.1. The generalized range-energy curve for k = 0.1 is as follows[65,66].

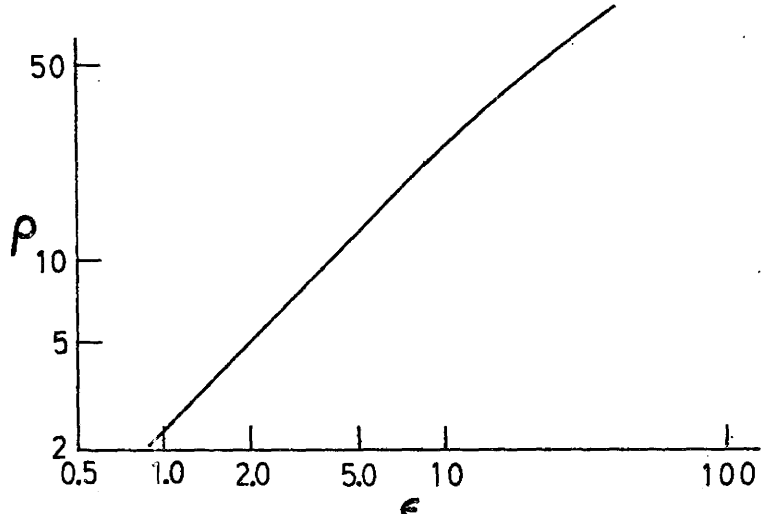

As an example, the theory is applied to ^{224}Th. Using equation A.1, the generalized range is 4.18 for ^{224}Th recoils traversing 1.2 cm of He at 1.9 atm. From the preceeding graph, ϵ is determined to be 2.0. Substituting this value into equation A.2 yields a ^{224}Th recoil energy of 2.8 MeV. A comparison between theory and experiment for heavy ions in He, however, reveals that this value could be low by as much as 20%[65].

REFERENCES

(1) Y. E. Kim and J. O. Rasmussen, Phys. Rev. 135 (1964) B44.

(2) Y. E. Kim, Phys. Rev. 131 (1963) 1712; UCRL-10865, Thesis, University of California (1963) unpublished.

(3) P. A. Mello and J. Flores, Nucl. Phys. 47 (1963) 177.

(4) Y. E. Kim and J. O. Rasmussen, Nucl. Phys. 47 (1963) 184.

(5) J. R. Erskine, Phys. Rev. 135 (1964) 110.

(6) P. Mukherjee and B. L. Cohen, Phys. Rev. 127 (1962) 1284.

(7) W. P. Alford, J. P. Schiffer, and J. J. Schwartz, Phys. Rev. Letters 21 (1968) 156.

(8) W. B. Jones, Phys. Rev. 130 (1963) 2042; UCRL-11238, Thesis, University of California (1964) unpublished.

(9) D. F. Torgerson, R. A. Gough, and R. D. Macfarlane, Phys. Rev. 174 (1968) 1494.

(10) D. F. Torgerson and R. D. Macfarlane, Bull. Am. Chem. Soc. (in press).

(11) D. F. Torgerson and R. D. Macfarlane, Bull. Am. Phys. Soc. 13 (1968) 1370.

(12) D. F. Torgerson, R. A. Gough, and R. D. Macfarlane, Bull. Am. Phys. Soc. 14 (1969) 588.

(13) J. O. Rasmussen, Alpha-, Beta-, Gamma-Ray Spectroscopy, vol 1, North Holland Publ. Co. (1964) p.701.

(14) J. O. Rasmussen, Phys. Rev. 115 (1959) 1675; Phys. Rev. 113 (1959) 1593.

(15) G. Igo, Phys. Rev. 115 (1959) 1665.

(16) H. A. Enge, Introduction to Nuclear Physics, Addison-Wesley Publ. Co. (1966) p.286.

(17) J. K. Poggenburg, UCRL-16187, Thesis, University of California (1965) unpublished.

(18) R. D. Woods and D. S. Saxon, Phys. Rev. 95 (1954) 577.

(19) G. H. Winslow, Phys. Rev. 96 (1954) 1032.

(20) P. J. Brussaard and H. A. Tolhoek, Physica 24 (1958) 263.

(21) D. H. Wilkinson, Proceedings of the Rutherford Jubilee International Conference, Heywood and Co. Ltd. (1961) p.339.

(22) R. G. Thomas, Prog. Theoret. Phys. 12 (1954) 253.

(23) H. J. Mang, Z. Phys. 148 (1957) 582.

(24) H. J. Mang, Phys. Rev. 119 (1960) 1069.

(25) H. J. Mang and J. O. Rasmussen, Mat. Fys. Skr. Dan. Vid. Selsk. 2, No. 3 (1962).

(26) H. D. Zeh and H. J. Mang, Nucl. Phys. 29 (1962) 529.

(27) H. J. Mang, Ann. Rev. Nucl. Sci. 14 (1964) 1.

(28) J. O. Rasmussen, Nucl. Phys. 44 (1963) 93.

(29) K. Harada and E. A. Rauscher, Phys. Rev. 169 (1968) 818.

(30) G. Benoze and A. Sandulescu, Phys. Letters 22 (1966) 473.

(31) K. Harada, Prog. Theoret. Phys. 27 (1962) 430.

(32) C. F. Von Weizsacker, Z. Physik 96 (1935) 431.

(33) P. A. Seeger, Proceedings of the Third International Conference on Atomic Masses, University of Manitoba Press (1967) 85.

(34) H. Kummel, J. H. E. Mattauch, W. Thiele, and A. H. Wapstra, Nucl. Phys. 81 (1966) 129.

(35) J. Myers and W. Swiatecki, Nucl. Phys. 81 (1966) 1.

(36) J. Myers and W. Swiatecki, UCRL-11980 (1965) unpublished.

(37) J. Viola and G. T. Seaborg, J. Inorg. Nucl. Chem. 28 (1966) 697.

(38) R. D. Macfarlane and R. D. Griffioen, Nucl. Instr. and Meth. 24 (1963) 461

(39) R. D. Macfarlane, R. A. Gough, N. S. Oakey, and D. F. Torgerson, Nucl. Instr. and Meth. (in press).

(40) R. D. Macfarlane, Arkiv. for Fysik 36 (1967) 431.

(41) R. D. Macfarlane and J. Cerny, Proceedings of the Third International Conference on Atomic Masses, University of Manitoba Press (1967) 431.

(42) V. L. Mikeev, Pribory i Tekhnika Eksperimenta 4 (1966) 22 (translation: Instr. Exptl. Tech. (USSR) 4 (1967) 785).

(43) R. A Gough, private communication (1969).

(44) W. Parker and A. Falk, Nucl. Instr. and Meth. 16 (1962) 355.

(45) L. Winsberg and J. M. Alexander, Phys. Rev. 121 (1961) 518.

(46) A. H. Wapstra, Nucl. Phys. 28 (1961) 29.

(47) L. C. Northcliffe, Phys. Rev. 120 (1960) 1744.

(48) P. G. Roll and F. E. Steigert, Nucl. Phys. 17 (1960) 54.

(49) J. R. Walton, Lawrence Rad. Lab., Berkeley (1959) unpublished data.

(50) L. W. Nordheim, Phys. Rev. 78 (1950) 294.

(51) R. D. Griffioen and R. D. Macfarlane, Bull. Am. Phys. Soc. 7 (1962) 541.

(52) H. Rotter, A. G. Demin, L. P. Pashchenko, and H. F. Brinkman, Yadern. Fiz. 4 (1966) 246 (translation: Soviet J. Nucl. Phys. 4 (1967) 178).

(53) K. Valli, W. Treytl, and E. K. Hyde, Phys. Rev. 161 (1967) 1284.

(54) K. Valli, E. K. Hyde, and W. Treytl, J. Inorg. Nucl. Chem. 29 (1967) 2503.

(55) R. D. Griffioen and R. D. Macfarlane, Phys. Rev. 133 (1964) 1373.

(56) R. D. Macfarlane, Phys. Rev. 126 (1962) 274.

(57) K. Valli and E. K. Hyde, Phys. Rev. 176 (1968) 1377.

(58) I. Perlman, A. Ghiorso, and G. T. Seaborg, Phys. Rev. 77 (1950) 26.

(59) K. Valli, W. Treytl, and E. K. Hyde, Phys. Rev. 167 (1968) 1094.

(60) C. M. Lederer, J. M. Hollander, and I. Perlman, Table of Isotopes, 6th ed., Wiley and sons (1967).

(61) H. D. Zeh, Thesis, University of Heidelburg (1962) unpublished.

(62) J. Blomqvist and S. Wahlborn, Arkiv for Fysik 16 (1960) 545.

(63) J. H. E. Mattauch, W. Theile, and A. H. Wapstra, Nucl. Phys. 67 (1965) 1.

(64) R. L. Hahn, M. F. Roche, and K. S. Toth, Nucl. Phys. 113 (1968) 206.

(65) J. Lindhard, M. Scharff, and H. E. Schiott, Mat. Fys. Medd. Dan. Vid. Selsk. 33, No. 14 (1963).

(66) I. Bergstrom and B. Domeij, Nucl. Instr. and Meth. 43 (1966) 146.

(67) R. D. Macfarlane and R. D. Griffioen, unpublished results (1961).